

AD-A140 920

AFWAL-TR-82-4040
VOLUME II



STATISTICS OF CRACK GROWTH IN ENGINE MATERIALS

Volume II Spectrum Loading and Advanced Techniques

R. J. Schwartz
C. G. Annis, Jr.
Pratt & Whitney Aircraft
West Palm Beach, Florida 33402

G. C. Salivar
Florida Atlantic University
Boca Raton, Florida 33431

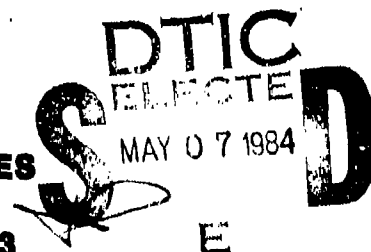
J. N. Yang
The George Washington University
Washington, D.C. 20052

February 1984

Final Report for Period 15 January 1981 - 30 November 1982

Approved for Public Release; Distribution Unlimited

MATERIALS LABORATORY
AIR FORCE WRIGHT AERONAUTICAL LABORATORIES
AIR FORCE SYSTEMS COMMAND
WRIGHT-PATTERSON AIR FORCE BASE, OHIO 45433



DTIC FILE COPY

84 05 07 010

NOTICE

When Government drawings, specifications, or other data are used for any purpose other than in connection with a definitely related Government procurement operation, the United States Government thereby incurs no responsibility nor any obligation whatsoever; and the fact that the government may have formulated, furnished, or in any way supplied the said drawings, specifications, or other data, is not to be regarded by implication or otherwise as in any manner licensing the holder or any other person or corporation, or conveying any rights or permission to manufacture use, or sell any patented invention that may in any way be related thereto.

This report has been reviewed by the Office of Public Affairs (ASD/PA) and is releasable to the National Technical Information Service (NTIS). At NTIS, it will be available to the general public, including foreign nations.

This technical report has been reviewed and is approved for publication.




JOHN P. HENDERSON, Chief
Metals Behavior Branch
Metals and Ceramics Division



ROBERT C. DONATH, Project Engineer
Metals Behavior Branch
Metals and Ceramics Division

FOR THE COMMANDER


LAWRENCE N. HJELM, Asst Chief
Metals and Ceramics Division
Materials Laboratory

"If your address has changed, if you wish to be removed from our mailing list, or if the addressee is no longer employed by your organization please notify AFW AL/MLLN W-PAFB, OH 45433 to help us maintain a current mailing list".

Copies of this report should not be returned unless return is required by security considerations, contractual obligations, or notice on a specific document.

Unclassified

SECURITY CLASSIFICATION OF THIS PAGE (When Data Entered)

REPORT DOCUMENTATION PAGE		READ INSTRUCTIONS BEFORE COMPLETING FORM
1. REPORT NUMBER AFWAL-TR-82-4040, Vol II	2. GOVT ACCESSION NO. AD-A140920	3. RECIPIENT'S CATALOG NUMBER
4. TITLE (and Subtitle) STATISTICS OF CRACK GROWTH IN ENGINE MATERIALS Volume II: Spectrum Loading and Advanced Techniques	5. TYPE OF REPORT & PERIOD COVERED Final for Period 15 Jan 81 - 30 Nov 82	
7. AUTHOR(s) B. J. Schwartz G. C. Salivar C. G. Annis, Jr. J. N. Yang	6. PERFORMING ORG. REPORT NUMBER P&WA/GPD/FR-16727	
9. PERFORMING ORGANIZATION NAME AND ADDRESS Pratt & Whitney Aircraft Government Products Division, P.O. Box 2691 West Palm Beach, FL 33402	8. CONTRACT OR GRANT NUMBER(s) F33615-80-C-5189	
11. CONTROLLING OFFICE NAME AND ADDRESS Materials Laboratory (AFWAL/MLLN) Air Force Wright Aeronautical Laboratories Wright-Patterson Air Force Base, OH 45433	10. PROGRAM ELEMENT, PROJECT, TASK AREA & WORK UNIT NUMBERS 24200128	
14. MONITORING AGENCY NAME & ADDRESS (if different from Controlling Office)	12. REPORT DATE February 1984	
	13. NUMBER OF PAGES 100	
	15. SECURITY CLASS. (of this report) Unclassified	
16. DISTRIBUTION STATEMENT (of this Report) Approved for public release; distribution unlimited.		
17. DISTRIBUTION STATEMENT (of the abstract entered in Block 20, if different from Report)		
18. SUPPLEMENTARY NOTES		
19. KEY WORDS (Continue on reverse side if necessary and identify by block number) Statistical Fatigue Crack Growth Spectrum Loading Engine Materials Lognormal Distribution Elevated Temperature Fracture Mechanics		
20. ABSTRACT (Continue on reverse side if necessary and identify by block number) <i>These</i> A method is developed capable of incorporating the scatter observed in crack growth data into component residual life analyses, such as used in damage-tolerant and retirement-for-cause concepts. Two fracture mechanics-based statistical models for fatigue crack growth damage accumulation in engine materials are proposed. They are based on synergistic fracture mechanics models: a hyperbolic sine crack growth rate function (developed by Pratt & Whitney Aircraft), and a linear crack growth rate function of the Paris type.		

DD FORM 1 JAN 73 1473

EDITION OF 1 NOV 68 IS OBSOLETE
S/N 0102-014-6601

Unclassified

SECURITY CLASSIFICATION OF THIS PAGE (When Data Entered)

Unclassified

SECURITY CLASSIFICATION OF THIS PAGE(When Data Entered)

Test results of IN100 at various temperatures, loading frequencies and stress ratios were compiled and analyzed statistically. The statistical distributions of crack growth rate, propagation life to reach any given crack size, and crack size at any service life, are derived. Correlation between the IN100 test results and the two statistical models is very good.

Test results for IN100 under block type spectrum loading under various test conditions were used with a lognormal statistical model to predict statistical distributions of life to reach any given crack size, and of the crack size at any given service life. Good correlation is shown.

Available fatigue crack growth rate data for Ti 6-2-4-6 and Waspaloy under various test conditions are also analyzed statistically. The lognormal statistical model, using either the Paris or hyperbolic sine crack growth rate function, gives good correlation with extrapolated test results. When applied to a collection of 7475-T7351 aluminum fastener hole specimen data, the Paris relation does not give reasonable correlation.

Finally, a statistical theory, based on the concept of fracture mechanics and random processes, is proposed for the analysis of fatigue crack propagation. Examples are presented for the case where the crack growth rate is governed by a power law. Parameters are estimated from experimental data from 7475-T7351 aluminum fastener hole specimens subjected to an aircraft bomber load spectrum.

Unclassified

SECURITY CLASSIFICATION OF THIS PAGE(When Data Entered)

PREFACE

An investigation of the statistical nature of fatigue-crack growth rate data, resulting in the incorporation of the observed scatter into component residual life analyses, was conducted from February 1981 through January 1983. The authors wish to acknowledge the assistance of several Pratt & Whitney Aircraft employees who made significant contributions to the program. These include Messrs. M. L. Poormon, E. H. Hindle III, C. K. Kraft, G. Scott and D. W. Ogden who aided in the verification testing, and T. Watkins, Jr. who aided in data analysis.

This work was performed under Materials Laboratory Contract F33615-80-C-5189, "Statistics of Crack Growth in Engine Materials." The program was conducted by the Mechanics of Materials and Structures section of Pratt & Whitney Aircraft, Government Products Division, under the cognizance of Dr. R. C. Donath, AFWAL/MLLN. Mr. B. J. Schwartz and Dr. G. C. Salivar were the responsible engineers and Mr. C. G. Annis, Jr. was the program manager reporting to Mr. M. C. VanWanderham, Manager, Mechanics of Materials and Structures. Professor J. N. Yang, of The George Washington University, Washington, DC, was the principal investigator.

Accession For	
NTIS GRA&I	<input checked="" type="checkbox"/>
DTIC TAB	<input type="checkbox"/>
Unannounced	<input type="checkbox"/>
Justification	
By _____	
Distribution/	
Availability Codes	
Dist	Avail and/or Special
A-1	



TABLE OF CONTENTS

Section		Page
I	INTRODUCTION	1
II	FATIGUE CRACK GROWTH UNDER SPECTRUM LOADING CON- DITIONS	3
	1. Theoretical Model	3
	2. Experimental Program	7
	3. Correlation Between Statistical Model and Experimental Test Results	10
III	LOGNORMAL STATISTICAL MODEL APPLIED TO THE PARIS EQUATION FOR IN100	14
	1. Correlation With IN100 Test Results	21
IV	ANALYSIS OF TI 6-2-4-6 AND WASPALOY DATA	33
V	STATISTICAL ANALYSIS OF A HOMOGENEOUS DATA SET	60
VI	ADVANCED STATISTICAL MODEL FOR FATIGUE CRACK GROWTH	65
	1. Model for $X(t)$	66
	2. Approximation of $\bar{a}(t)$ by a Markov Random Process	68
	3. Time to Reach a Given Crack Size	70
	4. Power-Law Crack Propagation	72
	5. Estimation of Model Parameters	74
VII	CONCLUSIONS	83
	1. Spectrum Loading	83
	2. Related Developments	83
	REFERENCES	84
	APPENDIX	86

PRECEDING PAGE BLANK-NOT FILMED

LIST OF ILLUSTRATIONS

<i>Figure</i>		<i>Page</i>
1	Representation of One Cycle Block	4
2	γ Percentiles of Crack Length Versus Number of Cycles	6
3	Laboratory Spectrum Test Loading Conditions for IN100	7
4	Verification Test Results for IN100	9
5	Predicted Crack Size Versus Cycles Behavior Under Spectrum Loading	10
6	Distribution of Cycles to Reach 0.8 Inch, for the IN100 Mission Verification Test	11
7	Distribution of Cycles to Reach 1.4 Inches for the IN100 Mission Verification Test	11
8	Probability of Crack Exceedance at 24,000 Cycles for IN100 Mission Verification Testing	12
9	Probability of Crack Exceedance at 35,000 Cycles for IN100 Mission Verification Testing	12
10	Data for Crack Growth Rate Versus Stress Intensity Range for Test Condition No. 1	16
11	Normal Probability Plot for Z (Test Condition No. 3)	17
12	Percentiles of Log Crack Growth Rate as a Function of Log Stress Intensity Range for Test Condition No. 1	18
13	Distribution of Crack Size as Function of Load Cycles Based on Statistical Model; (a) Test Condition No. 1, (b) Test Condition No. 2	20
14	Distribution of Cycles To Reach Given Crack Size for Test Condition No. 1; (a) $a = 1.0$ Inch, and (b) $a = 2.0$ Inches	22
15	Crack Exceedance Curve After 25,000 Cycles for Test Condition No. 1	23
16	Distribution of Cycles To Reach Given Crack Size for Test Condition No. 2; (a) $a = 0.8$ Inch, and (b) $a = 2.0$ Inches	24
17	Crack Exceedance Curve after 10,000 Cycles for Test Condition No. 2	25
18	Distribution of Cycles To Reach Given Crack Size for Test Condition No. 3; (a) $a = 0.76$ Inch, and (b) $a = 1.7$ Inches	26
19	Crack Exceedance Curve after 40,000 Cycles for Test Condition No. 3	27

LIST OF ILLUSTRATIONS (Continued)

Figure		Page
20	Distribution of Cycles to Reach Given Crack Size for Test Condition No. 4; (a) $a = 0.8$ Inch, and (b) $a = 2.0$ Inches	28
21	Crack Exceedance Curve after 10,000 Cycles for Test Condition No. 4	29
22	Distribution of Cycles to Reach Given Crack Size for Test Condition No. 5; (a) $a = 0.8$ Inch, and (b) $a = 2.0$ Inches	30
23	Crack Exceedance Curve after 8,000 Cycles for Test Condition No. 5 .	31
24	Extrapolated Test Results for a Versus n ; (a) Test Condition No. 1 and (b) Test Condition No. 2	32
25	Crack Growth Rate Model for Waspaloy at 1200°F, 20 Hz, and $R = 0.05$	35
26	Crack Growth Rate Model for Titanium 6-2-4-6 at Room Temperature, 20 Hz, and $R = 0.1$	36
27	Distribution Curve and Crack Exceedance Curve for Waspaloy for Test Condition No. 1; (a) Distribution of Cycles to Reach Given Crack Size, and (b) Crack Exceedance Curve After 50,000 Cycles	39
28	Distribution Curve and Crack Exceedance Curve for Waspaloy for Test Condition No. 2; (a) Distribution of Cycles to Reach a Given Crack Size, and (b) Crack Exceedance Curve After 10,000 Cycles	40
29	Distribution Curve and Crack Exceedance Curve for Waspaloy for Test Condition No. 3; (a) Distribution of Cycles to Reach Given Crack Size, and (b) Crack Exceedance Curve After 50,000 Cycles	41
30	Distribution Curve and Crack Exceedance Curve for Titanium for Test Condition No. 1, Using the Hyperbolic Sine Model; (a) Distribution of Cycles to Reach Given Crack Size, and (b) Crack Exceedance Curve After 30,000 Cycles	42
31	Distribution Curve and Crack Exceedance Curve for Titanium for Test Condition No. 2, Using the Hyperbolic Sine Model; (a) Distribution of Cycles to Reach Given Crack Size, and (b) Crack Exceedance Curve After 20,000 Cycles	43
32	Distribution Curve and Crack Exceedance Curve for Titanium for Test Condition No. 3, Using the Hyperbolic Sine Model; (a) Distribution of Cycles to Reach Given Crack Size, and (b) Crack Exceedance Curve After 5,000 Cycles	44

LIST OF ILLUSTRATIONS (Continued)

Figure		Page
33	Distribution of Cycles to Reach Given Crack Size for Titanium for Test Condition No. 4, Using the Hyperbolic Sine Model; (a) Distribution of Cycles to Reach Given Crack Size, and (b) Crack Exceedance Curve After 5,000 Cycles	45
34	Distribution Curve and Crack Exceedance Curve for Titanium for Test Condition No. 5, Using the Hyperbolic Sine Model; (a) Distribution of Cycles to Reach Given Crack Size, and (b) Crack Exceedance Curve After 100,000 Cycles	46
35	Titanium Crack Growth Rate Specimen at Test Condition No. 1	48
36	Distribution Curve and Crack Exceedance Curve for Titanium for Test Condition No. 1, Without Specimen No. 1582; (a) Distribution of Cycles to Reach Given Crack Size, and (b) Crack Exceedance Curve After 30,000 Cycles	49
37	Distribution Curve and Crack Exceedance Curve for Waspaloy for Test Condition No. 1, Using the Paris Model; (a) Distribution of Cycles to Reach Given Crack Size, and (b) Crack Exceedance Curve After 50,000 Cycles	52
38	Distribution Curve and Crack Exceedance Curve for Waspaloy for Test Condition No. 2, Using the Paris Model; (a) Distribution of Cycles to Reach Given Crack Size, and (b) Crack Exceedance Curve After 10,000 Cycles	53
39	Distribution Curve and Crack Exceedance Curve for Waspaloy for Test Condition No. 3, Using the Paris Model; (a) Distribution of Cycles to Reach Given Crack Size, and (b) Crack Exceedance Curve After 50,000 Cycles	54
40	Distribution Curve and Crack Exceedance Curve for Titanium for Test Condition No. 1, Using the Paris Model; (a) Distribution of Cycles to Reach Given Crack Size, and (b) Crack Exceedance Curve After 30,000 Cycles	55
41	Distribution Curve and Crack Exceedance Curve for Titanium for Test Condition No. 2, Using the Paris Model; (a) Distribution of Cycles to Reach Given Crack Size, and (b) Crack Exceedance Curve After 20,000 Cycles	56
42	Distribution of Cycles to Reach Given Crack Size for Titanium for Test Condition No. 3, Using the Paris Model; (a) Distribution of Cycles to Reach Given Crack Size, and (b) Crack Exceedance Curve After 5,000 Cycles	57

LIST OF ILLUSTRATIONS (Continued)

Figure		Page
43	Distribution of Cycles to Reach Given Crack Size for Titanium for Test Condition No. 4, Using the Paris Model; (a) Distribution of Cycles to Reach Given Crack Size, and (b) Crack Exceedance Curve After 5,000 Cycles	58
44	Distribution Curve and Crack Exceedance Curve for Titanium for Test Condition No. 5, Using the Paris Model; (a) Distribution of Cycles to Reach Given Crack Size, and (b) Crack Exceedance Curve After 100,000 Cycles	59
45	Homogeneous Data Set of Virkler, et al. with $P_{max} = 23.35$ kn and $R = 0.2$	60
46	Lognormal Statistical Model Prediction of Virkler, et al. Data Set	61
47	Distribution Function of Number of Cycles to Reach 21mm Half-Crack Length	62
48	Distribution Function of Number of Cycles to Reach 49.8mm Half-Crack Length	63
49	Crack Exceedance Curves at 150,000 Cycles	64
50	Actual Crack Propagation Time-Histories of Some WPB Fastener Holes	66
51	Typical Sample Function of Random Process $X(t)$	67
52	Autocorrelation Function of Random Process $Y(t)$	69
53	Regression Analysis for the Estimation of Model Parameters for WPB Fastener Holes	76
54	Theoretical Mean and Standard Deviation of Random Time to Reach Various Crack Sizes Computed for Different Δ Values for WPB Fastener Holes	77
55	Mean and Standard Deviation of Random Time to Reach Various Crack Sizes Computed Directly from Some Actual Time-Histories of WPB Fastener Holes	77
56	Simulated Sample Functions of Crack Propagation Time-Histories for WPB Fastener Holes	78
57	Comparison Between Weibull-Type Approximation for the Distributions of Random Time to Reach a Given Crack Size and Actual Test Results for WPB Fastener Holes	79

LIST OF ILLUSTRATIONS (Continued)

<i>Figure</i>		<i>Page</i>
58	Actual Crack Propagation Time-Histories of Some XWPB Fastener Holes	80
59	Regression Analysis for the Estimation of Model Parameters for XWPB Fastener Holes	80
60	Theoretical Mean and Standard Deviation of Random Time to Reach Various Crack Sizes Computed for Different Δ Values for XWPB Fastener Holes	81
61	Mean and Standard Deviation of Random Time to Reach Various Crack Sizes Computed Directly from Some Actual Time-Histories of XWPB Fastener Holes	81
62	Comparison Between Weibull-Type Approximation for the Distribution of Random Time to Reach a Given Crack Size and Actual Sample Distribution of XWPB Fastener Holes	82
63	Simulated Sample Functions of Crack Propagation Time-History for XWPB Fastener Holes	82

LIST OF TABLES

Table		Page
1	Verification Test Results for IN100	8
2	Parameter Values C_2 , C_3 and C_4 as Well as Standard Deviation σ_x	10
3	Maximum Likelihood Estimate of b , Q , Standard Deviation σ_y and Coefficient of Variation of da/dn	16
4	Assumed Homogeneous Test Environments for Test Specimens	19
5	Specimen Geometry and Maximum Load for Each Test Specimen of Ti 6-2-4-6	33
6	Specimen Geometry and Maximum Load for Each Test Specimen of Waspaloy	34
7	Maximum Likelihood Estimate of C_2 , C_3 , C_4 , Standard Deviation $\sigma_y = \sigma_x$ and Coefficient of Variation, V , of da/dn for Ti 6-2-4-6 (Hyperbolic Sine Function)	34
8	Maximum Likelihood Estimate of C_2 , C_3 , C_4 , Standard Deviation $\sigma_y = \sigma_x$ and Coefficient of Variation, V , of da/dn for Waspaloy (Hyperbolic Sine Function)	34
9	Parameters C_2 , C_3 , and C_4 for Each Test Specimen of Titanium With $C_1 = 0.7$, Hyperbolic Sine Crack Growth Rate Function	37
10	Parameters C_2 , C_3 , and C_4 for Each Test Specimen of Waspaloy With $C_1 = 0.5$, Hyperbolic Sine Crack Growth Rate Function	37
11	Assumed Homogeneous Test Environments for Each Test Condition for Waspaloy	38
12	Assumed Homogeneous Test Environments for Each Test Condition for Titanium	47
13	Maximum Likelihood Estimate of b , Log Q and Standard Deviation $\sigma_x = \sigma_y$ for Waspaloy (Paris Function)	50
14	Maximum Likelihood Estimate of b , Log Q and Standard Deviation $\sigma_x = \sigma_y$ for Titanium (Paris Function)	50
15	Parameters b and Log Q for Each Test Specimen of Waspaloy, (Paris Function)	50
16	Parameters b and Log Q for Each Test Specimen of Titanium (Paris Function)	51
17	Maximum Likelihood Estimate of C_2 , C_3 , C_4 , Standard Deviation $\sigma_y = \sigma_x$ and Coefficient of Variation, V , of da/dn ; $C_1 = 0.5$	61

SECTION I

INTRODUCTION

Engine components have traditionally been designed using a crack initiation criterion. This approach has been very successful from a safety standpoint, but the conservatism inherent in this method has resulted in poor utilization of the intrinsic life of the component. The development of high temperature fracture mechanics has permitted basing residual life analyses on a crack propagation criterion. Using this approach, lives from a specified defect size can be calculated and combined with periodic inspection to determine component retirement.

Propagation analyses classically employed in residual life predictions are deterministically based. They typically account for materials scatter by the incorporation of a safety factor. A more rigorous treatment of materials scatter is necessary to permit maximum utilization of component life.

The objective of this program was to develop a methodology capable of incorporating the scatter observed in crack growth data into component residual life analyses. Such a methodology is desired for use in damage-tolerant and retirement-for-cause (RFC) concepts. This objective included: identification of the distribution functions which best describe crack growth rate (da/dn) behavior; characterization of fatigue-crack propagation (FCP) controlling parameters as to their effects on crack growth rate variability; examination of the correlations between this variability and propagation life distributions; and development of a generic methodology applicable to all engine materials, although particular program emphasis was placed on IN100, Waspaloy, and Ti 6-2-4-6.

Two fracture mechanics-based statistical models for fatigue crack growth damage accumulation in engine materials were proposed and investigated (Reference 1). These models were based on hyperbolic sine crack growth rate functions developed by Pratt & Whitney Aircraft (Reference 2). Test results of IN100 (a superalloy used in the F100 engine) at various elevated temperatures, loading frequencies, stress ratios, etc., were compiled and analyzed statistically. The statistical distributions of (1) crack growth rate; (2) propagation life to reach any given crack size; and (3) crack size at any service life, were derived and reported. It was demonstrated that the correlation between the IN100 test results and the two statistical models was very good.

In this report, the lognormal statistical model (Reference 1) is extended to the case of spectrum loading. Test results for IN100 under block type loading are generated and used to evaluate the capability of this model for predicting the statistical distributions of (1) the life to reach any given crack size; and (2) the crack size at any given service life. A good correlation is shown between the model and the test results.

The lognormal statistical model is also applied to a power law (linear) crack growth rate function (i.e., Paris equation). Test results for IN100 under various conditions used to evaluate the hyperbolic sine function (Reference 1) are also used to evaluate the Paris function. This model is only applicable within a certain range of stress intensity and care should be exercised in its application. The Paris model proves to be mathematically simple for practical engineering applications.

Available fatigue crack growth rate data for Ti 6-2-4-6 and Waspaloy under various test conditions are also analyzed statistically. The lognormal statistical model, along with either the Paris or hyperbolic sine crack growth rate function, is shown to correlate well with the test results.

The lognormal model, using both the hyperbolic sine and the Paris equations, is applied to the homogeneous data set of Virkler, et al. (References 3 and 4). It is shown that the Paris relation does not provide a reasonable representation of this data set. Finally, a new statistical theory is proposed for the analysis of fatigue crack propagation. This theory is based on the concept of fracture mechanics and random processes. Examples are presented to demonstrate the application of the new theory using available test results.

SECTION II

FATIGUE CRACK GROWTH UNDER SPECTRUM LOADING CONDITIONS

Two statistical fracture mechanics-based models for predicting the fatigue crack propagation life of engine materials under any single test condition have been proposed and investigated in Reference 1. These models are based on the hyperbolic sine crack growth rate function developed by Pratt & Whitney Aircraft. It has been demonstrated that the correlations between the proposed statistical models and the test results are very good.

A single test condition is defined by a single constant value of each of the following parameters: temperature T , loading frequency ν , stress ratio R and maximum load P_{\max} . Service loading spectra to engine components, however, consist of variable histories of temperature T , frequency ν , loading magnitude R and P_{\max} , and holding time T_h . The objectives of this section are: (1) to extend a statistical model proposed in Reference 1 for any single test condition to be capable of predicting the fatigue crack propagation of engine materials under spectrum loadings, (2) to conduct experimental tests using IN100 compact tension specimens subject to loading spectra in order to generate statistically meaningful data, and (3) to correlate the test results with the proposed statistical model for verification purposes.

1. Theoretical Model

The lognormal crack growth rate model proposed in Reference 1 for a single test condition is expressed as

$$Y = C_1 \sinh[C_2(X + C_3)] + C_4 + Z \quad (1)$$

in which C_1 is a material constant, C_2 , C_3 and C_4 are functions of test conditions (T , ν , R) and

$$Y = \log \frac{da}{dn}, \quad X = \log \Delta K \quad (2)$$

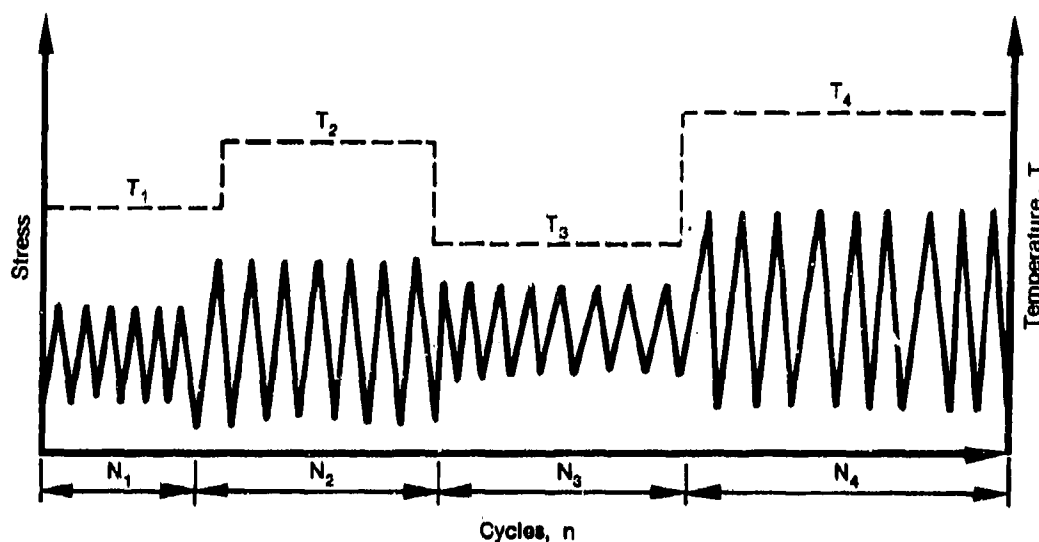
where ΔK is the stress intensity range. In Equation 1, Z is a normal random variable with zero mean and standard deviation σ_z that also depends on the test conditions (see Reference 1).

In order to extend the statistical model given by Equation 1 to account for the crack propagation under spectrum loadings, the composition of loading spectra will be described as follows: A loading spectrum is assumed to consist of repeated identical cycle blocks (or missions or duty cycles). Each cycle block (or duty cycle) is composed of m different segments (or m test conditions). Each segment or test condition is defined by constant values of temperature T , loading frequency ν , stress ratio R , maximum load P_{\max} and numbers of load cycles n . Therefore, the j th segment in one cycle block (or duty cycle) can be denoted by $(T_j, \nu_j, R_j, P_{j\max}, n_j)$ whereas one cycle block consists of $(T_j, \nu_j, R_j, P_{j\max}, n_j)$ for $j=1,2,\dots,m$, as schematically shown in Figure 1.

For the j th test condition, or segment, in one cycle block, it follows from Equation 1 that

$$Y_j = C_1 \sinh[C_2(X + C_{3j})] + C_4 + Z_j \quad ; \quad j=1,2,\dots,m \quad (3)$$

in which Z_j is a normal random variable with zero mean and standard deviation σ_{zj} . Values of C_2 , C_{3j} , C_4 and σ_{zj} for different test conditions are given in Reference 1.



FD 260798

Figure 1. Representation of One Cycle Block

Since Z_j is a statistical variable, a specimen having a faster crack growth rate will preserve it over the entire crack propagation life in the j th test condition, and the variability of Z_j is exclusively contributed by the material variability (loading is deterministic) as described in Reference 1. Hence, under spectrum loadings Z_j for $j=1,2,3,\dots,m$ are completely correlated not only in one cycle block but also over the entire crack propagation life. Consequently, Equation 5 can be integrated segment-by-segment not only in one cycle block but also over the entire propagation life to obtain the crack length $a(n)$ as a function of the number of load cycles, n (or cycle blocks).

For simplicity, the crack propagation in the first cycle block is illustrated by the following. Let $z_{j\gamma}$ be the γ percentile of the normal random variable Z_j associated with the j th segment.

$$\gamma\% = P[Z_j > z_{j\gamma}] = 1 - \Phi(z_{j\gamma}/\sigma_{z_j}) \quad (4)$$

in which $\Phi(\cdot)$ is the standardized normal distribution function and σ_{z_j} is the standard deviation of Z_j . The determination of σ_{z_j} was described in Reference 1.

The γ percentile, $z_{j\gamma}$, of Z_j can be obtained from Equation 4 as

$$z_{j\gamma} = \sigma_{z_j} \Phi^{-1}(1 - \gamma\%) \quad \text{for } j=1,2,\dots,m \quad (5)$$

where $\Phi^{-1}(\cdot)$ is the inverse standardized normal distribution function.

The γ percentile of the crack growth rate for the j th segment, denoted by $Y_{j\gamma}$, follows from Equation 3 as

$$Y_{j\gamma} = C_1 \sinh [C_{2j}(X + C_{3j})] + C_{4j} + z_{j\gamma} \quad \text{for } j=1,2,\dots,m \quad (6)$$

Then, Equation 6 can be integrated segment-by-segment to yield the γ percentile of the crack length $a_\gamma(n)$ versus the number of load cycles n as follows:

$$\begin{aligned} a_\gamma(n_1) &= a_0 + \sum_{k=1}^{n_1} \Delta a_{1,k} \\ a_\gamma(n_1 + n_2) &= a_\gamma(n_1) + \sum_{k=1}^{n_2} \Delta a_{2,k} \\ a_\gamma\left(\sum_{j=1}^m n_j\right) &= a_\gamma\left(\sum_{j=1}^{m-1} n_j\right) + \sum_{k=1}^{n_m} \Delta a_{m,k} \end{aligned} \quad (7)$$

in which a_0 is the initial crack size, $a_\gamma(n_1)$ is the γ percentile crack length after the first segment that consists of n_1 load cycles, and $\Delta a_{1,k}$ is the increment of the crack length during the k th load cycle in the first segment which is computed numerically using Equation 6 for $j=1$ as follows:

$$Y_{1\gamma} = C_1 \sinh [C_{21}(X + C_{31})] + C_{41} + z_{1\gamma} \quad (8)$$

In Equation 8, $z_{1\gamma}$ is determined from Equation 5 with $j=1$. Other notations appearing in Equation 7 are self-explanatory for segment by segment numerical integrations.

Repeating numerical integrations similar to Equation 7 and using appropriate initial crack lengths for each segment and cycle block, we obtain one γ percentile for the crack length, $a_\gamma(n)$, as a function of load cycles n . Furthermore, by varying values of γ , we obtain the distribution of the crack length as a function of load cycles as shown in Figure 2. It should be noted that the numerical integration to generate a set of $a_\gamma(n)$ is deterministic, straightforward, and very simple.

The approach described above recognizes the difference of the statistical dispersion of the crack growth rate, da/dn , for each segment (or test condition). However, since the spectrum loading is idealized by repeated identical cycle blocks, it may be reasonable to average the statistical dispersion of the crack growth rate for each segment over one cycle block and to approximate the statistical dispersion of the crack growth rate for one cycle block by such an average value. Such an approximate approach is described in the following:

The coefficient of variation of the crack growth rate V_j in the j th segment is related to σ_{aj} through

$$V_j = [e^{(\sigma_{aj}/a_{10})^2} - 1]^{1/2} \quad (9)$$

Then, the coefficient of variation, V , of the crack growth rate for one cycle block is approximated by the weighted average of V_j associated with all segments in one cycle block, i.e.,

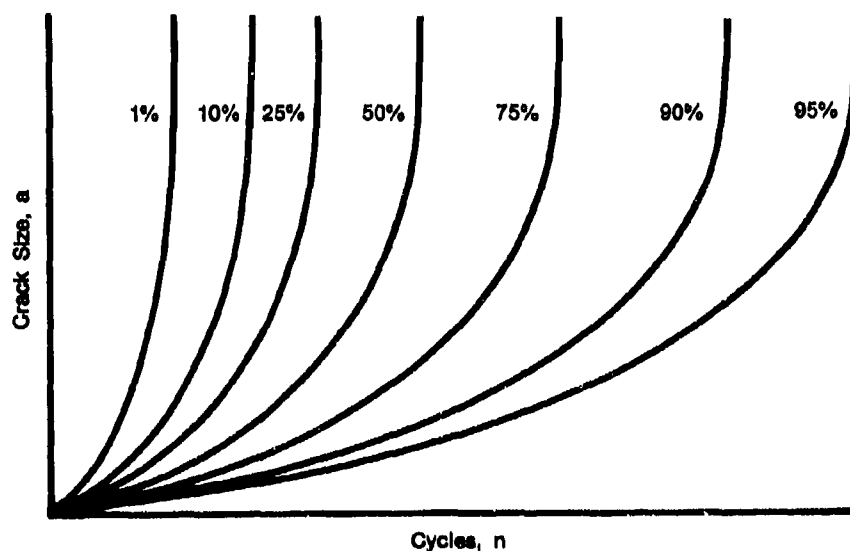
$$V = \sum_{j=1}^m V_j n_j / \sum_{j=1}^m n_j \quad (10)$$

and Equation 3 is approximated by

$$Y_j = C_1 \sinh [C_2(X + C_3)] + C_4 + Z \quad (11)$$

in which Z is a normal random variable with zero mean and standard deviation σ_z which is related to V (Equation 10) through

$$\sigma_z = \sqrt{\ln(1 + V^2) / \ln 10} \quad (12)$$



FD 235894

Figure 2. γ Percentiles of Crack Length Versus Number of Cycles

Therefore, the statistical dispersion of the crack growth rate over the entire loading spectrum is characterized, in approximation, by the random variable Z .

Applying the same procedures described previously, with all Z_j ($j=1,2,\dots,m$) being replaced by Z , one can obtain the distribution of the crack length as a function of load cycles shown in Figure 2.

To account for the scatter of crack propagation life in the prediction of engine components, two distributions are of practical importance: (1) the distribution $F_{N(a_1)}(n)$ of the propagation life $N(a_1)$ to reach any given crack length a_1 (including the critical crack length), and (2) the distribution, $F_{a(n)}(x)$, of the crack length $a(n)$ after any specific number, n , of load cycles. In fact, the distribution of the crack length as a function of load cycles shown in Figure 2 contains all the information mentioned above. For instance, by drawing a horizontal line through any specific crack length a_1 in Figure 2, one obtains the distribution, $F_{N(a_1)}(n)$, of the number of load cycles to reach that crack length. Likewise, the distribution, $F_{a(n)}(x)$, of the crack length $a(n)$ after a given number, n , of load cycles can be obtained by drawing a vertical line through n in Figure 2.

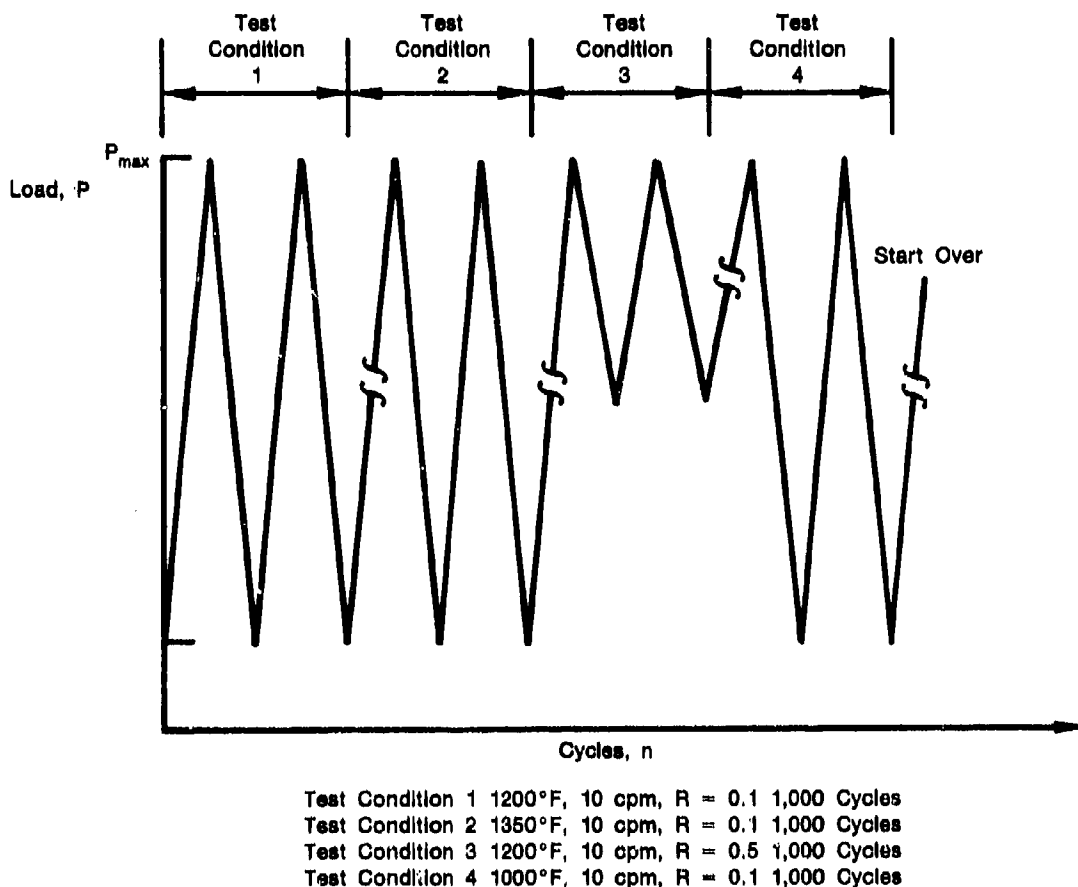
A computer program based on the above theoretical model (Equations 6-8) has been established to predict the crack growth damage accumulation for any given loading spectrum.

No attempt was made in this program to account for retardation or acceleration effects, although the statistical model developed can be modified to take these effects into account.

2. Experimental Program

An experimental test program has been carried out in order to verify the capability of the proposed statistical model in predicting the crack propagation behavior of engine materials under spectrum loading. The specimens used were ASTM compact tension specimens with a thickness (B) of 0.5 inches (12.7 mm) and width (W) of 2.5 inches (63.5 mm). The initial flaw size (a_0) is 0.5 inches (12.7 mm) and the final flaw size (a_f) is 2.0 inch (50.8 mm).

The spectrum loading employed was composed of repeated block loading (or cycle block) consisting of four test conditions (segments) as shown in Figure 3. Each segment was applied for 1,000 cycles with the next test condition in succession. The entire block was repeated after test condition number 4. This procedure was continued until specimen fracture occurred.



FD 247364

Figure 3. Laboratory Spectrum Test Loading Conditions for IN100

In one block loading, the maximum load, P_{max} , for each segment was fixed at 2.4 kips (10.7 kn) with all positive stress ratios, R , in order to eliminate the need for consideration of retardation or acceleration effects due to overloads or underloads. The results of twelve tests are summarized in Table 1, and displayed in Figure 4. A complete listing of these tests is shown in the Appendix. The three solid curves shown in Figure 4 are the theoretical predictions that will be described later.

TABLE 1. VERIFICATION TEST RESULTS FOR IN100

	Specimen No.	Final Crack Length a_f	Cycles to Failure N	Cycles at 1.4 inches
1.	2396	1.74	100,000	97,600
2.	2397	1.68	85,000	82,000
3.	2398	1.68	88,000	85,800
4.	2399	1.43	73,000	72,800
5.	2400	1.84	70,000	68,500
6.	2401	1.48	97,000	96,500
7.	2402	1.63	85,000	82,000
8.	2403	1.63	75,000	73,300
9.	2404	1.59	115,000	113,600
10.	2405	1.41	81,000	81,000
11.	2406	1.53	81,000	80,000
12.	2407	1.45	85,000	84,500
Failure: Mean Life (N) = 82,900				
Standard Deviation = 14,800				
Mean Life at 1.4 in. = 81,500				
Standard Deviation = 15,000				

For theoretical predictions the parameter values C_{2j} , C_{3j} and C_{4j} , as well as the standard deviation σ_{Z_j} of Z_j under each test condition (or segment) in one block loading, Figure 3, have been estimated using the method of maximum likelihood in Reference 1. The results are shown in Table 2 along with the total number of test specimens used. The parameter C_1 is a material constant which is equal to 0.5 for IN100. Note that the parameter values presented in Table 2 were estimated using compiled IN100 crack growth rate data, which were generated over a long period of time for different purposes (Reference 1). The total number of test specimens under each test condition is very small. Even with such a small sample size, the specimen dimensions, the initial and final flaw sizes, and the maximum cyclic load for each test specimen are all different. Thus, the data base used for estimating the parameter values is highly nonhomogeneous; however, it is representative of the expected data base found in industry (see Reference 1).

Using the statistical model described in the previous section, Equation 7, and Table 1, we construct various γ percentiles for the crack size, $a_\gamma(n)$, as a function of the number of load cycles n . The results are shown in Figure 5 as solid curves and the numerical values are presented in the Appendix. For instance, the curve associated with $\gamma=10$ indicates that the probability is 10% that a specimen will have a crack size growing faster than that denoted by the curve. These solid curves are the predicted distribution of crack growth damage accumulation based on the statistical model. The crack propagation associated with $\gamma=5$, 50 and 95 percentiles are also shown in Figure 4 as solid curves for the purpose of comparison with test results.

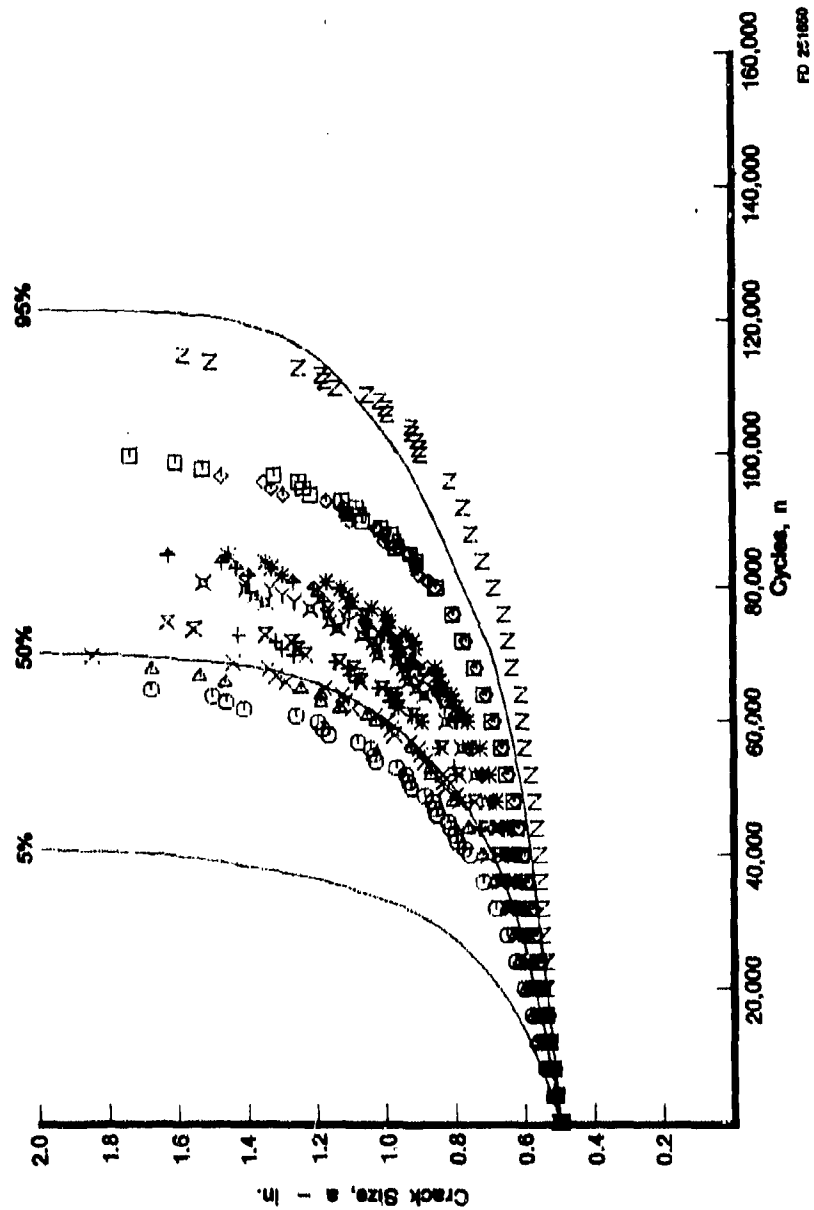


Figure 4. Verification Test Results for IN100

TABLE 2. PARAMETER VALUES C_2 , C_3 AND C_4 AS WELL AS STANDARD DEVIATION σ_s

Segment	Test Condition	C_2	C_3	C_4	σ_s	Number of Specimens
1	5	3.8982	-1.5376	-3.9341	0.1028	9
2	2	4.9323	-1.4073	-3.9895	0.1692	4
3	3	4.3098	-1.3032	-4.4450	0.1240	4
4	1	3.8033	-1.5239	-4.3563	0.1673	5

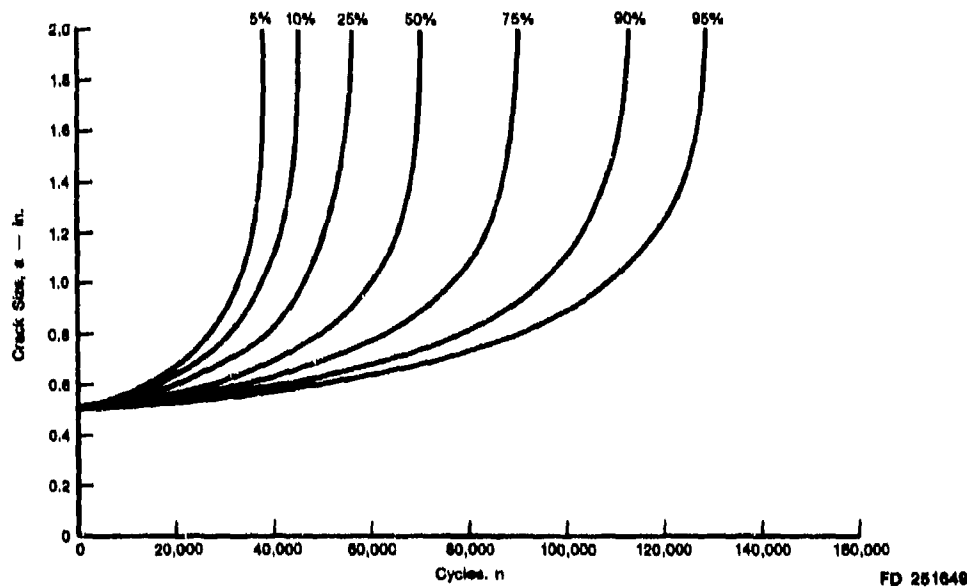
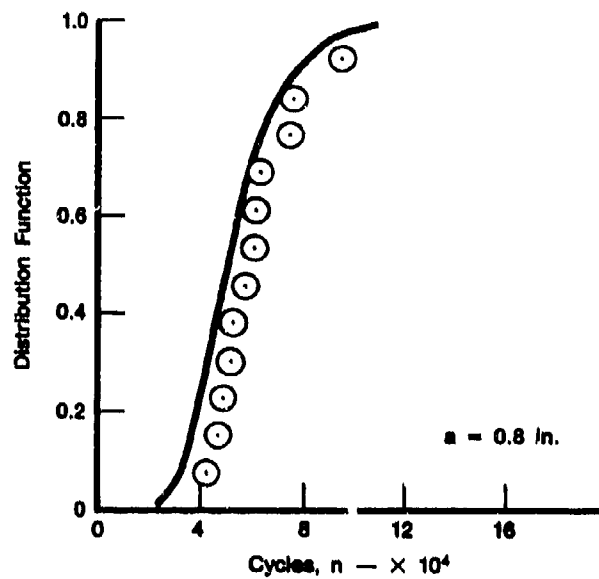


Figure 5. Predicted Crack Size Versus Cycles Behavior Under Spectrum Loading

3. Correlation Between Statistical Model and Experimental Test Results

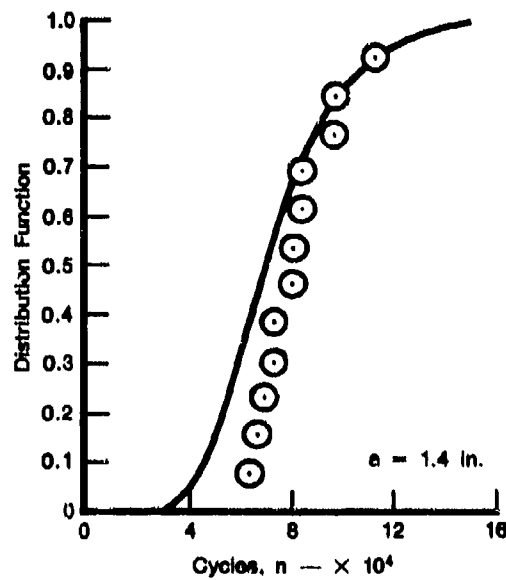
As observed from Figure 4, the statistical model predicts faster *average* crack growth damage accumulation and slightly *larger* statistical dispersion. Thus, from the analysis and design standpoint, the statistical model is conservative. The correlation between the test results and theoretical prediction appears to be very reasonable.

The theoretical predictions for the statistical distribution of the number of load cycles to reach crack sizes 0.8 and 1.4 inches (20.3 and 35.6 mm) are presented as solid curves in Figures 6 and 7, respectively. Also plotted in these figures as circles are the experimental test results for twelve specimens. Furthermore, predictions for the probability of crack exceedance, which is equal to one minus the distribution function of the crack size, at 24,000, and 35,000 load cycles are displayed in Figures 8 and 9 as solid curves, respectively. Also shown in these figures as circles are the corresponding experimental test results. Again, Figures 6 to 9 indicate that the statistical model is slightly conservative, in the sense that the model predicts shorter crack propagation life and larger statistical dispersion. The correlation between the theoretical model and the test results is very reasonable.



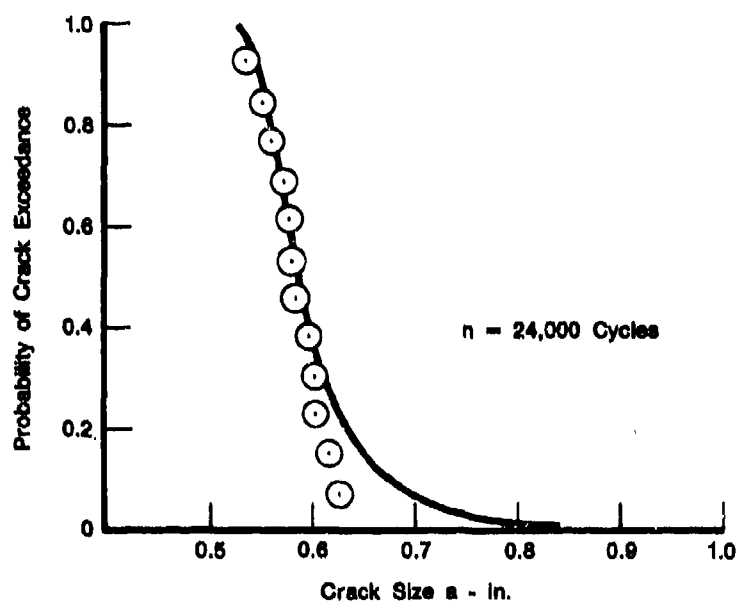
FD 265064

Figure 6. Distribution of Cycles to Reach 0.8 Inch, for the IN100 Mission Verification Test



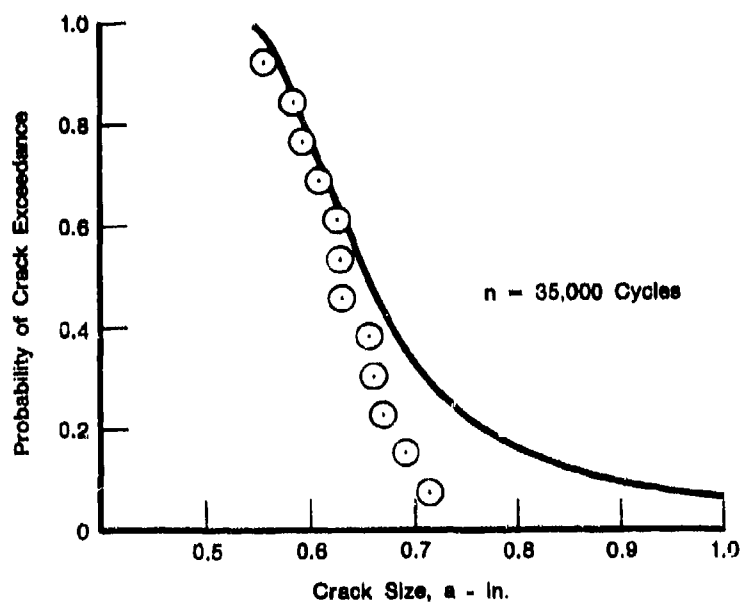
FD 265065

Figure 7. Distribution of Cycles to Reach 1.4 Inches for the IN100 Mission Verification Test



FD 265066

Figure 8. Probability of Crack Exceedance at 24,000 Cycles for IN100 Mission Verification Testing



FD 265067

Figure 9. Probability of Crack Exceedance at 35,000 Cycles for IN100 Mission Verification Testing

Since the initial crack size is deterministic, which is equal to 0.5 inch (12.7 mm), the deviation between the theoretical predictions and the test results is expected to increase as the number of load cycles increases. This is clearly demonstrated by the crack exceedance curves shown in Figures 8 and 9. Furthermore, the statistical dispersion of the crack size increases with respect to the number of load cycles as exemplified by these figures. Hence, the maximum discrepancy occurs when the random number of load cycles reaches a 1.4 inch (35.6 mm) crack, that is very close to the critical crack size (see Figure 4). It is observed from Figure 7 that the discrepancy in predicting the average number of load cycles to reach a 1.4 inch (35.6 mm) crack is approximately 13%.

Some of this conservatism may be due to retardation at the crack tip caused by the change in yield stress as a function of temperature. The size of the plastic zone is inversely proportional to the square of the yield stress. At the 1350°F test condition, the lower yield stress will cause a larger plastic zone which will retard the crack when the temperature is decreased to 1200°F. This will also occur from the 1200°F to the 1000°F temperature change. The initial retardation of the crack growth rate in each test condition would result in a longer test life than the predicted life, as the computer program (theoretical model) does not address retardation effects.

From the statistical standpoint, the main reason for a slight discrepancy comes from the compiled data base as described in the following.

The theoretical prediction is computed based on the parameter values C_2 , C_3 , C_4 , and σ_{ij} for $j = 1, 2, 3, 4$. These parameter values were estimated using a compiled data set for each test condition which was generated over a long period of time for different purposes. As a result, the specimen preparations, heat treatments and processes of materials, test machines, measurements and environments, etc. will not be identical to those specimens tested under the present program. The number of test specimens compiled for the data base for each test condition is also very small (see Table 1). Likewise, the data base is highly inhomogeneous, indicating that the specimen dimension, initial and final flaw sizes, and the maximum applied load are all different for each test specimen. Consequently, it may be reasonable to expect some inconsistencies between the highly inhomogeneous data base, from which the theoretical model parameters are calibrated, and the homogeneous test results generated in the present program. Nevertheless, the worst discrepancy is only 13% on the conservative side, which is quite reasonable in practice.

In practical situations, however, the data base is usually not plentiful, highly nonhomogeneous, and compiled over a long period of time under different test environments. Nevertheless, such a homogeneous and limited data base can be used to calibrate the model parameters, and the present statistical model is capable of predicting the crack propagation behavior under spectrum loading.

One important aspect of the fracture mechanics approach is that available crack growth rate data from inhomogeneous data bases can be pooled together to estimate the crack growth rate parameters, although the type of specimen, the specimen dimension, initial and final flaw lengths, and the maximum cyclic load for each test specimen may be different in the data base. In contrast to other statistical models (e.g., References 14, 15, 18-21), the statistical model proposed herein is based on fracture mechanics, thus it possesses the same important advantage pertinent to the fracture mechanics approach.

Finally, the present statistical model does not address the retardation or acceleration effects. Further research is needed in this regard in order to provide a better prediction capability necessary for retirement-for-cause analysis of engine components under service loading spectra.

SECTION III

LOGNORMAL STATISTICAL MODEL APPLIED TO THE PARIS EQUATION FOR IN100

The lognormal crack growth rate model has been applied to data for IN100 at various test conditions using the hyperbolic sine (SINH) function (Reference 1). In this section, the lognormal model is developed for the Paris crack growth rate function. Emphasis is on the simplicity of this model for practical application. The distributions of propagation life to reach any specific crack size and the distribution of crack size at any service life are derived. The correlation between the extrapolated test results for IN100 and the statistical model is shown to be reasonable.

The Paris crack growth rate equation is given by

$$\frac{da}{dn} = Q[\Delta K]^b \quad (13)$$

in which a = crack size after n load cycles, ΔK = stress intensity range, Q and b are functions of temperature T , loading frequency ν , stress ratio R and others.

To account for the statistical variability of the crack growth rate $da(n)/dn$, the deterministic crack growth rate function (Equation 13) is randomized as follows

$$\frac{da}{dn} = X(\Delta K)Q[\Delta K]^b \quad (14)$$

in which $X(\Delta K)$ is a non-negative random function taking values around unity, and introduced to reflect the statistical nature of the crack growth rate.

Taking the logarithm on both sides of Equation 14, one obtains

$$Y = bU + q + Z(\Delta K) \quad (15)$$

in which

$$Y = \log \frac{da}{dn}, \quad U = \log \Delta K \quad (16)$$

$$q = \log Q, \quad Z(\Delta K) = \log X(\Delta K)$$

Whereas $X(\Delta K)$ is a random function, the solution for the statistical distribution of the crack growth damage accumulation is rather complicated (e.g., Reference 5). In this connection, two extreme cases of the random function $X(\Delta K)$ should be mentioned. At one extreme, $X(\Delta K)$ is completely independent at any two values of the stress intensity range, referred to as the white noise process. Based on the central limit theorem, it can be shown that the statistical variability of the crack size or the fatigue life, after integrating Equation 14, is the smallest within the class of random functions. Hence, it is unconservative for engineering analyses and applications. Also, the mathematical solution for the white noise random process model is difficult. At another extreme, the random function $X(\Delta K)$ is totally correlated at any two values of the stress intensity range, indicating that $X(\Delta K)$ is a random variable, i.e., $X(\Delta K) = X$. For the case of random variable X , the statistical dispersion of the fatigue crack growth damage

accumulation is the largest in the class of random functions. Consequently, the random variable model is conservative for the prediction of the crack propagation life and for practical applications.

Because of mathematical simplicity in analysis and the conservative nature in crack propagation prediction, we shall investigate the random variable model, i.e., $X(\Delta K) = X$ is a positive random variable taking values around unity. It is assumed that X follows the lognormal distribution with a median equal to unity. Tests for goodness of fit for the lognormal distribution will be performed later.

It follows from Equation 16 that $Z = \log X$ is a normal random variable with zero mean. By virtue of Equation 15 the log crack growth rate, $Y = \log(da/dn)$, is a normal random variable with mean value μ_y and standard deviation σ_y given by

$$\mu_y = bU + q \quad (17)$$

$$\sigma_y = \sigma_z \quad (18)$$

in which it is obvious that the mean value μ_y is a function of ΔK , and the standard deviation σ_y is a constant.

The parameters b and q (or Q), as well as the standard deviation σ_z (or σ_y), given in Equations 15 through 18 can be estimated from the test results of the crack growth rate versus the stress intensity range using Equation 15 and the method of maximum likelihood estimate. Since Y and Z are normal random variables and Equation 3 is linear, the method of maximum likelihood is identical to the linear regression analysis and the method of least squares.

Test results from compact tension specimens, for log crack growth rate $Y = \log(da/dn)$ versus the log stress intensity range $U = \log \Delta K$ are presented in Figure 10 as discrete points for five IN100 specimens in the test condition No. 1 ($T = 1000^\circ\text{F}$, $\nu = 10$ cpm, $R = 0.1$). The crack growth rate data shown in Figure 8 have been used to estimate b , Q and σ_y using the method of maximum likelihood. The results are presented in the first row of Table 3 and plotted in Figure 10 as a solid straight line for $\sigma_y = 0$. The maximum likelihood estimates of b , Q and σ_y , determined from the test results of Y versus U using ASTM CT specimens, are shown in Table 3 for different test conditions (ν, R, T).

The power law for the crack growth rate (Equation 14) holds only in the central region of ΔK . In the regions where ΔK is either too low or too high, the crack growth rate appears to behave asymptotically. Hence several data points for the crack growth rate have already been censored in Figure 10. Also, the crack growth rate data seem to scatter around the solid straight line indicating the validity of the Paris function.

To show the validity of the assumption that Z follows the normal distribution, sample values of Z , denoted by z_j , are computed from test results of the log crack growth rate $Y = \log da/dn$ versus log stress intensity range $U = \log \Delta K$, denoted by (y_j, u_j) , using Equation 15

$$z_j = y_j - bu_j - q \quad \text{for } j=1, 2, \dots, n \quad (19)$$

in which b and q have been estimated by the method of maximum likelihood and n is the total number of test data.

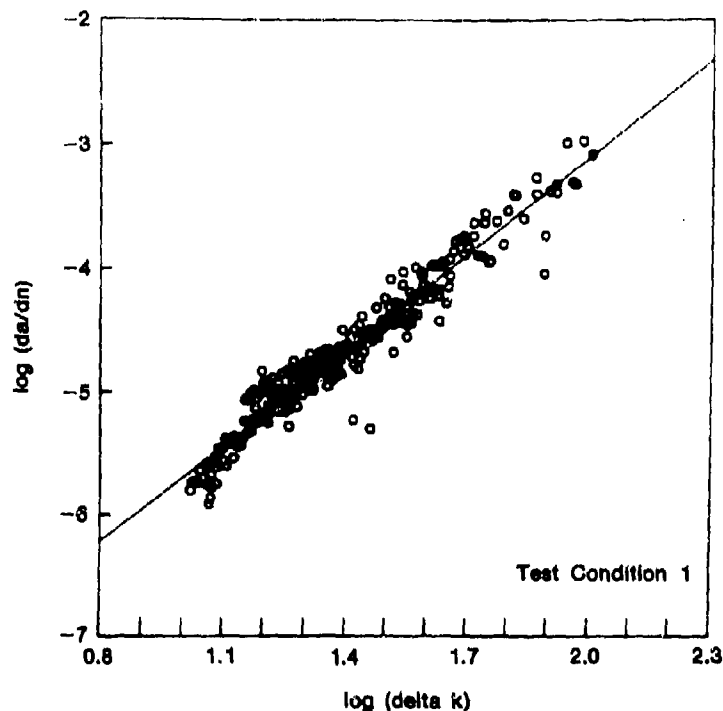


Figure 10. Data for Crack Growth Rate Versus Stress Intensity Range for Test Condition No. 1

TABLE 3. MAXIMUM LIKELIHOOD ESTIMATE OF b , Q , STANDARD DEVIATION σ_y AND COEFFICIENT OF VARIATION OF da/dn

Test Condition*	b	Q	$\sigma_y = \sigma_z$	Coef. of Variation	No. of Data
1	2.0617	5.016×10^{-9}	0.1515	36.0%	251
2	2.9216	7.409×10^{-9}	0.1455	34.3%	147
3	2.8439	7.141×10^{-9}	0.1038	24.3%	129
4	2.3850	1.870×10^{-8}	0.1961	45.2%	185
5	2.3180	3.141×10^{-8}	0.1131	26.5%	338
Average				33.3%	

*Test Conditions

1. $T = 1000^\circ\text{F}$, $\nu = 10$ cpm, $R = 0.1$
2. $T = 1350^\circ\text{F}$, $\nu = 10$ cpm, $R = 0.1$
3. $T = 1200^\circ\text{F}$, $\nu = 10$ cpm, $R = 0.5$
4. $T = 1200^\circ\text{F}$, $\nu = 20$ cpm, $R = 0.05$
5. $T = 1200^\circ\text{F}$, $\nu = 10$ cpm, $R = 0.1$

Sample data of Z ($j=1, 2, \dots, n$) for test condition No. 3 are plotted on normal probability paper in Figure 11 as circles along with a straight line representing the estimated normal distribution for Z (with zero mean and standard deviation σ_z determined previously, see Table 3). A linear scale is used in Figure 11 in which the sample data z_j are arranged in an ascending order, i.e., $z_1 \leq z_2 \leq z_3 \leq \dots \leq z_n$, and the ordinate corresponding to z_j is given by $\Phi^{-1}[j/(n+1)]$ with

$\Phi^{-1}(\cdot)$ being the inversed standardized normal distribution function. It is observed from Figure 11 that the sample values of Z are scattered around the straight line without a nonlinear trend, indicating that the normal distribution is acceptable.

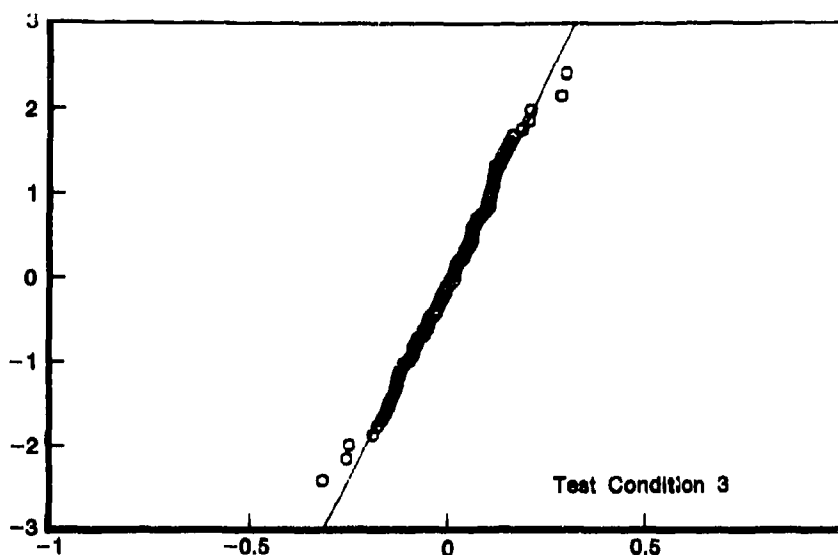


Figure 11. Normal Probability Plot for Z (Test Condition No. 3)

The Kolmogorov-Smirnov test for goodness of fit was performed to determine the observed K-S statistic D_n . The normal distribution was found to be acceptable at least at a 10% level of significance.

Since $Z = \log X$ and $Y = \log da/dn$ are normal random variables, the crack growth rate $G = da/dn$ follows the lognormal distribution. The coefficient of variation, V , of da/dn is related to the standard deviation, $\sigma_y = \sigma_x$, through

$$V = [e^{(\sigma_x \sqrt{n} 10)^2} - 1]^{1/2} \quad (20)$$

The coefficients of variation, V , for the crack growth rate, $G = da/dn$, for five test conditions are also presented in Table 3.

The distribution of Z , and $Y = \log[da/dn]$, are both normal with the same standard deviation, $\sigma_x = \sigma_y$, that has been determined previously. Let z_γ be the γ percentile of Z , i.e.,

$$\gamma \% = P[Z > z_\gamma] = 1 - \Phi(z_\gamma / \sigma_x) \quad (21)$$

or inversely,

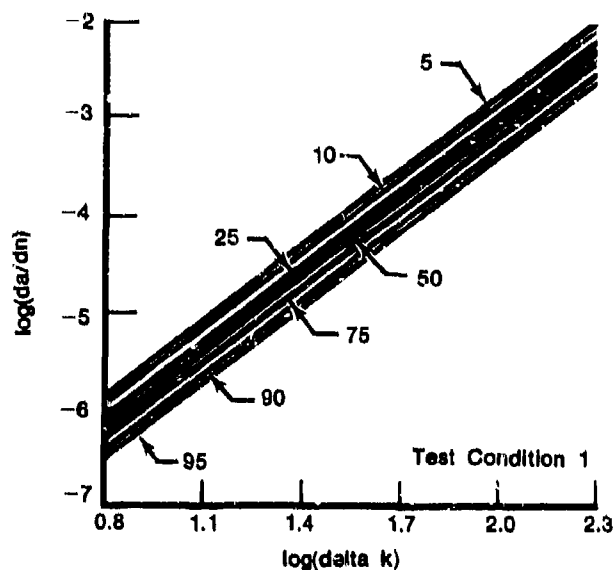
$$z_\gamma = \sigma_x \Phi^{-1}(1 - \gamma \%) \quad (22)$$

The γ percentile of the log crack growth rate Y , denoted by $y_\gamma(\Delta K, b, q)$, follows from Equation 3 as

$$y_\gamma(\Delta K, b, q) = bU + q + z_\gamma \quad (23)$$

in which z_γ is given by Equation 22. Note that $y_\gamma(\Delta K, b, q)$ is a function of b and q which in turn depend on test conditions (ν , R , and T).

Therefore, by varying the value of γ , one obtains the distribution of the log crack growth rate in terms of percentiles. The results are shown in Figure 12 for test condition No. 1 ($\nu = 10$ cpm, $R = 0.1$ and $T = 1000^\circ\text{F}$). As an example, the crack growth rate path associated with $\gamma = 10$ indicates that the probability is 10% that a specimen will have a growth rate faster than that shown by the curve.



FD 255034

Figure 12. Percentiles of Log Crack Growth Rate as a Function of Log Stress Intensity Range for Test Condition No. 1

The γ percentile of the random variable X , denoted by X_γ , is computed from Equation 4 as

$$X_\gamma = (10)^{z_\gamma} \quad (24)$$

in which z_γ is given by Equation 10.

The γ percentile of the crack size after n load cycles, denoted by a_γ , is obtained by substituting Equation 24 into Equation 4

$$\frac{da_\gamma}{dn} = X_\gamma Q(\Delta K_\gamma)^b \quad (25)$$

in which the stress intensity range ΔK_γ for the ASTM CT specimen is expressed as

$$\Delta K_\gamma = \frac{\Delta P}{B \sqrt{W}} f[a_\gamma] \quad (26)$$

where B = specimen thickness, W = specimen width, ΔP = applied load range and

$$f[a_\gamma] = \frac{2 + \alpha}{(1 - \alpha)^{3/2}} (0.866 + 4.64\alpha - 13.32\alpha^2 + 14.72\alpha^3 - 5.6\alpha^4) \quad (27)$$

$$\alpha = \frac{a_\gamma}{W} \quad (28)$$

Thus, Equation 25 can be integrated numerically over particular limits to obtain a set of crack lengths, $a_\gamma(n)$, versus the number of load cycles, n , for different γ percentiles. It should be mentioned that the numerical integration using Equation 25 for each γ percentile of the crack length, $a_\gamma(n)$, is deterministic and straightforward.

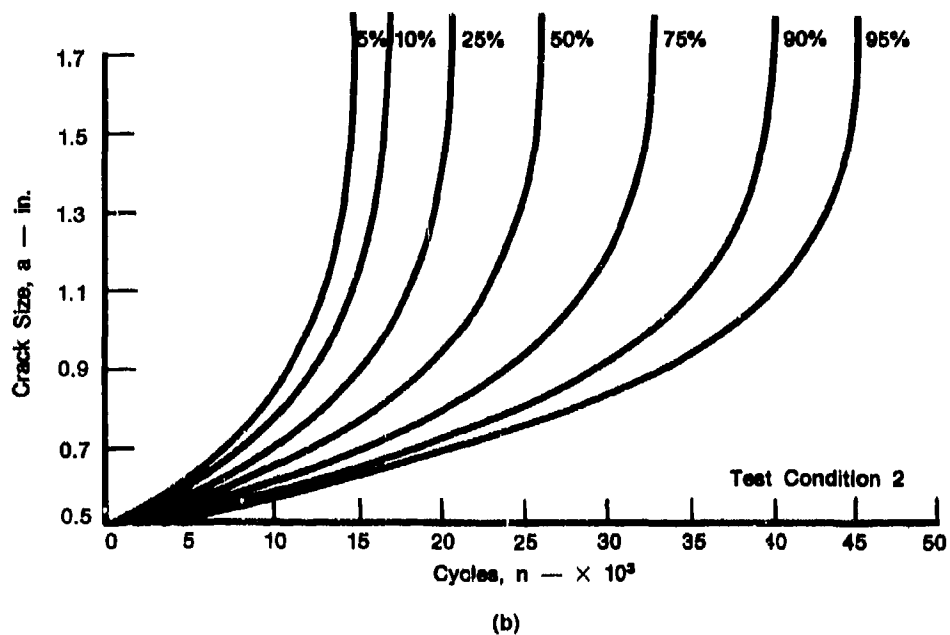
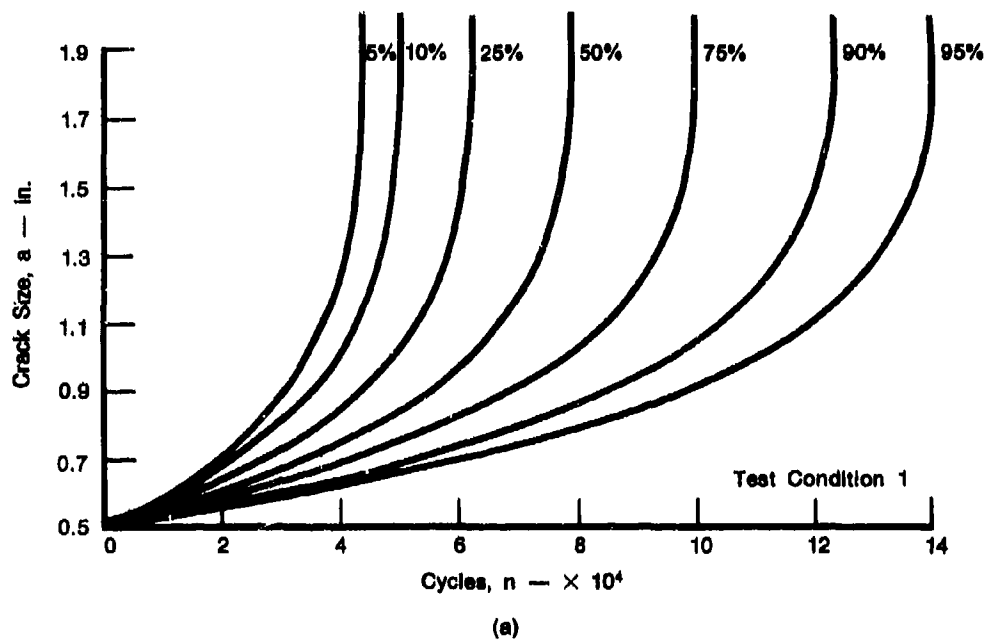
Test environments, including the initial crack size a_0 , the final crack size a_f , the maximum load P_{max} , and the width W and thickness B of the ASTM CT specimen, are assumed for each test condition as shown in Table 4. The necessity to assume homogeneous test environments in Table 4 for the correlation study has been described previously (Reference 1). Integrating Equation 25 and using Tables 3 and 4, one obtains five sets of crack length, a_γ , as a function of the number of load cycles, n , for different γ percentiles. Only the results for test conditions No. 1 and No. 2 are displayed in Figure 13.

TABLE 4. ASSUMED HOMOGENEOUS TEST ENVIRONMENTS FOR TEST SPECIMENS

Test Condition	a_0 (in.)	a_f (in.)	W (in.)	B (in.)	P_{max} (kips)
1	0.5	2.0	2.502	0.250	1.400
2	0.5	2.0	2.503	0.501	2.600
3	0.5	1.8	2.000	0.500	2.600
4	0.5	2.0	2.506	0.500	3.000
5	0.5	2.0	2.497	0.501	3.533

a_0 = initial crack size
 a_f = final crack size
 W = specimen width
 B = specimen thickness
 P_{max} = maximum load

In the life prediction of engine components, two statistical distributions are of practical importance; (1) the distribution function, $F_{N(a_1)}$, of the number of cycles, $N(a_1)$, to reach any given crack length, a_1 and (2) the distribution function, $F_a(x)$, of the crack length a after any number of load cycles n . Since Figure 13 represents the distribution of the crack length as a function load cycles n , it contains all the information needed to determine the distributions mentioned above. For instance, by drawing a horizontal line in Figure 13 through a crack length of interest, the distribution for the number of cycles to reach that crack length is obtained. Likewise drawing a vertical line in Figure 13 through a given load cycle n , one obtains the distribution of the crack length after n load cycles. The complement, $F'_a(x)$, of the distribution function, $F_a(x)$, of the crack length, i.e., $F'_a(x) = 1 - F_a(x)$, is the probability that the crack length after n cycles will exceed a certain value x . Hence, the plot of $F'_a(x)$ is referred to as the crack exceedance curve.



FD 255035

Figure 13. Distribution of Crack Size as Function of Load Cycles Based on Statistical Model; (a) Test Condition No. 1, (b) Test Condition No. 2

For instance, the distribution function, $F_{N(a_i)}$, for the number of load cycles to reach the crack lengths $a_1 = 1.0$ and 2.0 inches is obtained from Figure 13 and displayed in Figure 14 as a solid curve for test condition No. 1. For the same condition, the crack exceedance curve $F'_n(x)$ after $n = 25,000$ cycles is shown in Figure 15 as a solid curve.

In a similar manner, the distribution functions for the number of load cycles to reach certain crack sizes and the exceedance curves after certain number of load cycles for test conditions No. 2 to No. 5 are presented in Figures 16 through 23 as solid curves. Note that the solid curves depicted in Figures 14 through 23 are obtained based on the statistical model that utilizes only the crack growth rate data, e.g., Figure 10, for estimating the model parameters b , Q and $\sigma_y = \sigma_x$ as shown in Table 3.

1. Correlation with IN100 Test Results

A qualitative correlation study of the IN100 results is carried out in the following manner.

Test results of the crack growth rate for each specimen are best fitted by the hyperbolic sine crack growth rate function proposed by Pratt & Whitney Aircraft (Reference 2).

$$Y = C_1 \sinh [C_2(U + C_3)] + C_4 \quad (29)$$

in which Y and U are given in Equation 16, C_1 is a material constant, and C_2 , C_3 and C_4 are constants depending on the test condition (ν , R , T). Equation 29 involving four parameters is supposed to provide a better fit to the crack growth rate data.

Given the crack growth rate data, the least squares best fit procedures to estimate values of C_2 , C_3 and C_4 for each specimen were described in Reference 2 and the results of C_2 , C_3 and C_4 for each specimen in five test conditions were presented in Reference 1. Then, Equations 29 and 16 can be integrated to yield the crack size, a , as a function of load cycles, n . It has been shown that the crack growth damage accumulation a thus reproduced by integrating Equations 29 and 16 correlates very well with the test results for each specimen (Reference 1).

In order to correlate the nonhomogeneous test results with the predictions based on the statistical model proposed previously, homogeneous test environments have been assumed for each test condition, as shown in Table 4. The maximum loads P_{max} given in Table 4 are chosen in order to avoid excessive extrapolation far into the region of ΔK in which actual test results do not exist.

By integrating Equations 16 and 29 over the homogeneous test environments, with appropriate values of C_1 , C_2 , C_3 and C_4 for each specimen (see Reference 1), one obtains five sets of the homogeneous crack size, a , as a function of load cycles n . These homogeneous data sets are referred to as the extrapolated test results, since they are not the results obtained directly from experimental tests. The extrapolated test results for the crack size a versus load cycles n for the five test conditions are given in Reference 1 and only the results for test conditions No. 1 and No. 2 are depicted in Figure 24. A comparison between Figures 13 and 24 indicates that the correlation between the theoretical model and the extrapolated test results is reasonable.

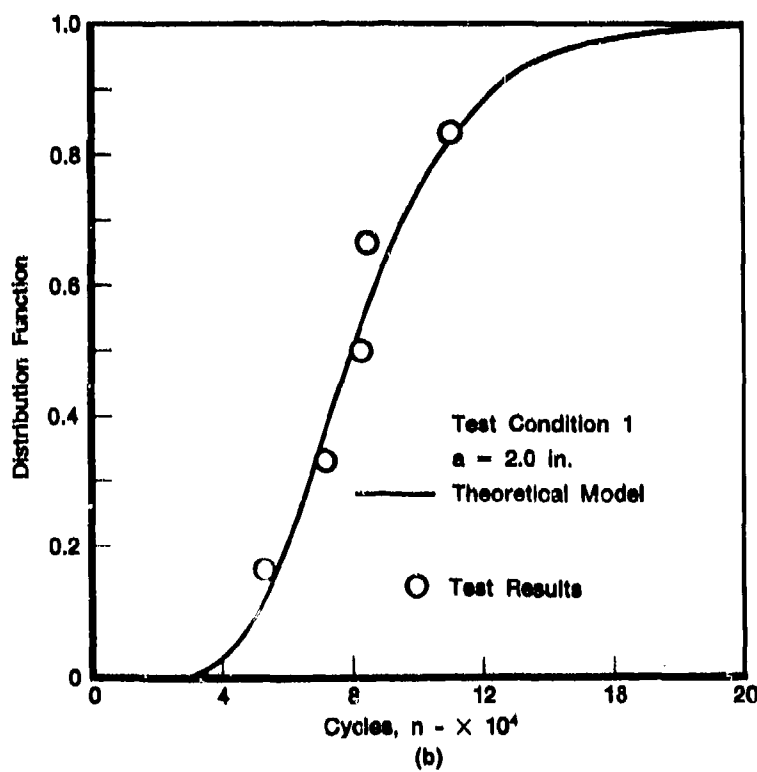
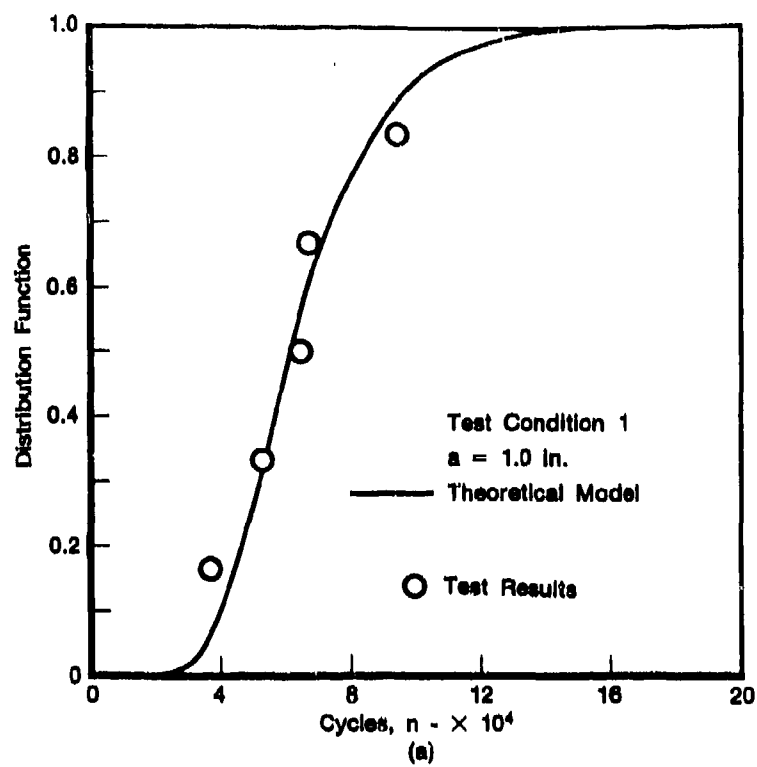


Figure 14. Distribution of Cycles To Reach Given Crack Size for Test Condition No. 1; (a) $a = 1.0$ Inch, and (b) $a = 2.0$ Inches

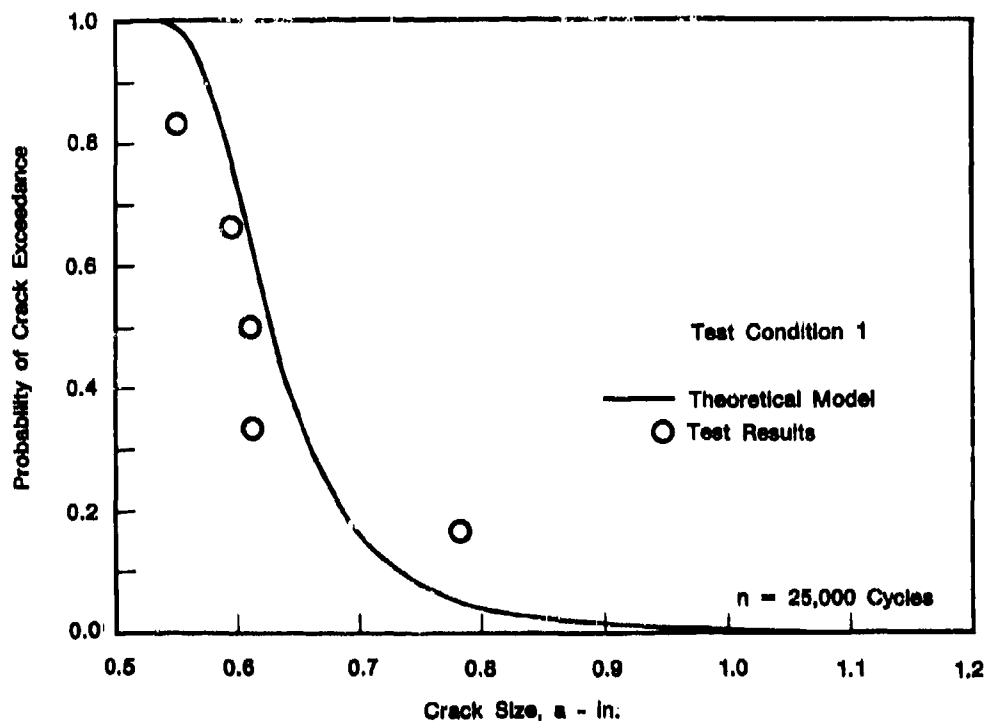


Figure 15. Crack Exceedance Curve After 25,000 Cycles for Test Condition No. 1

From the extrapolated test results for the crack size a versus the number of load cycles n , one obtains (1) extrapolated test data for the number of load cycles to reach any given crack size a_1 by drawing a horizontal line through a_1 , and (2) extrapolated test data for the crack size after any number of load cycles n_1 by drawing a vertical line through n_1 .

The distribution function is constructed from the extrapolated test data obtained above by arranging them in an ascending order. The ordinate of the i th data is given by $i/(m+1)$ where m is the total number of data points. For instance, one obtains five data points from Figure 22 by drawing a horizontal line through $a_1 = 1.0$ inch. These five data points, for the number of cycles to reach a crack size of $a_1 = 1$ inch, are ranked in an ascending order where the ordinate of the i th data point is equal to $i/6$ ($i=1, 2, \dots, 5$). These results are shown in Figure 14(a) by circles. In like manner, the distributions of the extrapolated test results for the number of load cycles to reach other crack sizes, as well as their crack exceedances after some numbers of cycles have been constructed and shown in Figures 14 through 23 as circles. It is observed from Figures 14 through 23 that the correlation between the statistical model (solid curves) and the extrapolated test results (circles) is very reasonable.

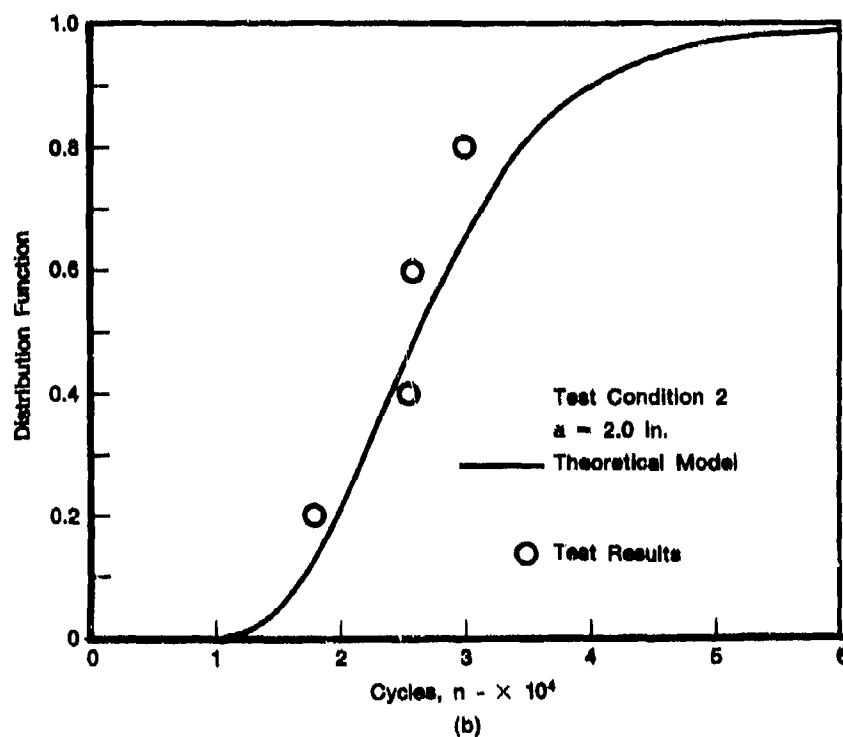
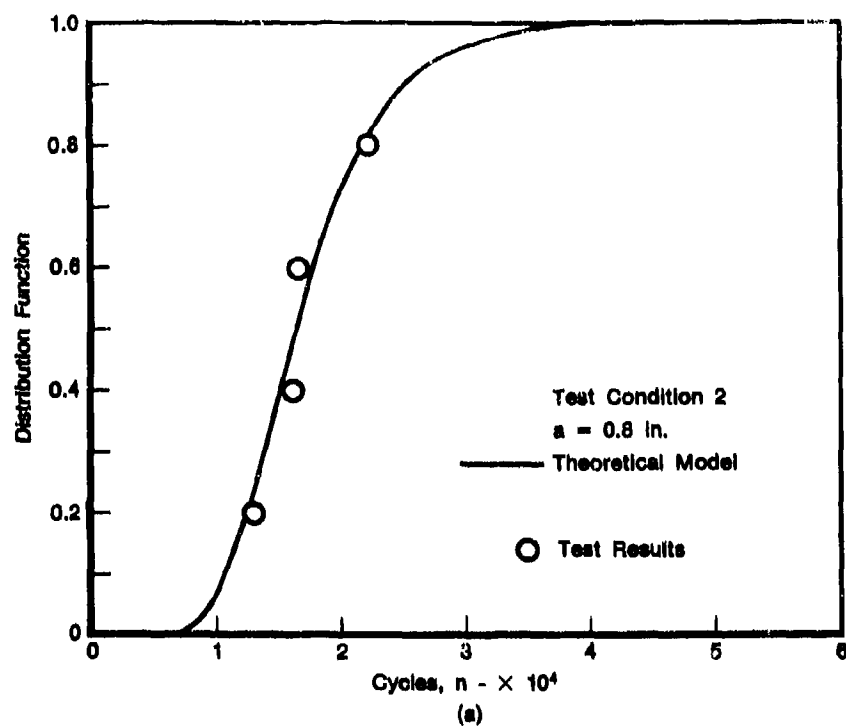


Figure 16. Distribution of Cycles To Reach Given Crack Size for Test Condition No. 2;
 (a) $a = 0.8$ Inch, and (b) $a = 2.0$ Inches

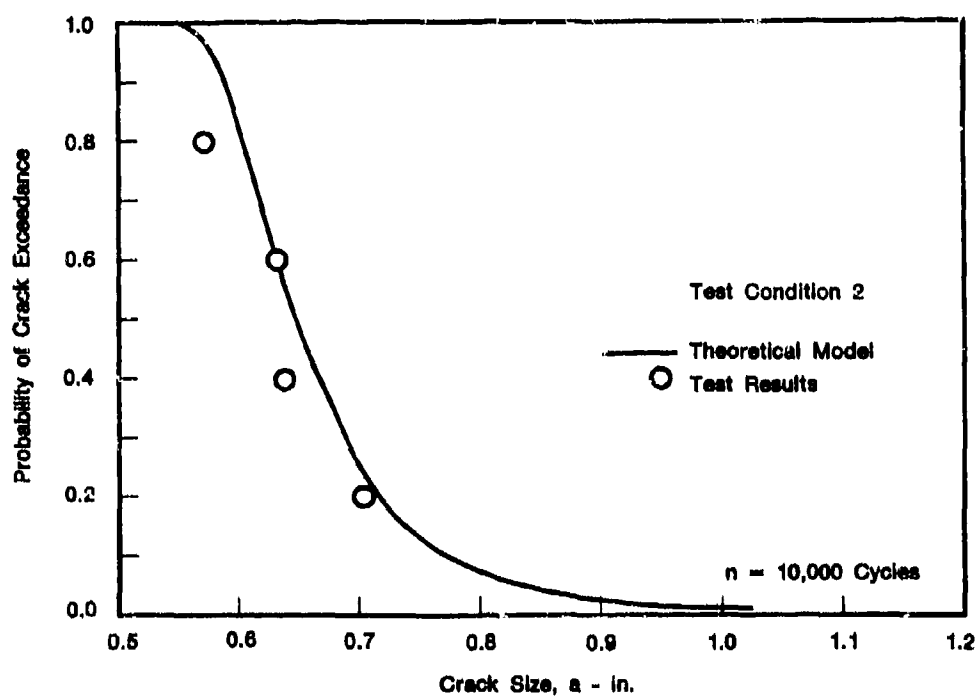


Figure 17. Crack Exceedance Curve after 10,000 Cycles for Test Condition No. 2

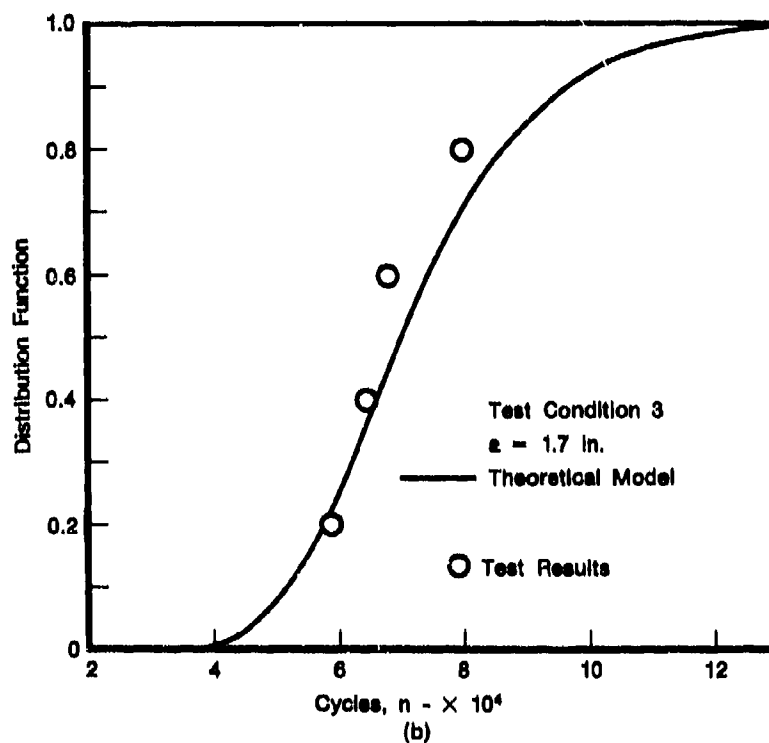
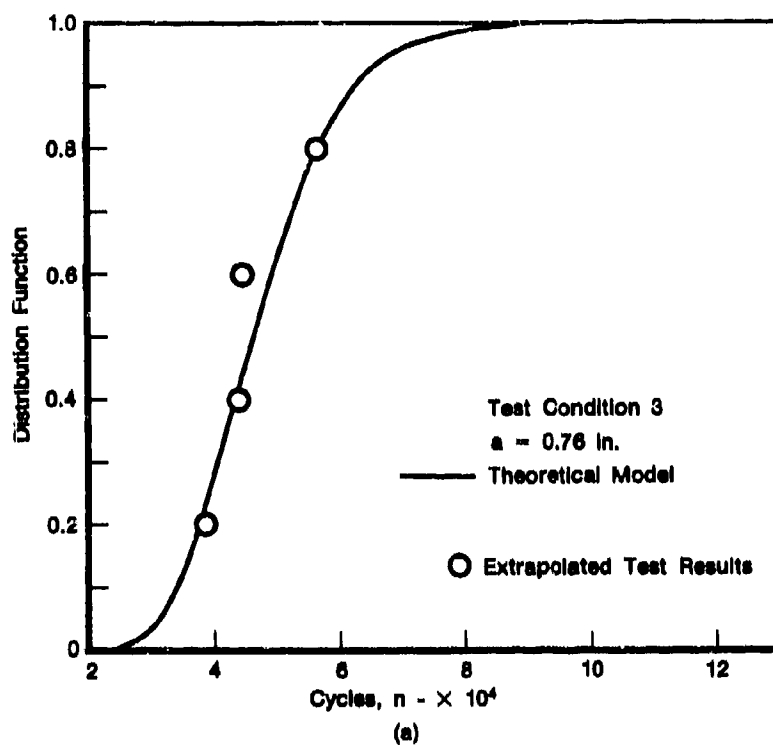


Figure 18. Distribution of Cycles To Reach Given Crack Size for Test Condition No. 3; (a) $a = 0.76$ Inch, and (b) $a = 1.7$ Inches

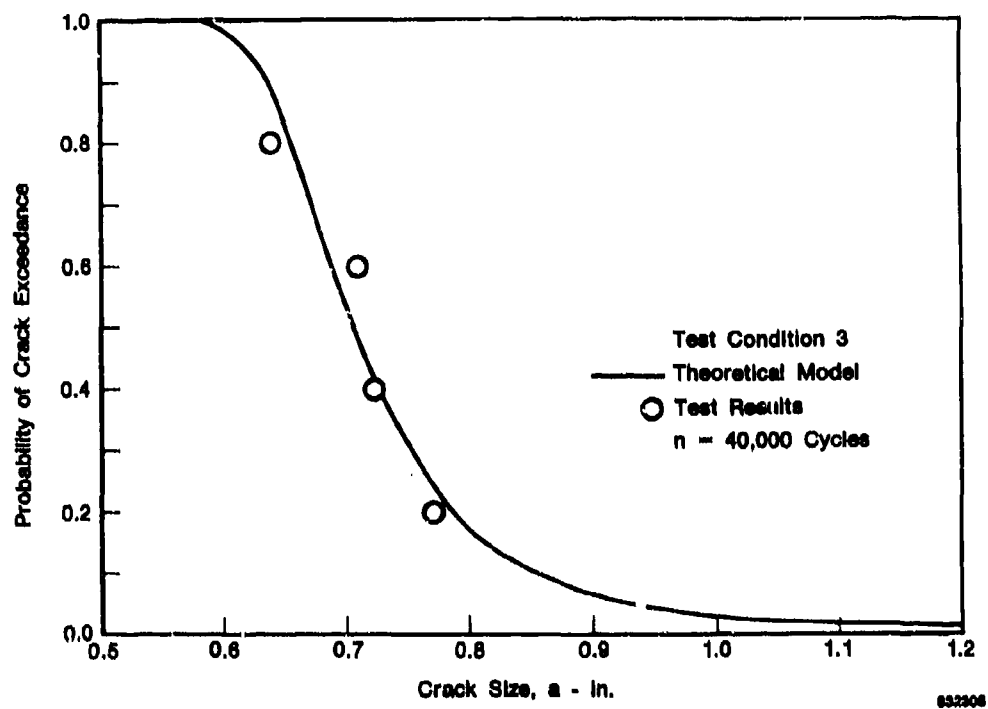


Figure 19. Crack Exceedance Curve after 40,000 Cycles for Test Condition No. 3

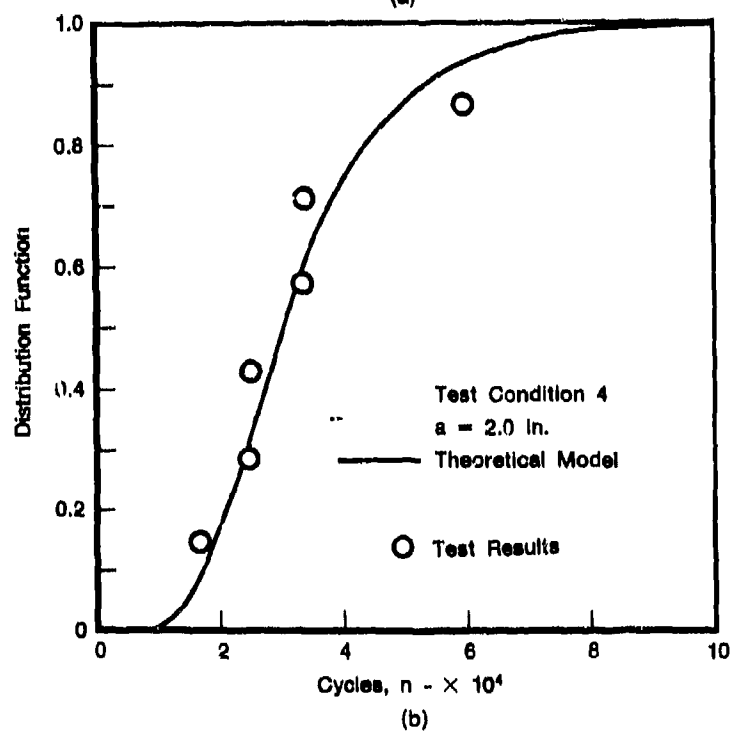
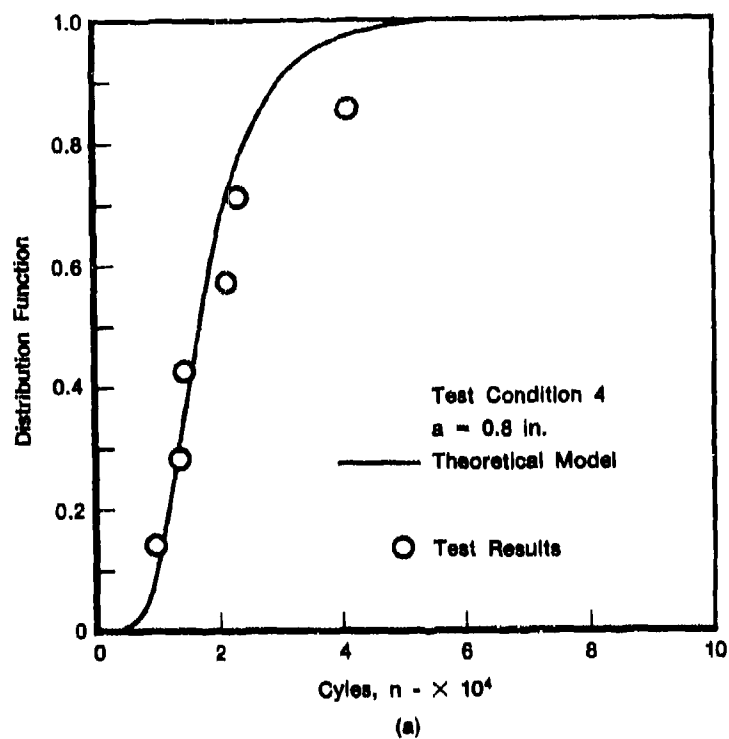


Figure 20. Distribution of Cycles to Reach Given Crack Size for Test Condition No. 4; (a) $a = 0.8$ Inch, and (b) $a = 2.0$ Inches

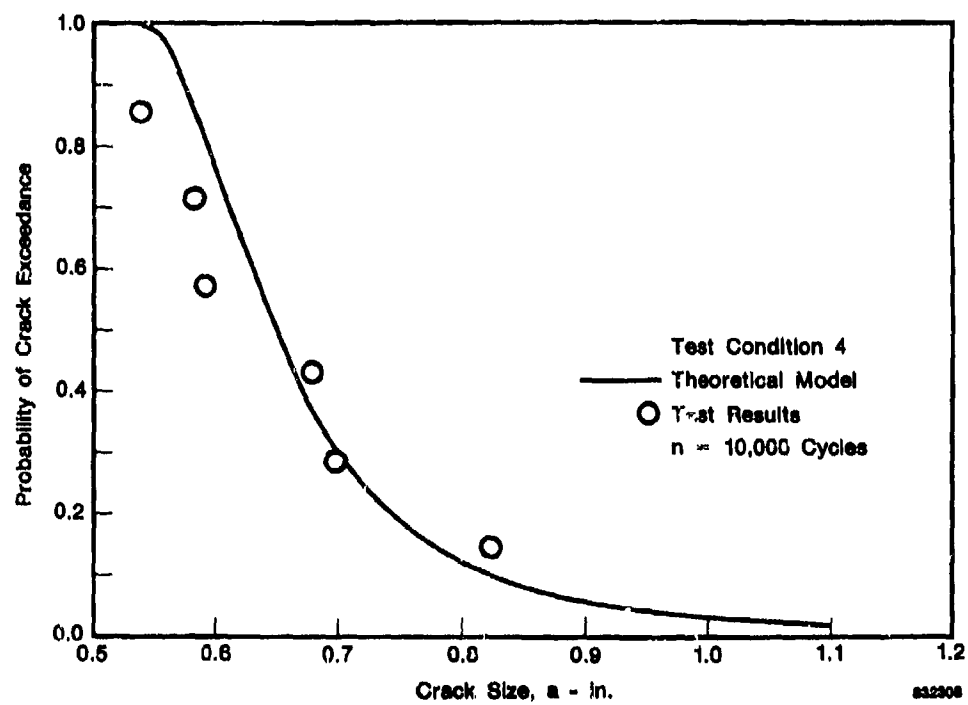
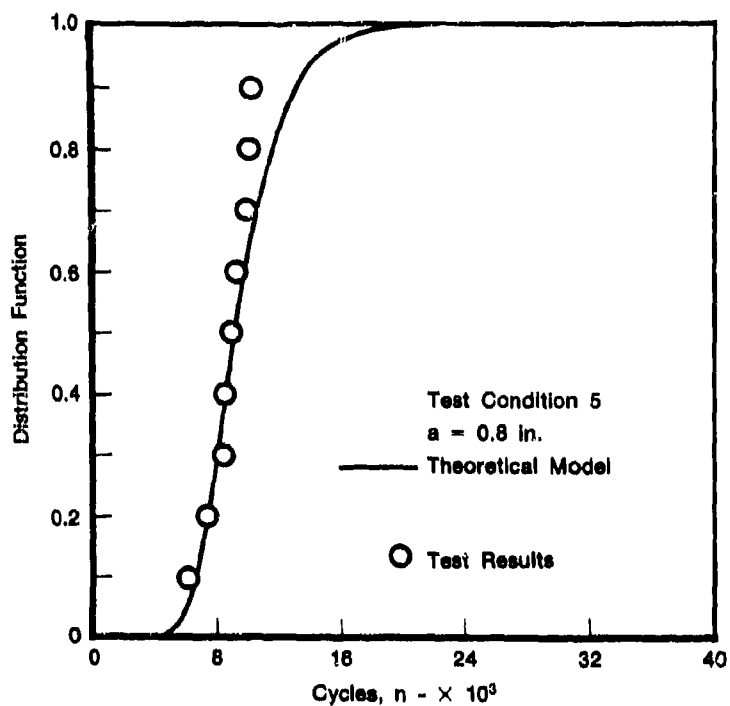
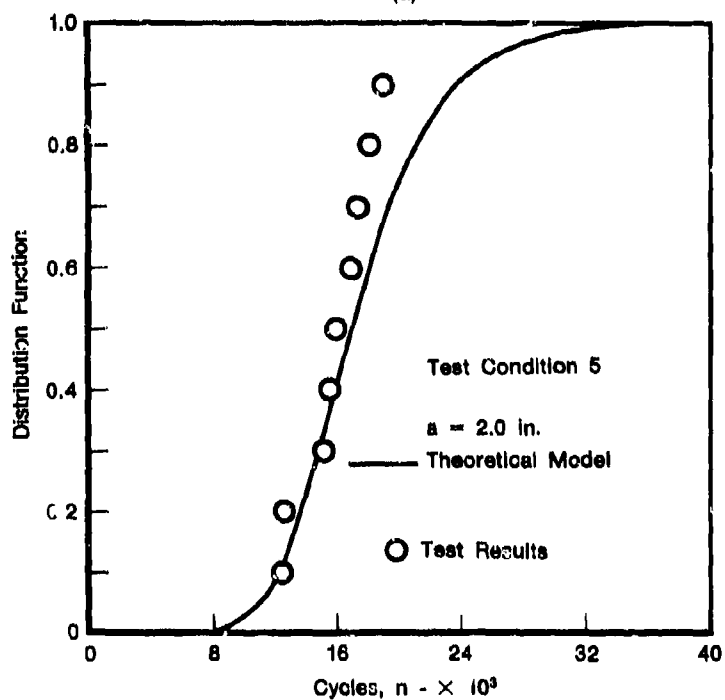


Figure 21. Crack Exceedance Curve after 10,000 Cycles for Test Condition No. 4



(a)



(b)

Figure 22. Distribution of Cycles to Reach Given Crack Size for Test Condition No. 5; (a) $a = 0.8$ Inch, and (b) $a = 2.0$ Inches

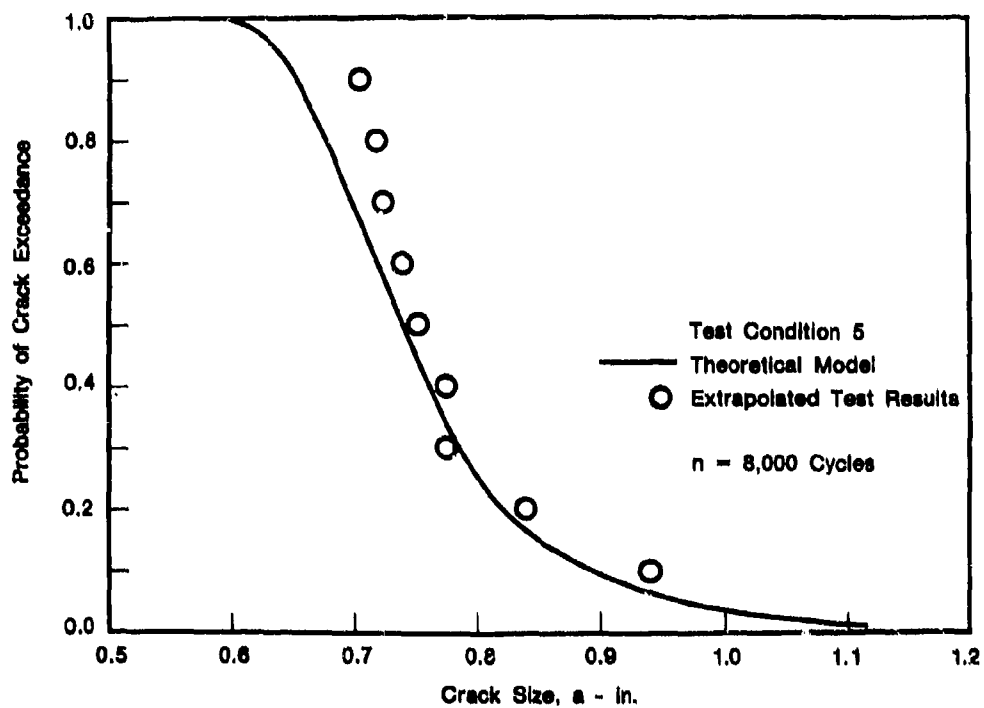
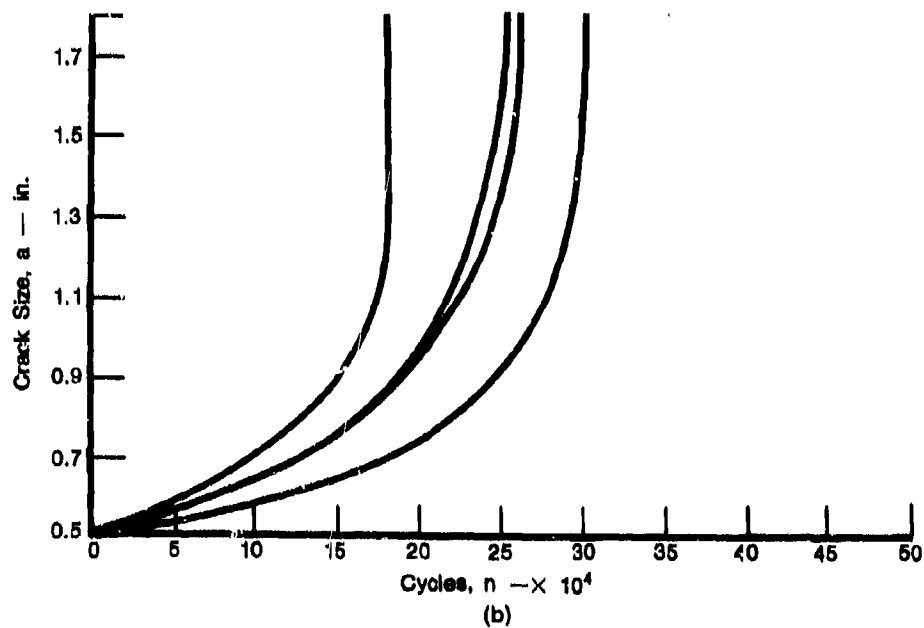
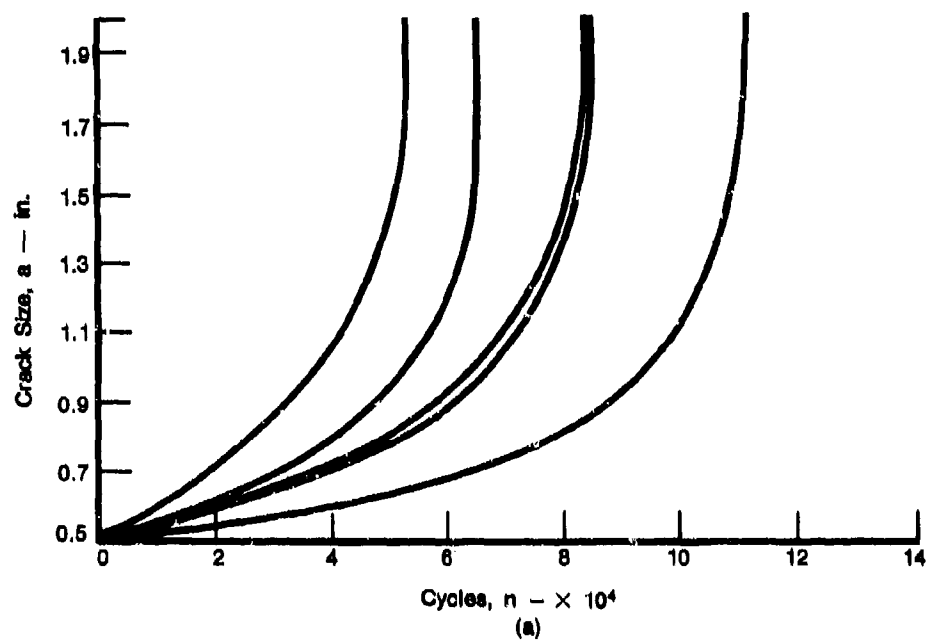


Figure 23. Crack Exceedance Curve after 8,000 Cycles for Test Condition No. 5



FD 255036

Figure 24. Extrapolated Test Results for a Versus n ; (a) Test Condition No. 1 and (b) Test Condition No. 2

SECTION IV

ANALYSIS OF Ti 6-2-4-6 AND WASPALOY DATA

Available Ti 6-2-4-6 and Waspaloy crack propagation test results from constant amplitude cyclic loading with various test conditions were compiled. The specimen dimensions, initial crack size, final crack size, and maximum load for each specimen in each test condition are shown in Tables 5 and 6. The crack growth rate data for all specimens in each test condition are also pooled together for analysis purposes. The pooled data for Waspaloy and Ti 6-2-4-6 from test condition Number 1 are shown therein, respectively.

TABLE 5. SPECIMEN GEOMETRY AND MAXIMUM LOAD FOR EACH TEST SPECIMEN OF Ti 6-2-4-6

Test Condition	Specimen No.	a_0 (in.)	a_f (in.)	B (in.)	W (in.)	P_{max} (kips)
1						
T = Room Temperature	1536	0.8138	1.7724	0.249	2.496	0.5450
$\nu = 20$ Hz	1580	0.8130	1.6130	0.2970	2.5007	0.7200
R = 0.1	1582	0.6880	2.2080	0.3690	2.0085	1.0640
	1662	0.7360	1.0620	0.4990	1.4970	0.6900
	1663	0.7580	1.0690	0.4990	1.4990	0.6810
	1676	0.3990	1.1780	0.3520	1.9910	0.9580
	1677	0.4040	1.1900	0.3630	1.9987	0.9880
	1680	0.4730	1.1164	0.3735	1.9955	1.0060
	1972	0.1919	0.6025	0.4990	0.9999	1.1960
	1535	0.7835	1.7618	0.2485	2.4999	0.5090
2						
T = Room Temperature	0423	0.3850	0.7973	0.0970	2.0000	1.890
$\nu = 10$ cpm	0448	0.8628	1.7005	0.2520	2.5001	0.538
R = 0.1	1484	1.3789	1.7577	0.5000	2.4951	1.037
	1885	0.6786	1.1718	0.5004	1.9929	1.182
	1886	0.5733	1.1711	0.5005	2.0056	1.138
	1892	0.5149	1.4487	0.3890	2.4993	1.295
	2103	0.5577	1.2586	0.3760	2.5003	1.301
3						
T = Room Temperature	1744	0.0828	0.2261	0.2935	0.996	6.611
$\nu = 10$ cpm	1741	0.0786	0.1982	0.2900	0.996	7.157
R = 0.0	1742	0.0887	0.2637	0.2970	0.996	6.815
	1532	0.115	0.3120	0.2950	0.997	4.273
4						
T = 800°F	0358	0.597	1.7926	0.2750	2.2520	0.624
$\nu = 10$ cpm	0359	0.6697	1.5878	0.2750	2.2556	0.625
R = 0.1	0409	0.3696	0.8359	0.1250	2.0000	4.844
	0410	0.3874	0.6907	0.1205	2.0000	4.891
	1245	0.5453	0.7775	0.5010	1.0030	0.365
	1881	0.3068	1.4964	0.5240	1.9959	1.763
	1883	0.3679	1.4914	0.5040	2.0045	1.577
5						
T = 400°F	0413	0.6325	2.0500	0.2500	2.5000	0.3330
$\nu = 20$ Hz	0415	0.3741	0.8276	0.1260	2.0000	2.4500
R = 0.1	0416	0.8426	2.0489	0.2500	2.5002	0.2690
	1678	0.4260	0.9300	0.3440	1.9972	1.1160
	1886	0.6128	1.4754	0.5015	1.9986	1.1210

TABLE 6. SPECIMEN GEOMETRY AND MAXIMUM LOAD FOR EACH TEST SPECIMEN OF WASPALOY

Test Condition	Specimen No.	a_0 (in.)	a_1 (in.)	B (in.)	W (in.)	P_{max} (kips)
1						
T = 1200°F	0736	1.0706	1.7666	0.432	2.502	1.621
ν = 20 Hz	1464	0.6000	2.0820	0.500	2.500	1.240
R = 0.05	1470	0.8510	1.7460	0.491	2.491	1.224
	1304	1.0830	1.8670	0.500	2.509	2.263
2						
T = 1200°F	1004	0.0703	0.3326	0.301	0.998	11.513
ν = 10 cpm	1301	1.1072	1.7064	0.501	2.519	1.769
R = 0.05	1013	0.9688	1.8553	0.132	2.484	1.261
3						
T = 800°F	1002	0.8339	1.7598	0.499	2.505	2.574
ν = 10 cpm	1003	0.0635	0.3047	0.303	0.997	13.316
R = 0.05	1018	1.0134	1.8944	0.298	2.505	1.417

Using the hyperbolic sine crack growth rate function (Equation 29), and the lognormal statistical model (Reference 1), we obtain the maximum likelihood estimates for C_2 , C_3 , C_4 and the standard deviation $\sigma_y = \sigma_x$. These results are presented in Tables 7 and 8. The crack growth rates based on the values of C_1 , C_2 , C_3 and C_4 given in these tables, for $Z = 0$, are shown as solid curves in Figures 25 and 26 (test condition Number 1).

TABLE 7. MAXIMUM LIKELIHOOD ESTIMATE OF C_2 , C_3 , C_4 , STANDARD DEVIATION $\sigma_y = \sigma_x$ AND COEFFICIENT OF VARIATION, V, OF da/dn FOR Ti 6-2-4-6 (HYPERBOLIC SINE FUNCTION)

Test Condition	C_1	C_2	C_3	C_4	$\sigma_y = \sigma_x$	V	No. of Data Points
1	0.7	4.68	-1.0898	-5.4878	0.0672	15.6%	269
2	0.7	4.5715	-1.1088	-5.378	0.1156	27.1%	179
3	0.7	3.0949	-0.9951	-5.7946	0.1174	27.5%	50
4	0.7	2.1954	-0.9086	-5.4958	0.0561	13.0%	251
5	0.7	3.5301	-1.0641	-5.7081	0.0939	21.9%	153

TABLE 8. MAXIMUM LIKELIHOOD ESTIMATE OF C_2 , C_3 , C_4 , STANDARD DEVIATION $\sigma_y = \sigma_x$ AND COEFFICIENT OF VARIATION, V, OF da/dn FOR WASPALOY (HYPERBOLIC SINE FUNCTION)

Test Condition	C_1	C_2	C_3	C_4	$\sigma_y = \sigma_x$	V	No. of Data Points
1	0.5	3.5484	-1.4054	-5.0269	0.0783	18.2%	130
2	0.5	4.0154	-1.3694	-4.8774	0.0470	10.9%	60
3	0.5	4.3817	-1.4941	-4.9847	0.0554	12.8%	67

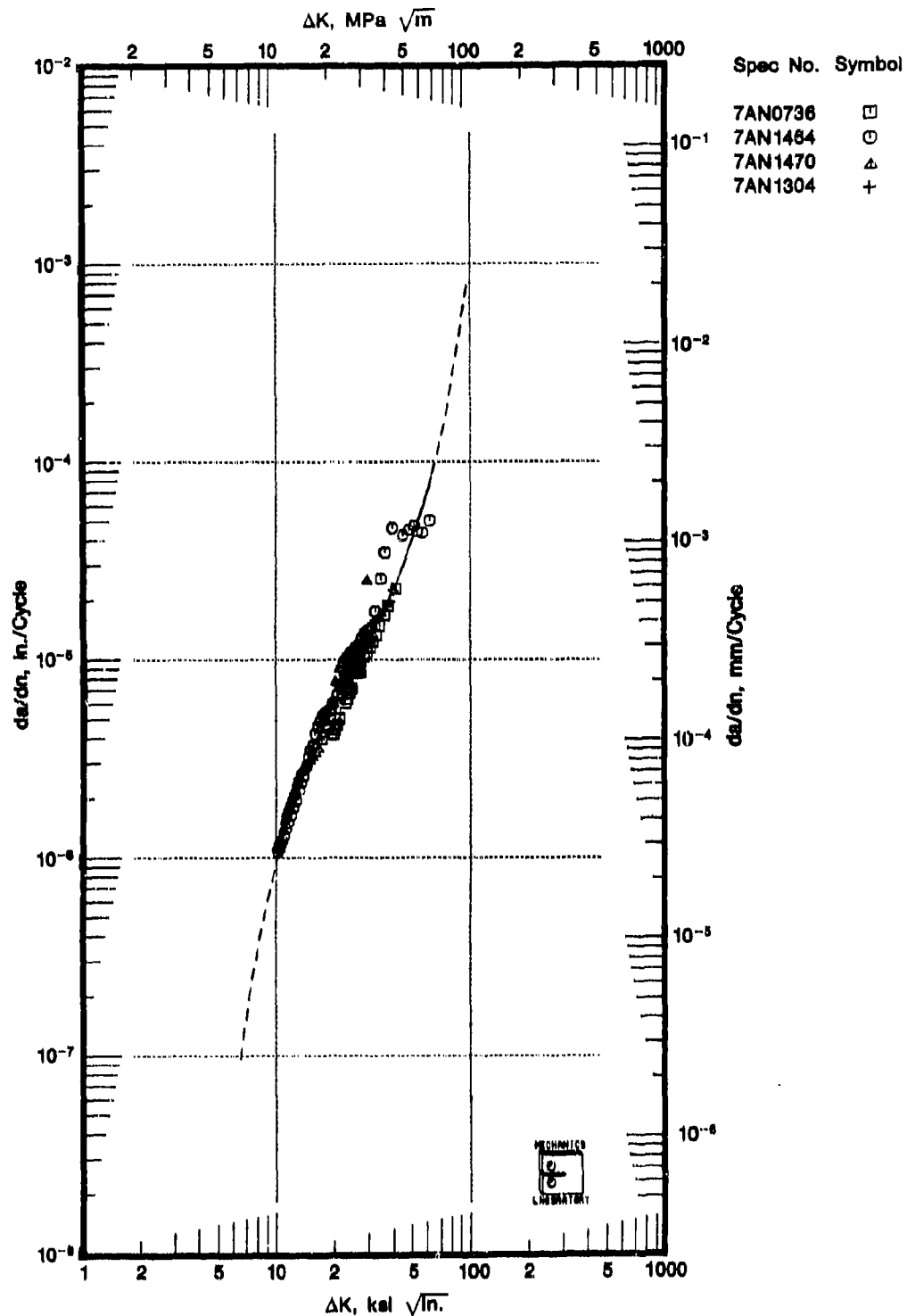


Figure 25. Crack Growth Rate Model for Waspaloy at 1200°F, 20 Hz, and $R = 0.05$

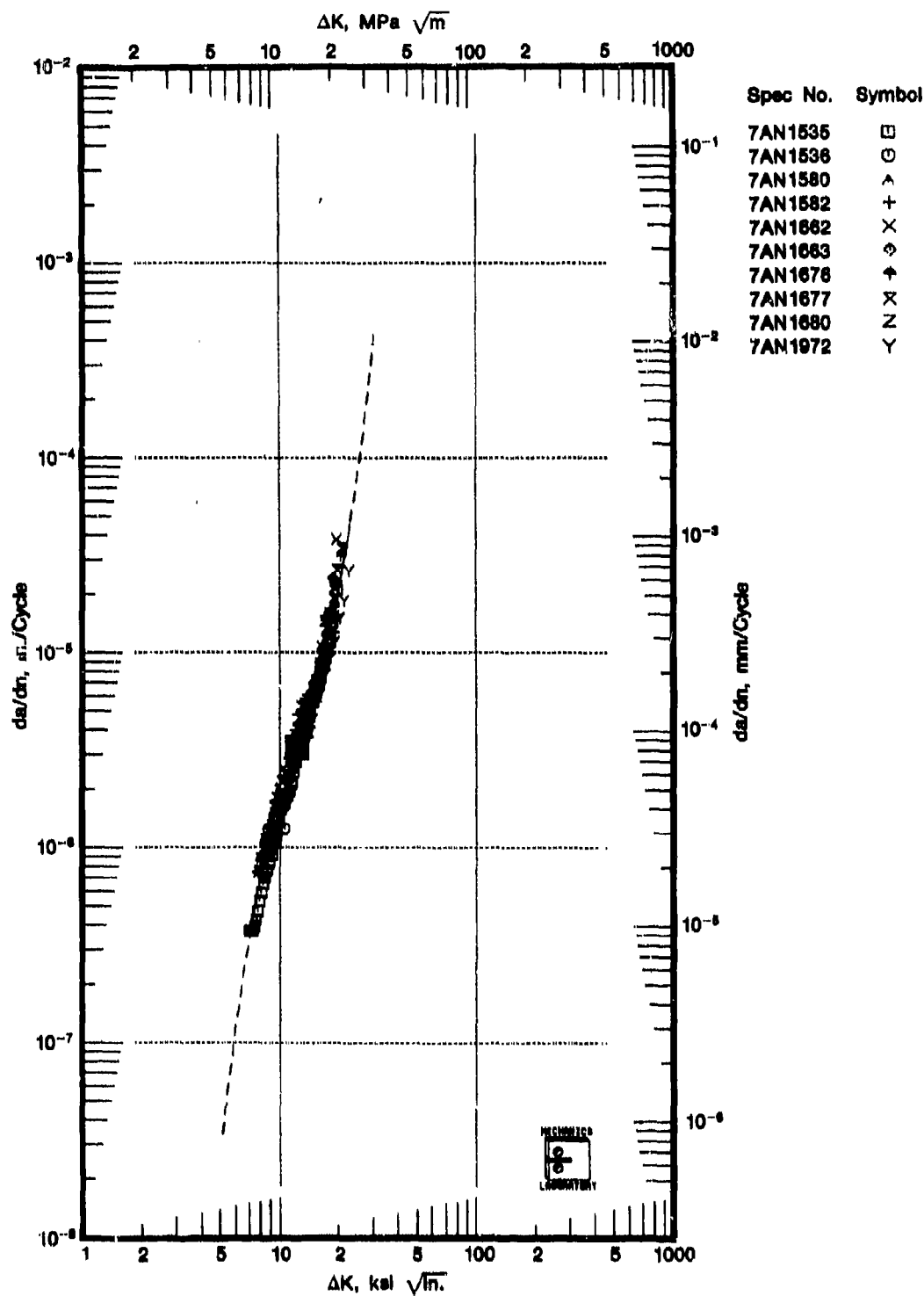


Figure 26. Crack Growth Rate Model for Titanium 6-2-4-6 at Room Temperature, 20 Hz, and $R = 0.1$

Crack growth rate data for each specimen are best-fitted by the hyperbolic sine function (Equation 3), to determine the parameter values C_2 , C_3 and C_4 . The results of the parameter values for each specimen are shown in Tables 9 and 10.

TABLE 9. PARAMETERS C_2 , C_3 , AND C_4 FOR EACH TEST SPECIMEN OF TITANIUM WITH $C_1 = 0.7$, HYPERBOLIC SINE CRACK GROWTH RATE FUNCTION

Test Condition	Specimen No.	C_2	C_3	C_4	R	Type of Specimen
1 —	1536	4.5592	-1.0205	-5.735	0.1	MCT
	1580	4.1696	-1.2051	-5.1217	0.1	MCT
	1582	5.0229	-1.3336	-4.6700	0.1	MCT
	1662	4.4731	-1.0217	-5.6851	0.1	MCT
	1683	4.7567	-1.0399	-5.6514	0.1	MCT
	1676	4.1695	-0.9856	-5.8264	0.1	MCT
	1677	4.2736	-0.9858	-5.8294	0.1	MCT
	1680	4.1694	-1.2454	-4.9161	0.1	MCT
	1972	3.7766	-1.0662	-5.5379	0.1	FRT
	1535	4.8335	-1.0530	-5.6762	0.1	MCT
	0423	4.6117	-1.1744	-5.2811	0.1	CN
	0448	4.4517	-1.0333	-5.6816	0.1	MCT
	1484	4.8831	-1.4252	-4.2558	0.1	MCT
	1885	5.2785	-1.1319	-5.2332	0.1	MCT
	1896	4.0642	-0.8937	-6.1048	0.1	MCT
2 —	1892	4.6282	-1.0629	-5.6214	0.1	MCT
	2103	5.1135	-0.9827	-5.7010	0.1	MCT
	1744	5.4566	-1.3166	-4.6476	0.0	CN
	1732	3.1613	-0.8446	-5.6793	0.0	CN
	1741	5.1208	-1.2970	-4.7369	0.0	CN
3 —	1542	4.7786	-1.4152	-4.3071	0.0	CN
	0558	2.1554	-0.8647	-5.5219	0.1	MCT
	0359	1.6211	-0.4380	-6.1690	0.1	MCT
	0409	3.0045	-1.7454	-3.7829	0.1	CN
	0410	3.3857	-1.4531	-4.4511	0.1	CN
4 —	1245	2.2045	-0.8054	-5.6619	0.1	MCT
	1881	2.7011	-1.0981	-5.1852	0.1	MCT
	1883	2.3800	-0.9634	-5.4186	0.1	MCT
	0413	3.5875	-1.1146	-5.5747	0.1	MCT
	0415	3.4328	-1.2919	-5.1373	0.1	CN
5 —	0416	3.8776	-0.8233	-6.4855	0.1	MCT
	1678	3.7288	-1.2226	-5.2324	0.1	MCT
	1886	3.5905	-1.1537	-5.3697	0.1	MCT

TABLE 10. PARAMETERS C_2 , C_3 , AND C_4 FOR EACH TEST SPECIMEN OF WSPALOY WITH $C_1 = 0.5$, HYPERBOLIC SINE CRACK GROWTH RATE FUNCTION

Test Condition	Specimen No.	C_2	C_3	C_4	R	Type of Specimen
1	0736	3.9744	-1.5278	-4.8472	0.05	MCT
	1464	3.4968	-1.4725	-4.8366	0.05	MCT
	1470	4.4457	-1.2349	-5.3545	0.05	MCT
	1304	3.8747	-1.5438	-4.7752	00.1	MCT
2	1004	4.9009	-1.4710	-4.6875	0.05	CN
	1301	3.7554	-1.2698	-5.1172	0.05	MCT
	1013	3.8140	-1.4935	-4.5702	0.1	MCT
3	1002	4.4664	-1.5408	-4.8281	0.05	MCT
	1003	4.9438	-1.5228	-4.9012	0.05	CN
	1018	3.827	-1.3911	-5.2284	0.05	MCT

In order to perform correlation studies, homogeneous test environments should be assumed, since each test specimen has different geometry, initial crack size, final crack size, and maximum load P_{max} , as shown in Tables 5 and 6. Homogeneous test environments assumed for Waspaloy are shown in Table 11.

TABLE 11. ASSUMED HOMOGENEOUS TEST ENVIRONMENTS FOR EACH TEST CONDITION FOR WASPALOY

Test Condition	a_0 (in.)	a_f (in.)	B (in.)	W (in.)	P_{max} (kips)	Type of Specimen
1	0.5	2.0	0.5	2.5	3.8	MCT
2	0.5	2.0	0.5	2.5	5.2	MCT
3	0.5	2.0	0.5	2.5	4.0	MCT

The distribution of the crack growth damage accumulation, a , as a function of load cycles, n , based on the lognormal statistical model can be obtained using Tables 8 and 11. Then, the distribution functions for (1) the number of load cycles to reach any specific crack size, and (2) the crack exceedance probability at any given number of load cycles, can easily be determined (Reference 1). The distribution functions for the number of load cycles to reach crack sizes 0.875 and 2.0 inches are displayed as solid curves in Figures 27(a), 28(a), and 29(a), for the three test conditions. Likewise, the probabilities of crack exceedance at $n = 50,000$, 10,000 and 50,000 cycles, for the three test conditions, are shown as solid curves in Figures 27(b), 28(b), and 29(b).

With the aid of the best-fitted parameter values for C_2 , C_3 , and C_4 , given in Table 10, the crack growth damage accumulation, a , for each individual specimen, is obtained by integrating the crack growth rate equation and using the assumed homogeneous test environments given in Table 11. The distribution of the number of load cycles to reach any specific crack size and the crack exceedance probability at any given number of load cycles is then established. These extrapolated results are presented as circles and triangles in Figures 27 through 29. The homogeneous test environment in Table 11, is assumed to avoid excessive extrapolation into the region of ΔK for which test data do not exist. This may be difficult to achieve because the crack growth rate data for each specimen do not cover the same region of ΔK . Therefore, the extrapolation cannot be avoided for some specimens. This problem becomes more serious for the Ti 6-2-4-6 data and will be discussed later.

It is observed from Figures 27 through 29 that the correlation between the lognormal statistical model and the extrapolated test results is very reasonable for Waspaloy.

In a similar manner, homogeneous test environments are assumed for Ti 6-2-4-6. Based on the lognormal statistical model, the distribution functions for the number of cycles to reach two different crack sizes are shown as solid curves in Figures 30(a) through 34(a) while the crack exceedance curves are shown in Figures 30(b) through 34(b). The corresponding extrapolated test results are shown in the same figures by circles and triangles. It is observed that except for test condition number 5, the correlation is less than satisfactory.

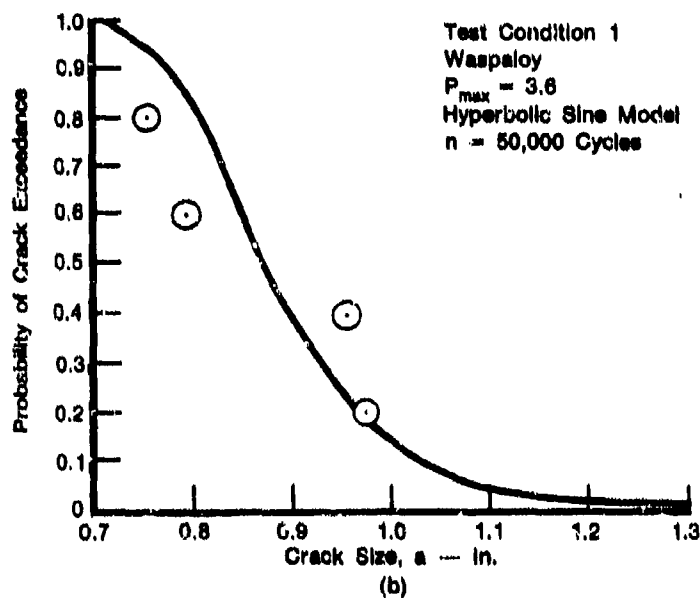
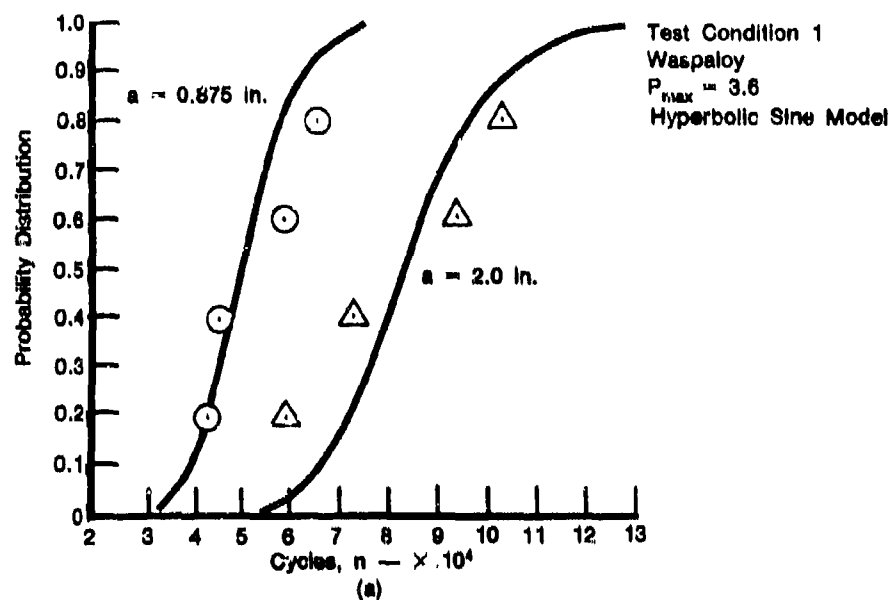
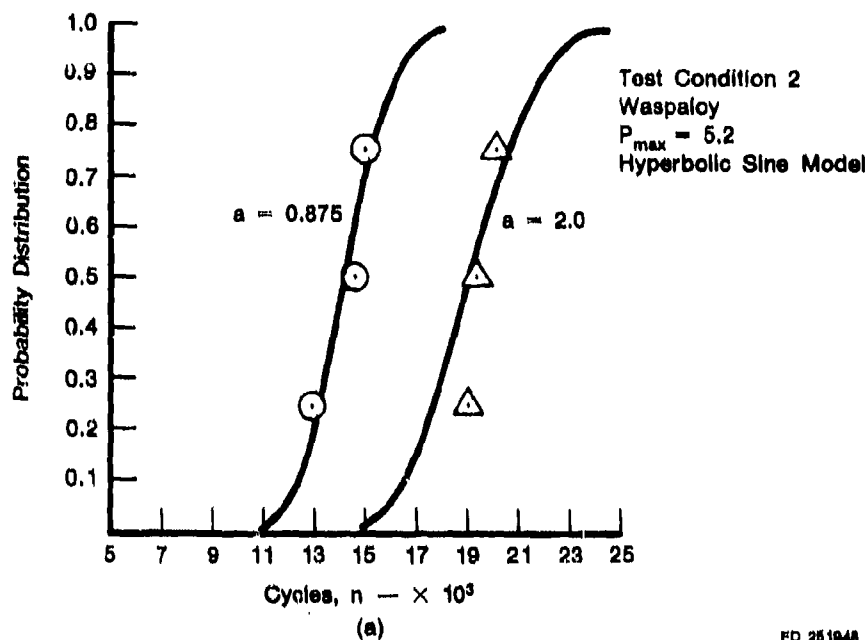
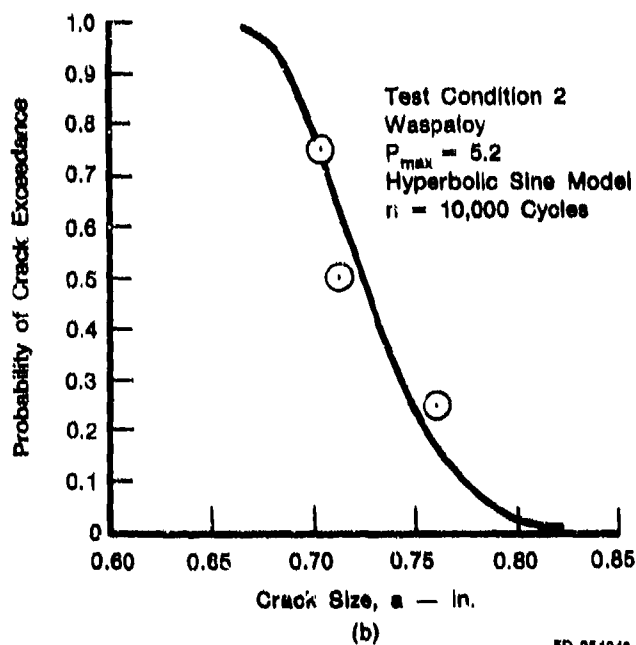


Figure 27. Distribution Curve and Crack Exceedance Curve for Waspaloy for Test Condition No. 1; (a) Distribution of Cycles to Reach Given Crack Size, and (b) Crack Exceedance Curve After 50,000 Cycles



FD 251948



FD 251948

Figure 28. Distribution Curve and Crack Exceedance Curve for Waspaloy for Test Condition No. 2; (a) Distribution of Cycles to Reach a Given Crack Size, and (b) Crack Exceedance Curve After 10,000 Cycles

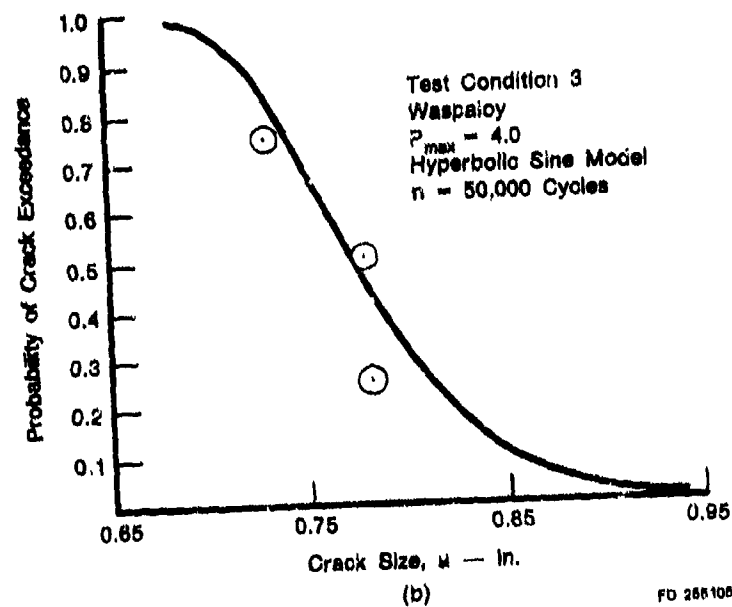
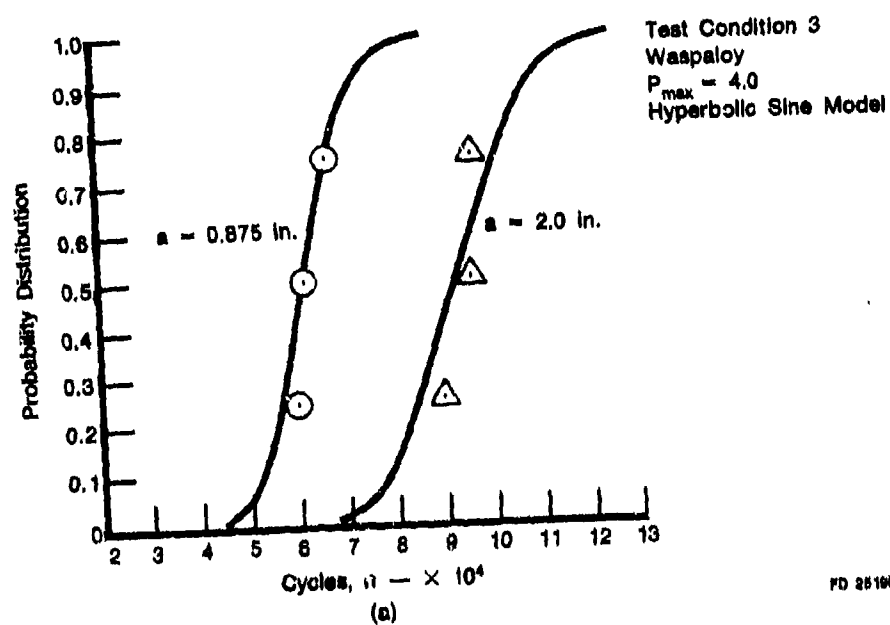
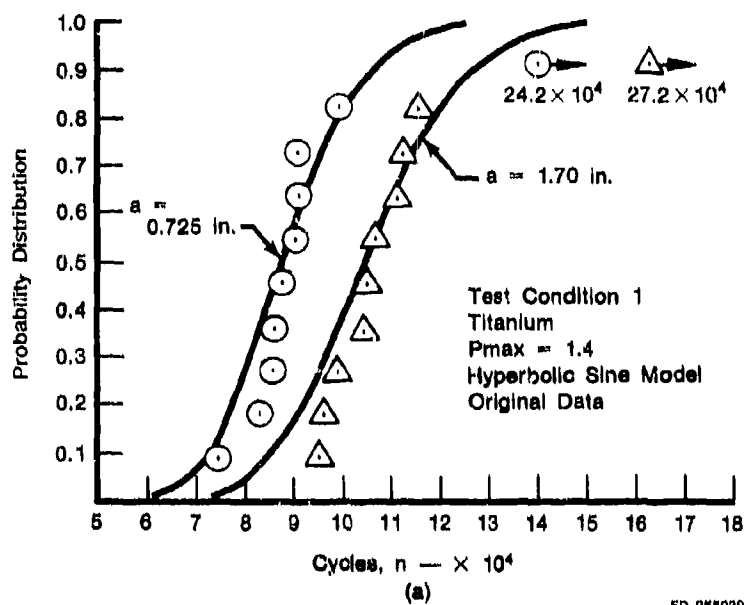
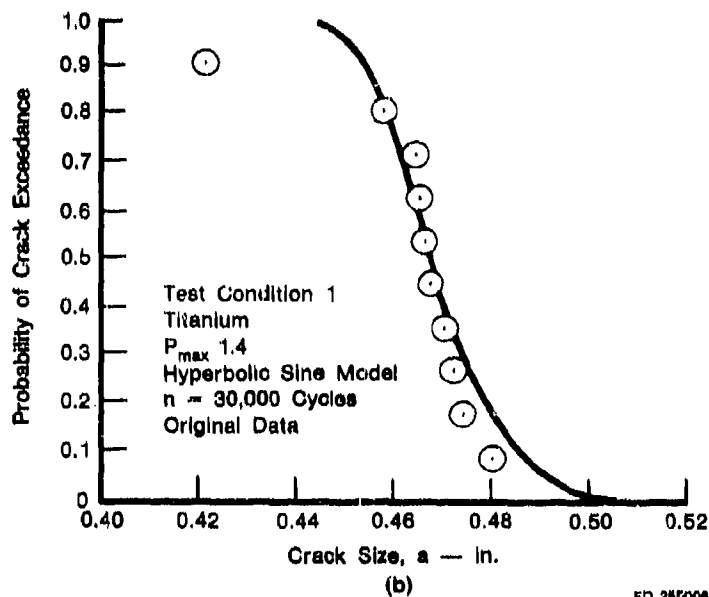


Figure 29. Distribution Curve and Crack Exceedance Curve for Waspaloy for Test Condition No. 3; (a) Distribution of Cycles to Reach Given Crack Size, and (b) Crack Exceedance Curve After 50,000 Cycles



FD 285030



FD 285006

Figure 30. Distribution Curve and Crack Exceedance Curve for Titanium for Test Condition No. 1, Using the Hyperbolic Sine Model; (a) Distribution of Cycles to Reach Given Crack Size, and (b) Crack Exceedance Curve After 30,000 Cycles

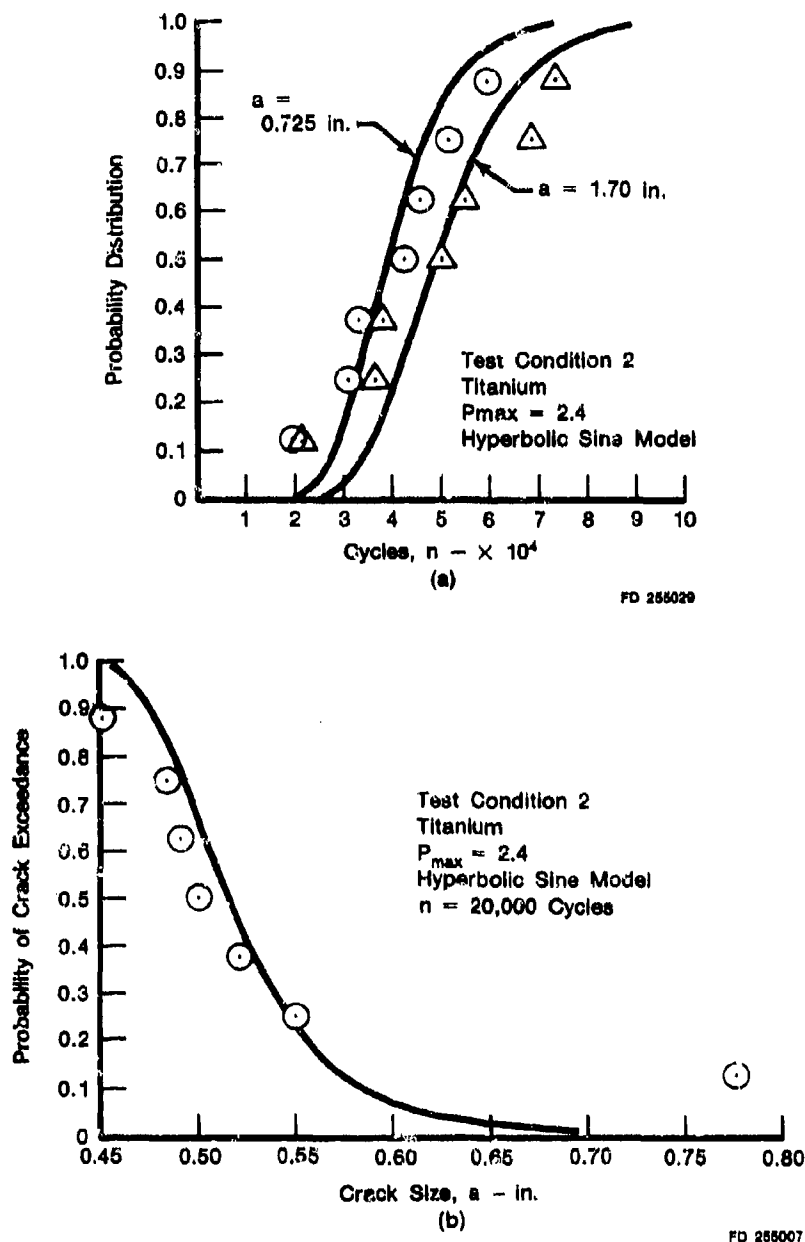
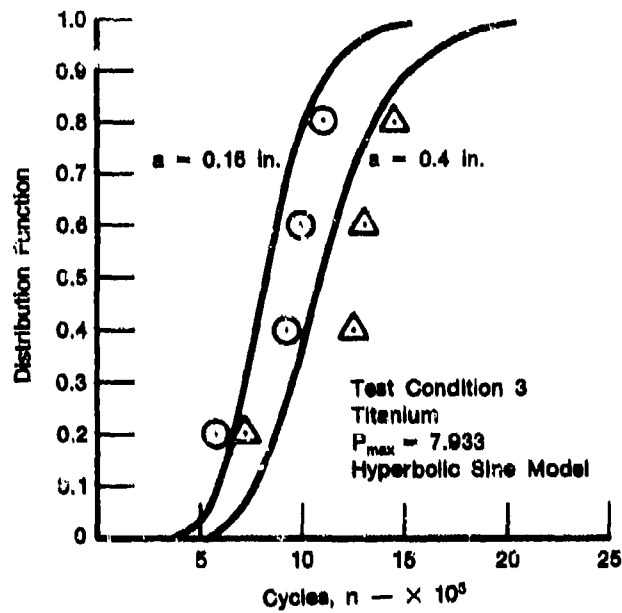
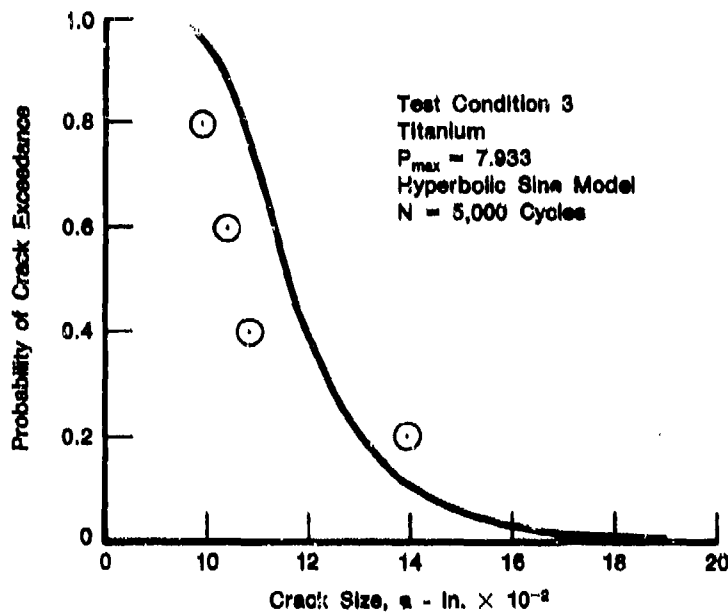


Figure 31. Distribution Curve and Crack Exceedance Curve for Titanium for Test Condition No. 2, Using the Hyperbolic Sine Model; (a) Distribution of Cycles to Reach Given Crack Size, and (b) Crack Exceedance Curve After 20,000 Cycles

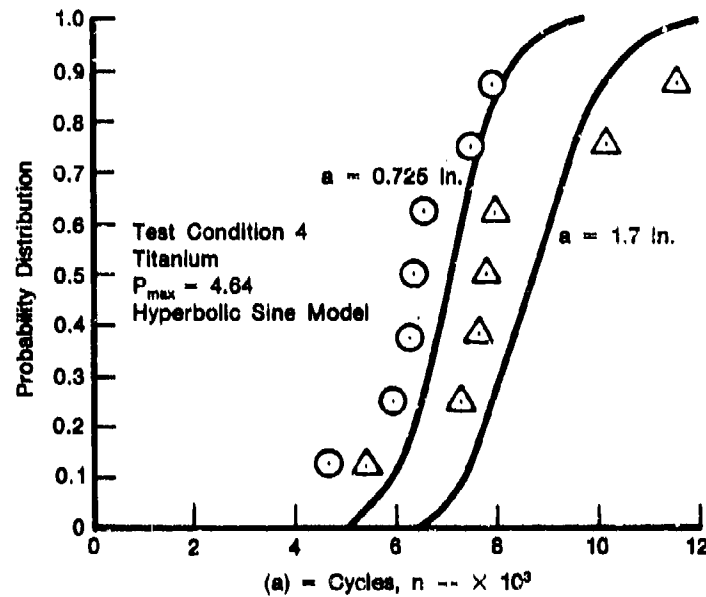


32(a)

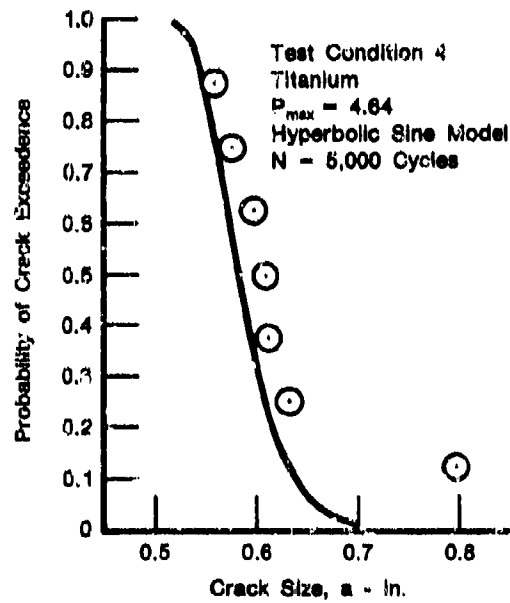


(b)

Figure 32. Distribution Curve and Crack Exceedance Curve for Titanium for Test Condition No. 3, Using the Hyperbolic Sine Model; (a) Distribution of Cycles to Reach Given Crack Size, and (b) Crack Exceedance Curve After 5,000 Cycles



(a)



(b)

Figure 33. Distribution of Cycles to Reach Given Crack Size for Titanium for Test Condition No. 4, Using the Hyperbolic Sine Model; (a) Distribution of Cycles to Reach Given Crack Size, and (b) Crack Exceedance Curve After 5,000 Cycles

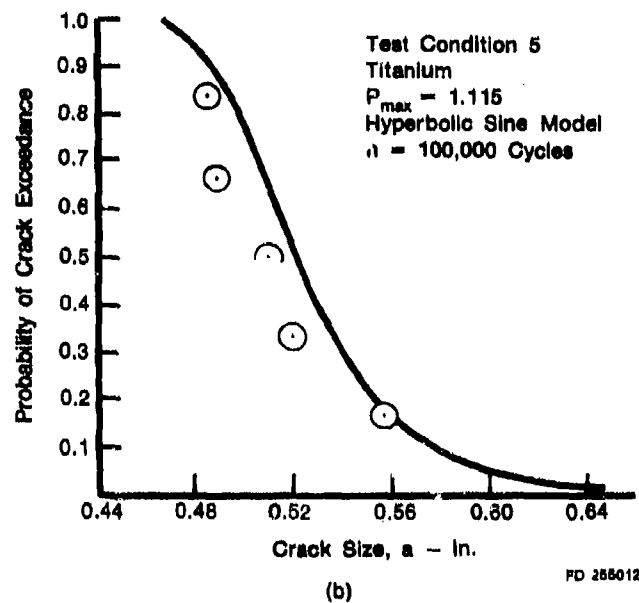
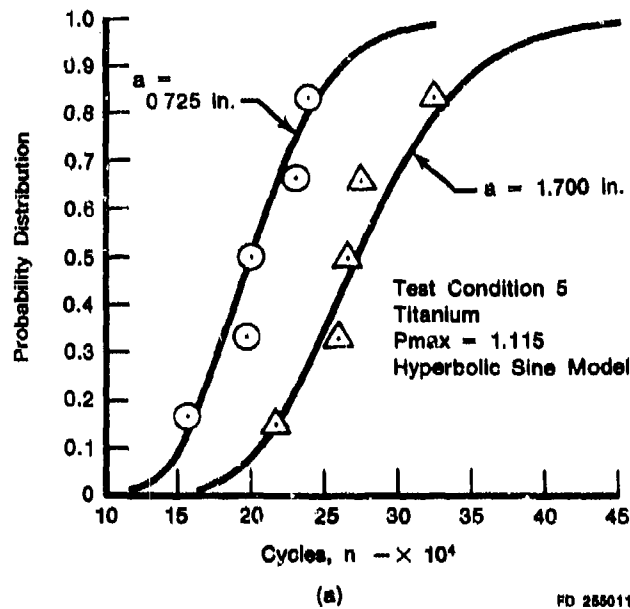


Figure 34. Distribution Curve and Crack Exceedance Curve for Titanium for Test Condition No. 5, Using the Hyperbolic Sine Model; (a) Distribution of Cycles to Reach Given Crack Size, and (b) Crack Exceedance Curve After 100,000 Cycles

A careful examination of the data indicates that the extrapolation for some specimens is excessive, due to the following reasons: (1) The crack growth rate data for each specimen cover different ranges of ΔK , and therefore, it is impossible to assume a homogeneous test environment without excessive extrapolations for some specimens, and (2) The hyperbolic sine function has two asymptotes, and the extrapolation is very sensitive in the region of ΔK where an asymptote occurs. In test condition Number 1, for instance, the crack growth rate data of one specimen (Number 7AN1592) covers only a very small range of ΔK . Consequently, the best-fitted hyperbolic sine function results when the left asymptote falls into the region of extrapolation as shown in Figure 35. Therefore, the propagation life is too long as indicated in Figure 30 by numerical values. Consequently, it seems reasonable to censor this specimen. With such a specimen being censored, the results are shown in Figures 36(a) and (b). It is observed that the correlation is very reasonable. Similar situations exist for test conditions Numbers 2 through 4.

The Paris crack growth model was also used to analyze statistically the Waspaloy and Titanium data.

From the pooled crack growth rate data for each test condition, the method of maximum likelihood was employed to estimate the parameters b and $\log Q$ as well as the standard deviation $\sigma_y = \sigma_x$. The results are presented in Tables 13 and 14, respectively, for Waspaloy and Titanium. Furthermore, the crack growth rate data for each test specimen were best-fitted by the Paris function to determine the corresponding b and $\log Q$ values. The results for each specimen are shown in Tables 15 and 16, respectively.

Following the same procedures described in Section III and using the assumed homogeneous test environments given in Tables 11 and 12, the correlation between the statistical model and the extrapolated test results was obtained. The correlation results for the distribution of random number of load cycles to reach any given crack size and the crack exceedance curve are depicted in Figures 37 through 44. It is observed that the correlation is very good for Waspaloy data sets whereas a considerable improvement in correlation has been achieved for Titanium data sets.

TABLE 12. ASSUMED HOMOGENEOUS TEST ENVIRONMENTS FOR EACH TEST CONDITION FOR TITANIUM

Test Condition	a_0 (in.)	a_1 (in.)	B (in.)	W (in.)	P_{max} (kips)	Type of Specimen
1	0.4	1.7	0.3630	1.9987	1.40	MCT
2	0.4	1.7	0.3890	2.4943	2.40	MCT
3	0.08	0.4	0.3000	1.0000	7.90	CN
4	0.4	1.7	0.5000	2.0000	4.84	MCT
5	0.4	1.7	0.3440	1.9972	1.12	MCT

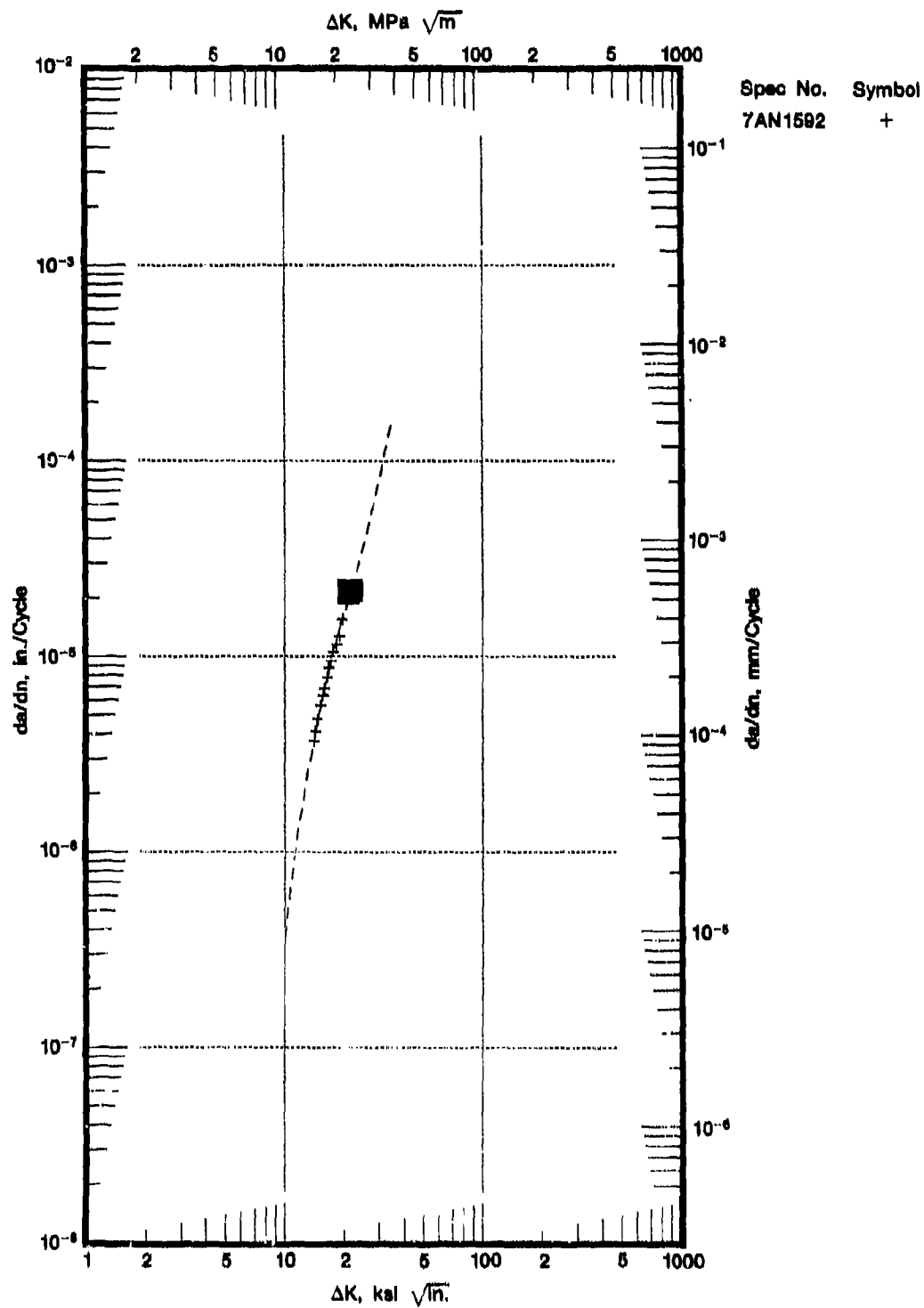


Figure 35. Titanium Crack Growth Rate Specimen at Test Condition No. 1

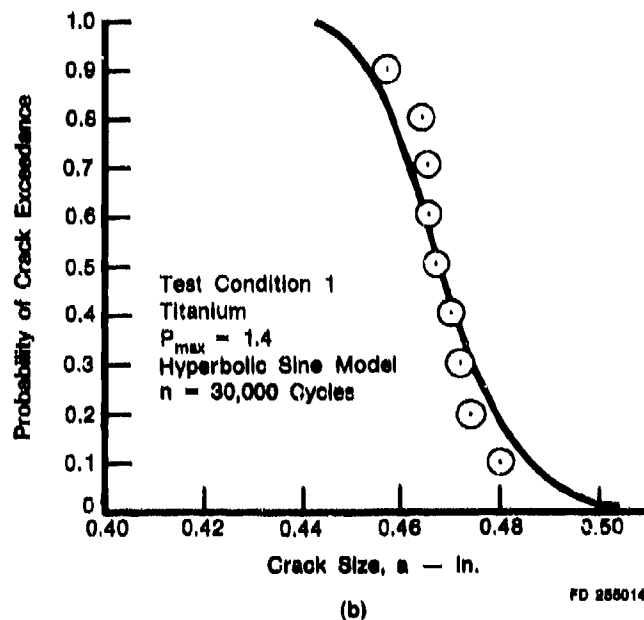
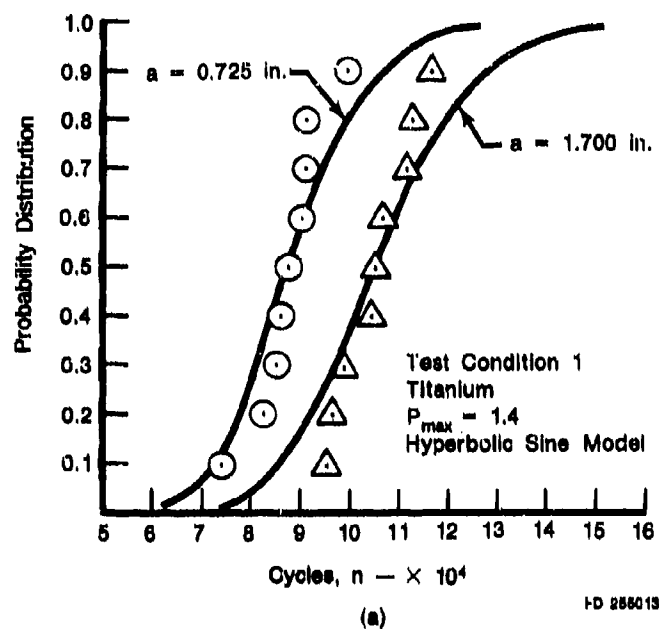


Figure 36. Distribution Curve and Crack Exceedence Curve for Titanium for Test Condition No. 1, Without Specimen No. 1582; (a) Distribution of Cycles to Reach Given Crack Size, and (b) Crack Exceedence Curve After 30,000 Cycles

TABLE 13. MAXIMUM LIKELIHOOD ESTIMATE OF b , LOG Q AND STANDARD DEVIATION $\sigma_x = \sigma_y$ FOR WASPALOY (PARIS FUNCTION)

Test Condition	b	$\log Q$	$\sigma_x = \sigma_y$
1	2.1841	-8.0979	0.0826
2	2.1429	-7.8101	0.0476
3	2.4193	-8.5940	0.0576

TABLE 14. MAXIMUM LIKELIHOOD ESTIMATE OF b , LOG Q AND STANDARD DEVIATION $\sigma_x = \sigma_y$ FOR TITANIUM (PARIS FUNCTION)

Test Condition	b	$\log Q$	$\sigma_x = \sigma_y$
1	3.6062	-9.4166	0.0797
2	3.5240	-9.2847	0.1180
3	2.8591	-8.4737	0.1273
4	2.1210	-7.5039	0.0928
5	3.1094	-9.0305	0.0787

TABLE 15. PARAMETERS b AND LOG Q FOR EACH TEST SPECIMEN OF WASPALOY, (PARIS FUNCTION)

Test Condition 1		
Specimen No.	b	$\log Q$
0736	2.2398	-8.2842
1484	2.2997	-8.2108
1470	2.5171	-8.4611
1304	2.0887	-7.9979
Test Condition 2		
Specimen No.	b	$\log Q$
1004	2.5790	-8.4792
1301	2.1521	-7.8826
1013	2.1302	-7.7509
Test Condition 3		
Specimen No.	b	$\log Q$
1002	2.4759	-8.8585
1003	2.8554	-9.2361
1016	2.1978	-8.2906

TABLE 16. PARAMETERS b AND $\log Q$
FOR EACH TEST SPECIMEN OF
TITANIUM (PARIS FUNCTION)

<i>Test Condition 1</i>		
<u>Specimen No.</u>	<u>b</u>	<u>$\log Q$</u>
1535	3.8179	-9.7058
1538	3.5989	-9.4006
1580	3.5938	-9.4074
1582	4.0285	-10.0185
1662	3.6577	-9.4299
1663	3.8253	-9.6413
1676	3.5012	-9.2797
1677	3.8373	-9.4230
1680	3.7600	-9.5362
1872	2.9832	-8.7004
<i>Test Condition 2</i>		
<u>Specimen No.</u>	<u>b</u>	<u>$\log Q$</u>
0423	3.3759	-9.2429
0448	3.3189	-9.1072
1484	5.0674	-11.2912
1885	4.0291	-9.7903
1886	3.4506	-9.2191
1892	3.6220	-9.4586
2103	4.3748	-10.0228
<i>Test Condition 3</i>		
<u>Specimen No.</u>	<u>b</u>	<u>$\log Q$</u>
1744	4.5104	-10.5876
1832	3.0972	-8.6325
1741	3.9922	-9.9043
1742	4.8892	-11.0534
<i>Test Condition 4</i>		
<u>Specimen No.</u>	<u>b</u>	<u>$\log Q$</u>
0358	1.9848	-7.2954
0359	1.9819	-7.3891
0409	2.7940	-8.5595
0410	2.4115	-7.9559
1245	1.7779	-7.1221
1821	2.3705	-7.8062
1883	2.2311	-7.6221
<i>Test Condition 5</i>		
<u>Specimen No.</u>	<u>b</u>	<u>$\log Q$</u>
0413	3.2859	-9.2172
0415	2.6355	-8.5358
0418	2.9530	-8.9137
1678	2.9355	-8.8684
1883	2.7563	-8.5453

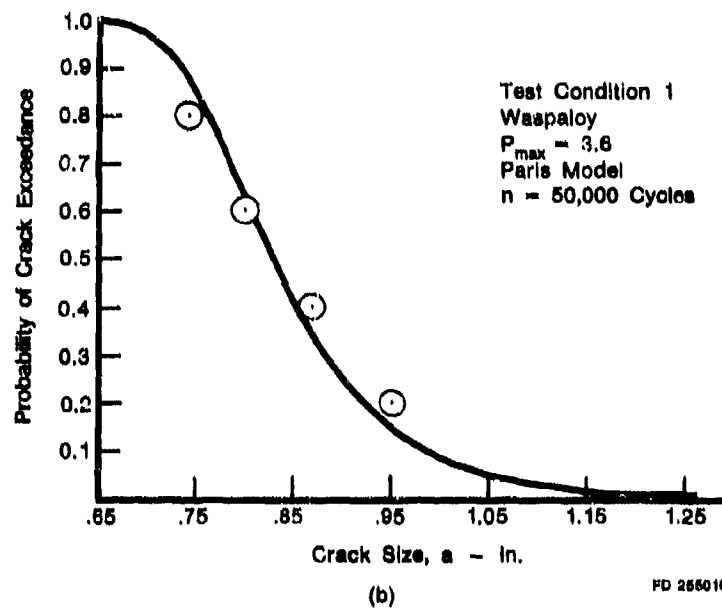
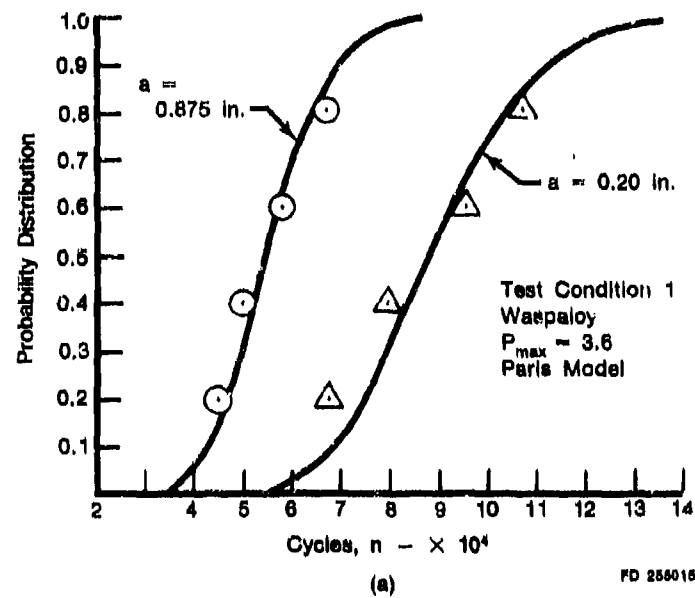


Figure 37. Distribution Curve and Crack Exceedance Curve for Waspaloy for Test Condition No. 1, Using the Paris Model; (a) Distribution of Cycles to Reach Given Crack Size, and (b) Crack Exceedance Curve After 50,000 Cycles

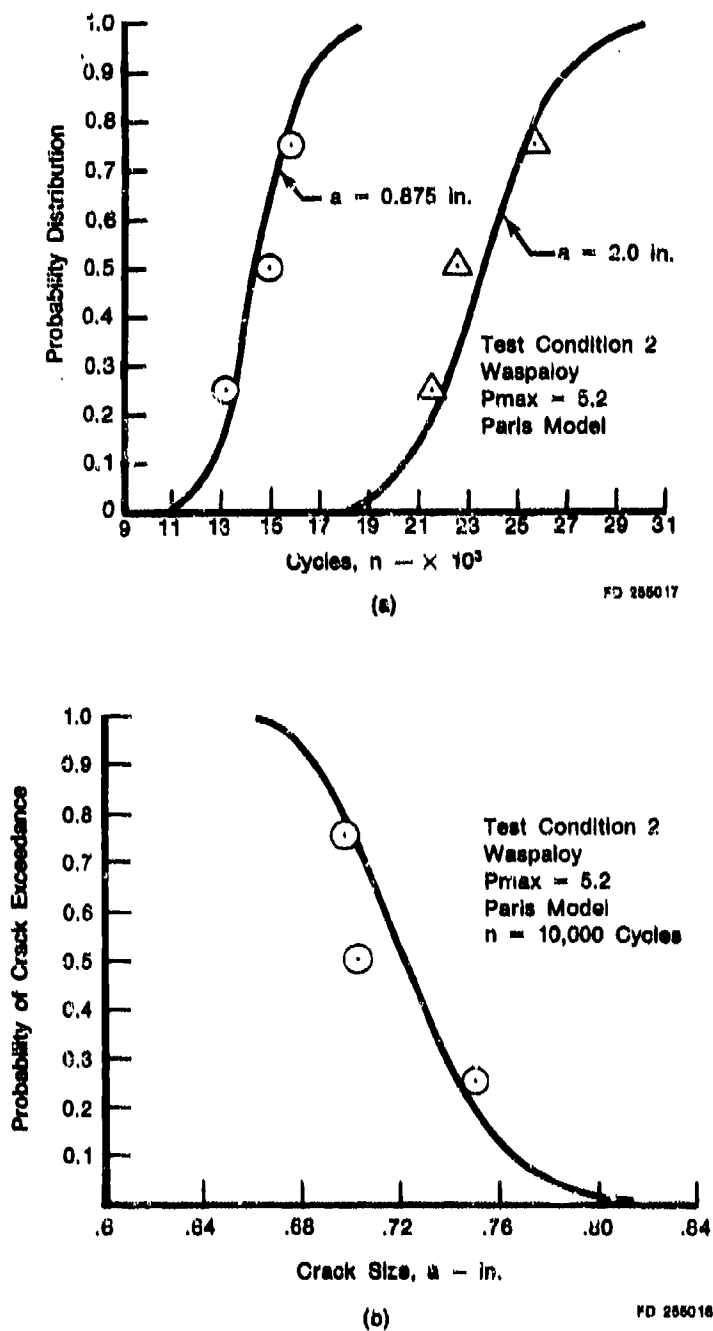


Figure 38. Distribution Curve and Crack Exceedance Curve for Waspaloy for Test Condition No. 2, Using the Paris Model; (a) Distribution of Cycles to Reach Given Crack Size, and (b) Crack Exceedance Curve After 10,000 Cycles

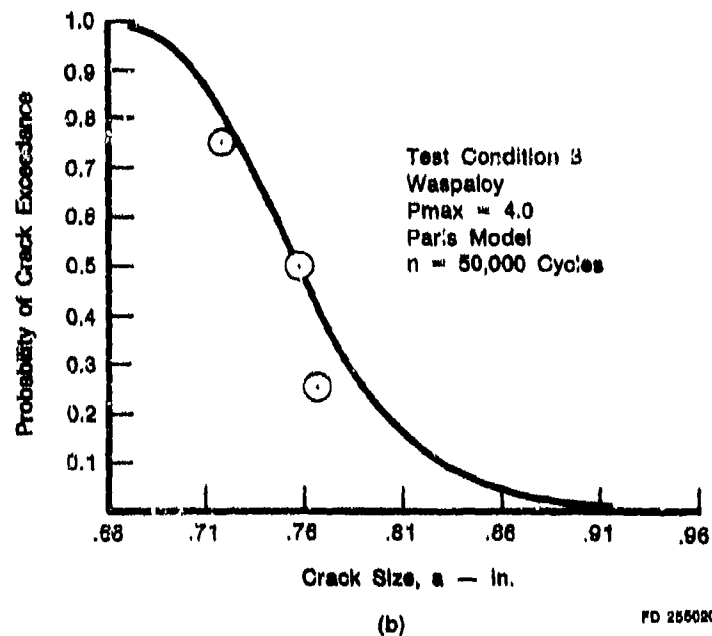
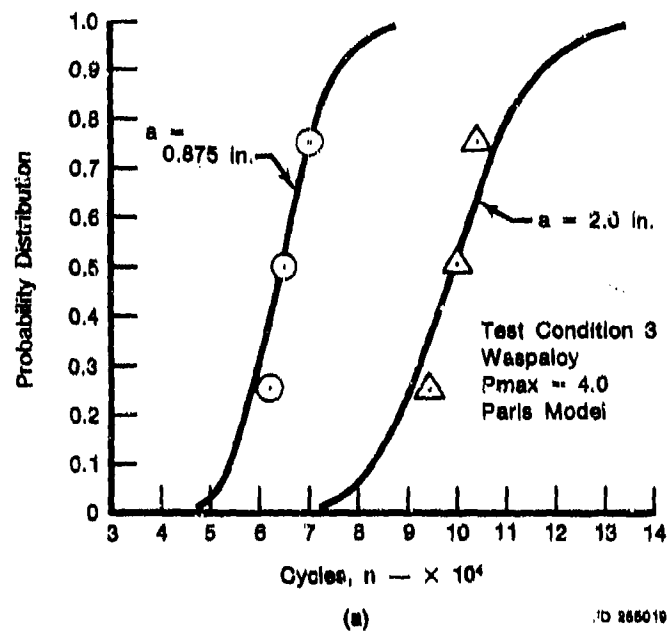
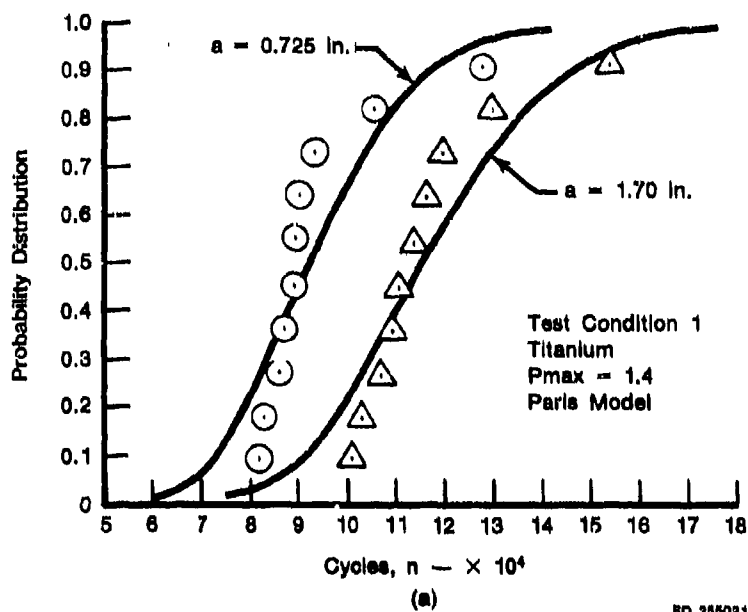
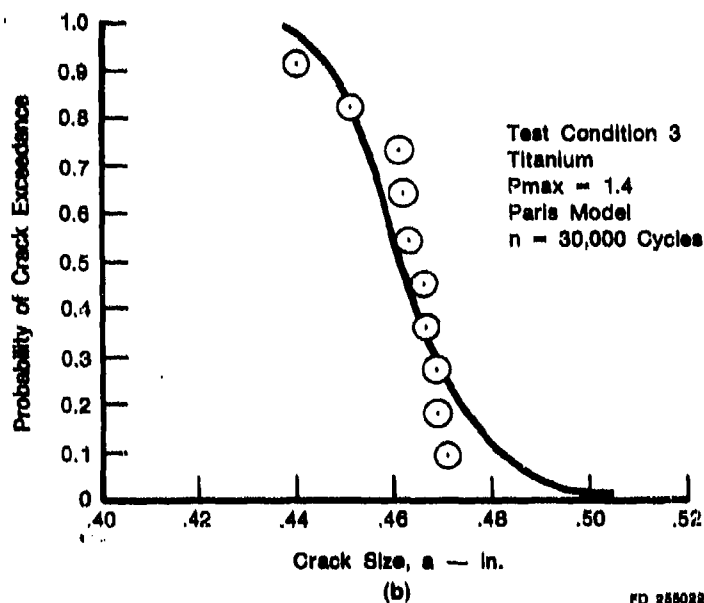


Figure 39. Distribution Curve and Crack Exceedance Curve for Waspaloy for Test Condition No. 3, Using the Paris Model; (a) Distribution of Cycles to Reach Given Crack Size, and (b) Crack Exceedance Curve After 50,000 Cycles



FD 255021



FD 255022

Figure 40. Distribution Curve and Crack Exceedance Curve for Titanium for Test Condition No. 1, Using the Paris Model; (a) Distribution of Cycles to Reach Given Crack Size, and (b) Crack Exceedance Curve After 30,000 Cycles

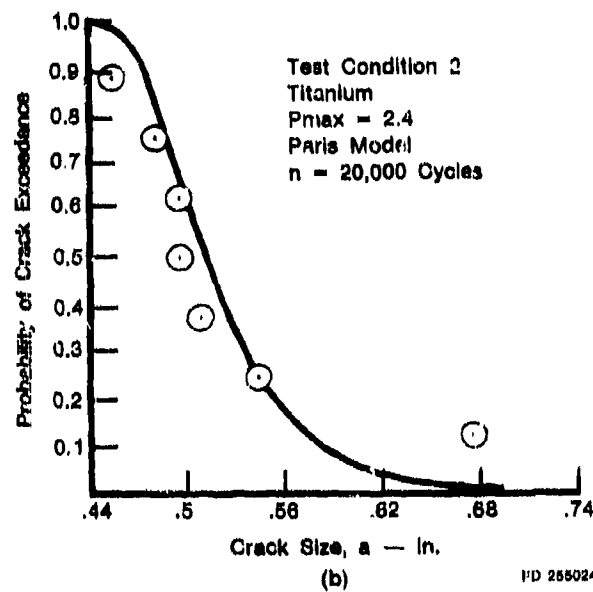
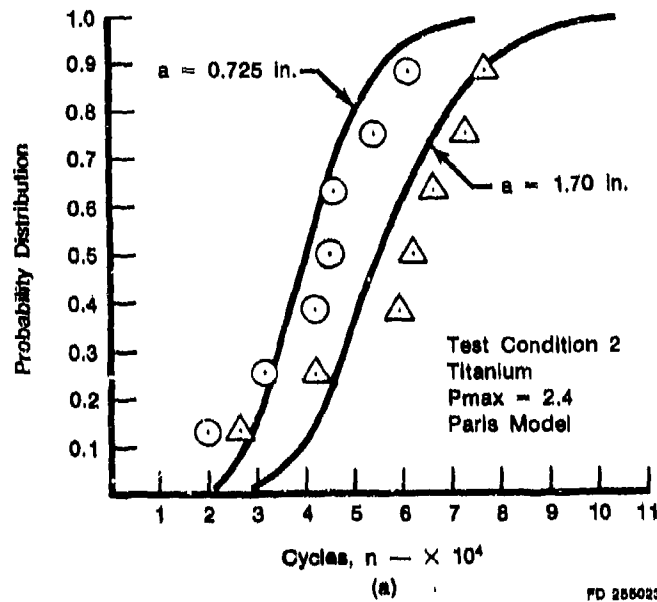
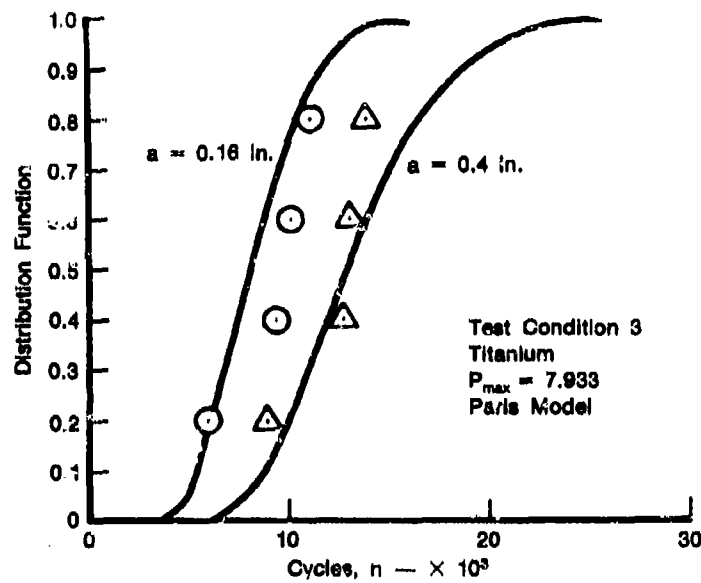
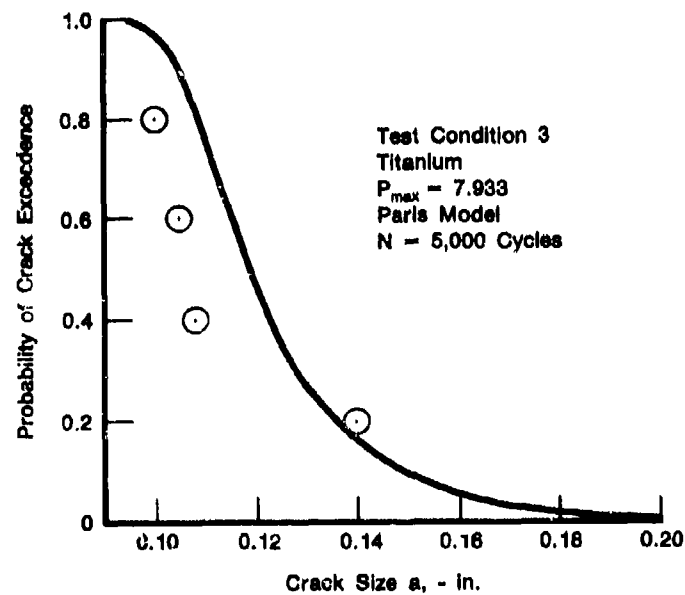


Figure 41. Distribution Curve and Crack Exceedance Curve for Titanium for Test Condition No. 2, Using the Paris Model; (a) Distribution of Cycles to Reach Given Crack Size, and (b) Crack Exceedance Curve After 20,000 Cycles

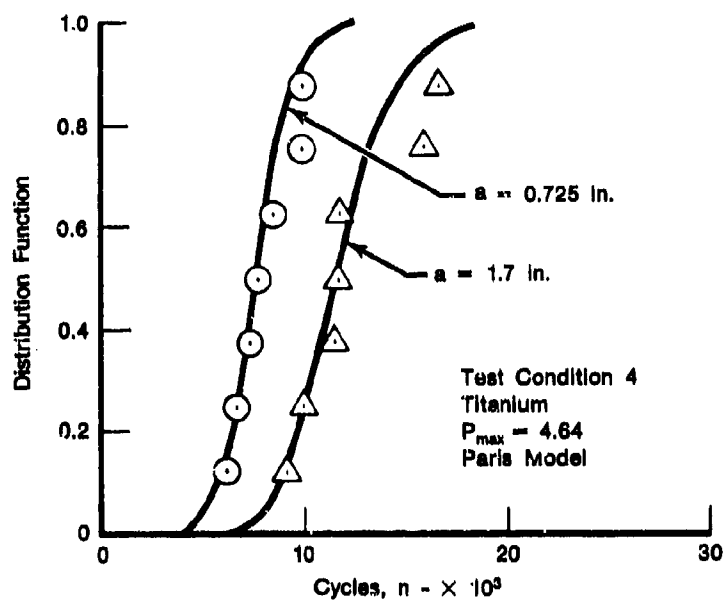


(a)

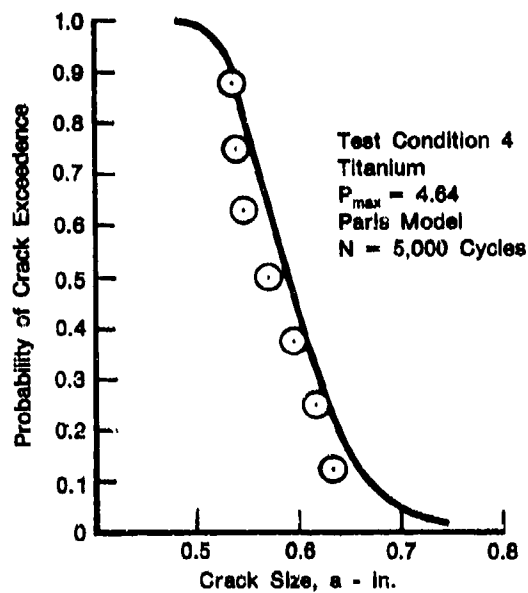


(b)

Figure 12. Distribution of Cycles to Reach Given Crack Size for Titanium for Test Condition No. 3, Using the Paris Model; (a) Distribution of Cycles to Reach Given Crack Size, and (b) Crack Exceedence Curve After 5,000 Cycles



(a)



(b)

Figure 43. Distribution of Cycles to Reach Given Crack Size for Titanium for Test Condition No. 4, Using the Paris Model; (a) Distribution of Cycles to Reach Given Crack Size, and (b) Crack Exceedance Curve After 5,000 Cycles

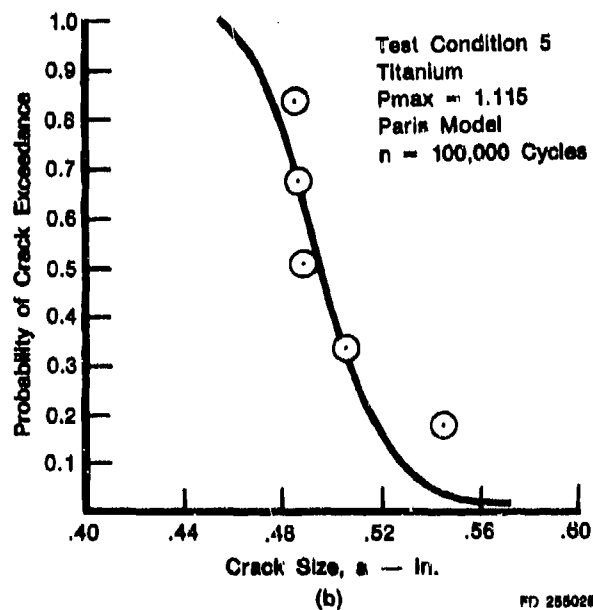
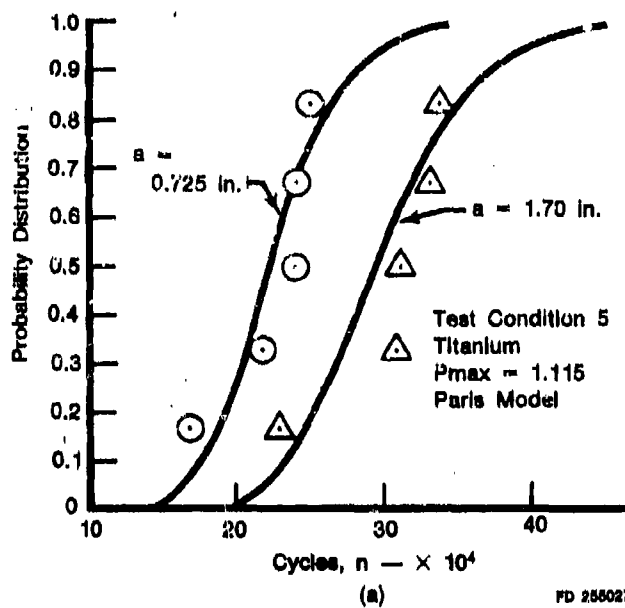


Figure 44. Distribution Curve and Crack Exceedance Curve for Titanium for Test Condition No. 5, Using the Paris Model; (a) Distribution of Cycles to Reach Given Crack Size, and (b) Crack Exceedance Curve After 100,000 Cycles

SECTION V

STATISTICAL ANALYSIS OF A HOMOGENEOUS DATA SET

A homogeneous crack propagation data set for 2024-T3 aluminum center-cracked specimens under constant amplitude cyclic loading generated in References 3 and 4 is analyzed. The lognormal statistical model, developed under the present program, and an advanced model currently being developed under another program, have been used. The results of such analyses reveal the importance of both the selection of the crack growth rate function and the data analysis technique used for deriving the crack growth rate data from the experimental measurements.

Sixty-four sample functions for the crack growth damage accumulation, a , versus the number of load cycles, n , are shown in Figure 45. The initial half-crack length is 9 mm and the final half-crack length is 49.8 mm. The crack growth rate data, da/dn , versus the stress intensity range, ΔK , are derived from Figure 45 using the seven-point polynomial method and the secant method. Based on the hyperbolic sine crack growth rate function, (Equation 1), the method of maximum likelihood is employed to estimate the parameters C_2 , C_3 , C_4 and the standard deviation $\sigma_y = \sigma_x$ (see Reference 1). The results are shown in Table 17. It is observed from Table 17 that the statistical dispersion of the crack growth rate, da/dn , is smaller when the seven-point polynomial method is applied.

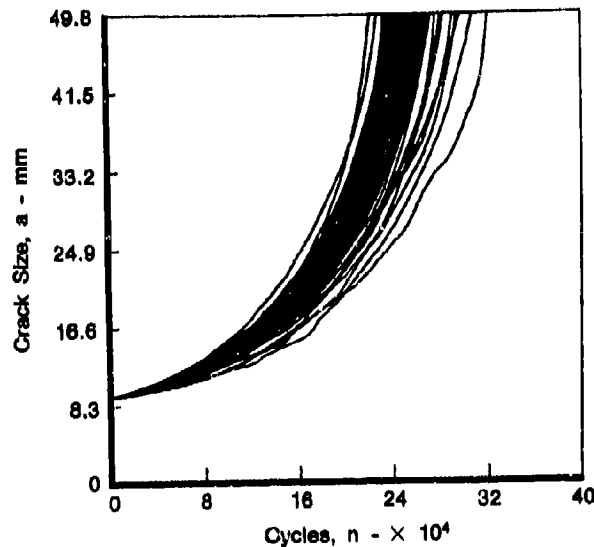


Figure 45. Homogeneous Data Set of Virkler, et al. with $P_{max} = 23.35$ kn and $R = 0.2$

Using the lognormal statistical model and integrating the crack growth rate equation (Equation 1), for different γ percentiles, one obtains the distribution of the half-crack length as a function of load cycles n . The results are shown in Figure 46, in which the seven-point polynomial method has been used. Note that the stress intensity range ΔK for the CCT specimen is given by

$$\Delta K = \frac{\Delta P}{BW} \sqrt{\frac{\pi a}{2} \sec(\pi a/2W)} \quad (30)$$

TABLE 17. MAXIMUM LIKELIHOOD ESTIMATE OF C_2 , C_3 , C_4 ,
STANDARD DEVIATION $\sigma_y = \sigma_x$ AND COEFFICIENT OF
VARIATION, V , OF da/dn ; $C_1 = 0.5$

Analysis Technique	C_2	C_3	C_4	$\sigma_y = \sigma_x$	V
7-Point Polynomial	3.4477	-1.3902	-4.5348	0.08235	19.13%
Secant method	5.0148	-1.1336	-5.0733	0.09569	22.35%

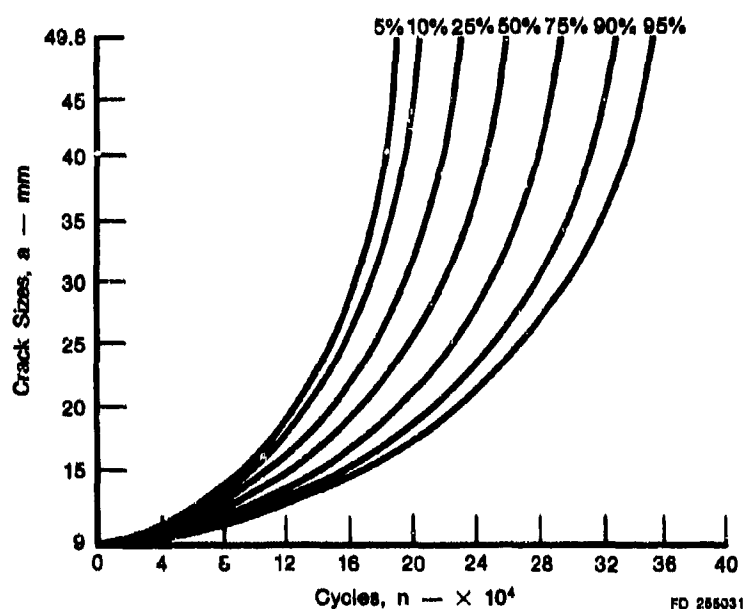


Figure 46. Lognormal Statistical Model Prediction of Virkler, et al. Data Set

A comparison between Figures 45 and 46 indicates that the lognormal statistical model correlates well with the test results for the 50% crack propagation life. However, the statistical dispersion of the crack growth damage accumulation based on the model is larger than the experimental test results.

The distribution functions for the number of cycles to reach half-crack lengths of 21 mm and 49.8 mm are presented in Figures 47 and 48, respectively. In these figures, the solid curve and the dashed curve represent the results based on the lognormal statistical model. The former is obtained using the 7-point polynomial method, whereas the latter is obtained using the secant method. The experimental test results, Figure 45, are shown by circles in Figures 47 and 48.

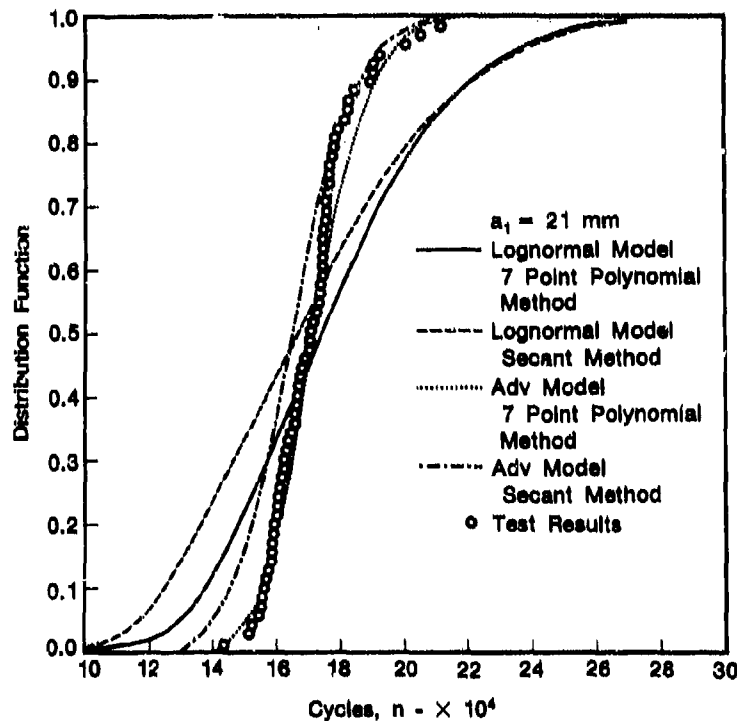


Figure 47. Distribution Function of Number of Cycles to Reach 21mm Half-Crack Length

The probabilities of crack exceedance at $n = 150,000$ cycles are shown in Figure 49 as a solid curve, a dashed curve, and circles which have the same meaning as those in Figures 47 and 48.

As observed from Figures 47 through 49, the correlation between the lognormal statistical model and the test results is very good for the 50% crack propagation life. However, the model predicts a larger statistical dispersion for crack growth damage accumulation than the actual test data which results in a conservative prediction for the crack propagation life. Furthermore, the seven-point polynomial method appears to be superior to the secant method.

The observation that the lognormal statistical model results in a larger statistical dispersion for the crack growth damage accumulation was expected as described in Reference 1. This stems from the assumption that the crack growth rate is completely correlated and hence Z is a random variable. At another extreme, when the crack growth rate is assumed to be completely uncorrelated at any two different values of $\log \Delta K$, one obtains a white noise process. The white noise process model results in the smallest statistical dispersion for the crack propagation life (Reference 1) as evidenced by the results presented in References 3 and 4. However, for the white noise model, the prediction for the crack propagation life is unconservative.

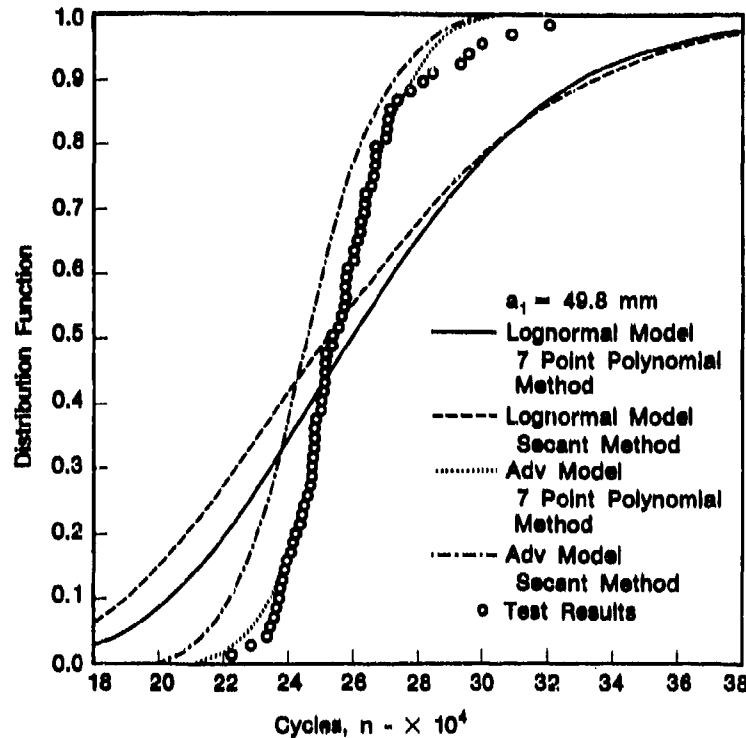


Figure 48. Distribution Function of Number of Cycles to Reach 49.8mm Half-Crack Length

The actual test results in Figure 45 indicate a definite correlation for the crack growth rate at different values of $\log \Delta K$. Therefore, a statistical model taking into account such a correlation has been explored in Section VI, which is referred to as the advanced statistical model. A complete development for the analytical solution of such a model has been accomplished under the sponsorship of another program (Reference 28). It can be shown that the statistical dispersion of the crack propagation life decreases as the correlation for the crack growth rate reduces.

Based on the advanced model with the correlation parameter $\Delta = 40,000$ (see Section VI), the distribution functions for the number of cycles to reach half-crack lengths 21 mm and 49.8 mm are indicated by dotted and dash-dot curves in Figures 47 and 48. The dotted curve represents the results of the advanced model using the seven-point polynomial method, while the dash-dot curve denotes the results using the secant method. Similarly, the crack exceedance curve at $n = 150,000$ cycles is shown in Figure 49 by dotted curve and dash-dot curve having the same meaning as those in Figures 47 and 48.

As indicated from Figures 47 through 49, the advanced model with the method of seven-point polynomial correlates well with the experimental test data (circles). For the advanced model, the 7-point polynomial method is definitely superior to the secant method.

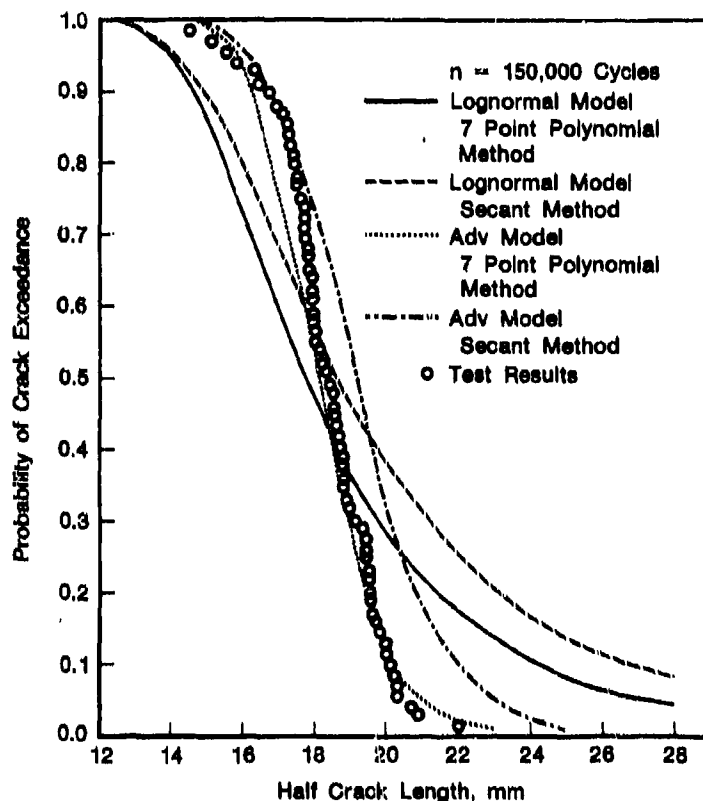


Figure 49. Crack Exceedance Curves at 150,000 Cycles

In conclusion, the Paris crack growth rate function, Equation 13, has been used in conjunction with both the lognormal and advanced statistical models. The correlation between the test data and the prediction based on the Paris crack growth rate function is extremely poor even for the 50% crack propagation life. Therefore, it is not worthwhile to present the results.

The results of analyses for the homogeneous data set presented above indicate two salient features associated with the prediction of fatigue crack propagation. For a particular type of specimen under a particular type of fatigue loading, one should select a crack growth rate function which can best describe the crack growth rate behavior. For the homogeneous data set analyzed, the hyperbolic sine function fit the crack growth rate data very well, whereas the Paris function did not. Using the method of maximum likelihood, the goodness-of-fit can be judged from the standard deviation $\sigma_y = \sigma_x$. A crack growth rate function has a better fit if the corresponding standard deviation σ_x is smaller.

Data for the crack size, a , versus the number of load cycles, n , are measured directly from experiments. Then, the crack growth rate data are derived from a versus n measurements. Various analysis techniques for obtaining the crack growth rate data have been proposed in the literature, such as the secant method, the method of seven-point polynomial, etc. Unfortunately, the accuracy for the statistical prediction of fatigue crack propagation depends on the data reduction methodology employed. Further research is needed to identify a best technique for the reduction of the crack growth rate data as well as the measurements of a versus n .

SECTION VI

ADVANCED STATISTICAL MODEL FOR FATIGUE CRACK GROWTH

Several mathematical models have been proposed for the prediction of crack growth damage accumulation for structures under dynamic loads based on the principles of fracture mechanics (References 6 and 7). These models have the general form of

$$\frac{da}{dt} = Q(K, \Delta K, s, a, R) \quad (31)$$

where $a(t)$ = crack size at time t , Q = a non-negative function, K = stress intensity factor, ΔK = stress intensity range, s = stress amplitude, R = stress ratio. For instance, the well-known Paris model is given by

$$\frac{da}{dt} = Q_1(\Delta K)^b \quad (32)$$

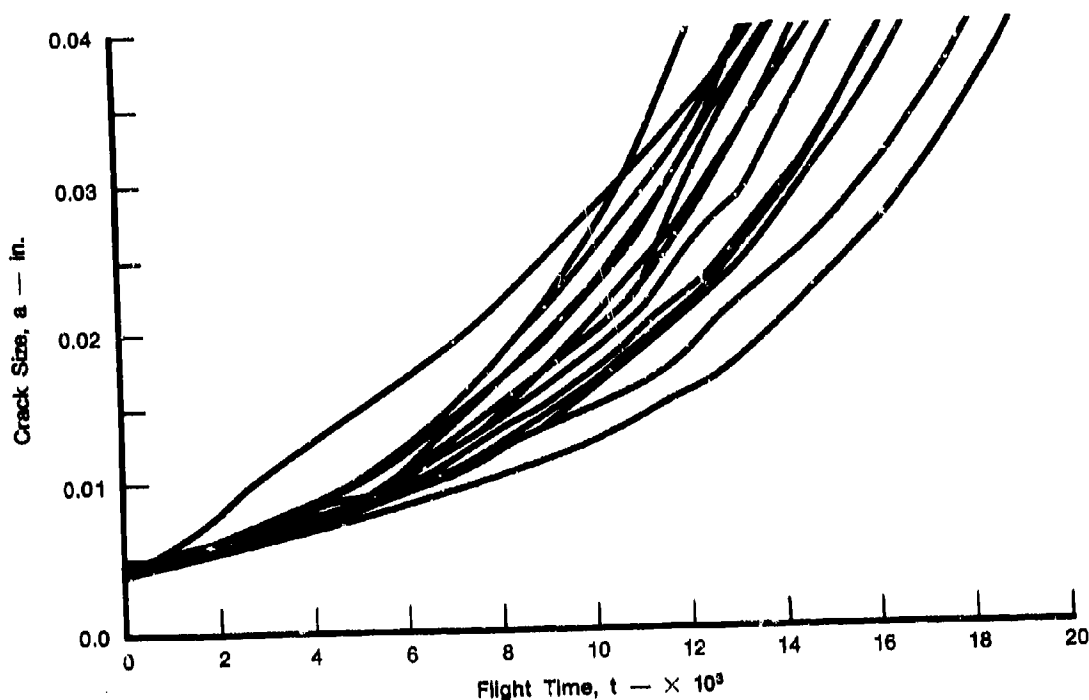
$$\Delta K = \alpha(a) \Delta s \sqrt{\pi a} \quad (33)$$

where Δs = stress range, $\alpha(\)$ = a function depending on the specimen and crack geometries. However, even in a well-controlled laboratory environment, results obtained from crack growth experiments under either a constant-amplitude cyclic loading or a given spectrum loading usually exhibit considerable statistical variability. This is illustrated in Figure 50, which shows the actual crack growth records of some fastener hole specimens subjected to the excitation of a specific load spectrum in a laboratory. It is, therefore, not surprising to find that statistical analyses have been applied quite frequently to such problems in recent years (References 6 through 22).

If we restrict our attention to a laboratory setting so that the loading time-variation is deterministic, then the mathematical model, Equation (1), can be "randomized" as follows:

$$\frac{d\bar{a}}{dt} = Q(K, \Delta K, s, \bar{a}, R) X(t) \quad (34)$$

where the additional factor $X(t)$ is a non-negative random process, and $\bar{a}(t)$ is a random process representing the crack length at time t . It is of interest to note that Virkler, Hillberry and Goel (References 3 and 4) have undertaken simulation studies of crack propagation which amount to assuming $X(t)$ in Equation (34) to be totally uncorrelated at any two different times. At the other extreme, Yang (References 1, 22, 17) has replaced the random process $X(t)$ in Equation (34) with a random variable, which is equivalent to the case where $X(t)$ is totally correlated at all times. It was pointed out in Reference 1 that a totally uncorrelated $X(t)$ would lead to the smallest statistical dispersion and a totally correlated $X(t)$ to the greatest statistical dispersion for the time at which a given crack size is reached. A more realistic modeling of fatigue crack growth should lie somewhere between the two extremes. Therefore, the ability to account for an arbitrary correlation in $X(t)$ is a major consideration in the present section.



FD 255038

Figure 50. Actual Crack Propagation Time-Histories of Some WPB Fastener Holes

From the standpoint of fatigue design and schedule maintenance (References 11, 14, 15), two types of statistical information are of interest: the distribution of the random crack size at any given time, and the distribution of the random time to reach a given crack size. As shown in Reference 1, these two problems are interrelated. Attention will be focused on the statistical properties of the latter problem. In particular, analytical solutions will be given for the statistical moments of the random time to reach any crack size, given the knowledge of an initial size. A procedure to estimate the parameters in a power-law mathematical model also will be presented, using the fractographical results (Reference 23) of some 7475-T7351 aluminum fastener hole specimens subjected to the excitation of a bomber load spectrum.

1. Model for $X(t)$

We shall model $X(t)$ as a random pulse train (see Reference 24), i.e.,

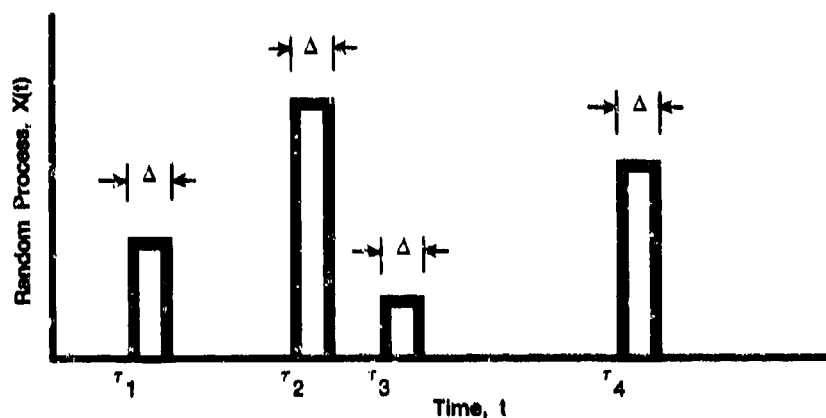
$$X(t) = \sum_{k=1}^{N(t)} Z_k w(t, \tau_k) \quad (35)$$

where $N(t)$ = a homogeneous Poisson counting process, giving the total number of pulses that arrive within the time interval $(-\infty, t)$; τ_k = the arrival time of the k th pulse; Z_k = the random amplitude of the k th pulse, and

$$w(t, \tau) = w(t - \tau) = \begin{cases} 1, & 0 < t - \tau \leq \Delta \\ 0, & \text{otherwise} \end{cases} \quad (36)$$

We further assume that Z_k for different k are independent, identically distributed random variables, with a common probability distribution Z .

A typical sample function of $X(t)$ is shown in Figure 51.



FD 255037

Figure 51. Typical Sample Function of Random Process $X(t)$

The statistical properties of $X(t)$ can be described by its cumulant (or semi-invariant) functions. The m th cumulant function is given by:

$$K_m[X(t_1), \dots, X(t_m)] = E[Z^m] \lambda \int_{-\infty}^{\min(t_1, \dots, t_m)} w(t_1 - \tau) \dots w(t_m - \tau) d\tau \quad (37)$$

in which $E[\]$ denotes an ensemble average, λ is the average arrival rate of the Poisson process, and $\min(\)$ indicates the smallest of the parenthesized quantities. In particular, the first cumulant is the mean function, and the second cumulant is the covariance function. These are found to be:

$$\begin{aligned} \mu &= E[X(t)] = E[Z] \lambda \int_{-\infty}^t w(t - \tau) d\tau \\ &= E[Z] \lambda \int_0^{\infty} w(u) du = E[Z] \lambda \Delta \end{aligned} \quad (38)$$

and

$$\begin{aligned}
\text{Cov}[X(t_1), X(t_2)] &= E[Z^2] \lambda \int_{-\infty}^{t_1} w(t_1 - \tau) w(t_2 - \tau) d\tau \\
&= E[Z^2] \lambda \int_0^{\infty} w(u) w(t_2 - t_1 + u) du \\
&= \begin{cases} 2\beta(1 - |t_2 - t_1|/\Delta), & |t_2 - t_1| < \Delta \\ 0, & |t_2 - t_1| \geq \Delta \end{cases}
\end{aligned} \tag{39}$$

in which $\beta = \frac{1}{2} E[Z^2] \lambda \Delta$.

2. Approximation of $\bar{a}(t)$ by a Markov Random Process

We now re-write Equation (34) as follows:

$$\frac{d\bar{a}}{dt} = Q(\bar{a})[\mu + Y(t)] \tag{40}$$

where the dependence of Q on K , ΔK , s and R has been suppressed for simplicity. Clearly, $Y(t)$ is a random process with a zero mean and the correlation function of $Y(t)$ is the same as the covariance function of $X(t)$; namely,

$$R_{YY}(\tau) = E[Y(t) Y(t+\tau)] = \begin{cases} 2\beta(1 - |\tau|/\Delta), & |\tau| < \Delta \\ 0, & \text{otherwise} \end{cases} \tag{41}$$

A sketch of this correlation function is shown in Figure 52. If the correlation time of $Y(t)$ is short compared with the characteristic time of $\bar{a}(t)$, then $\bar{a}(t)$ is close to a diffusive Markov process (Reference 25) which is governed by an Ito's stochastic differential equation (Reference 26):

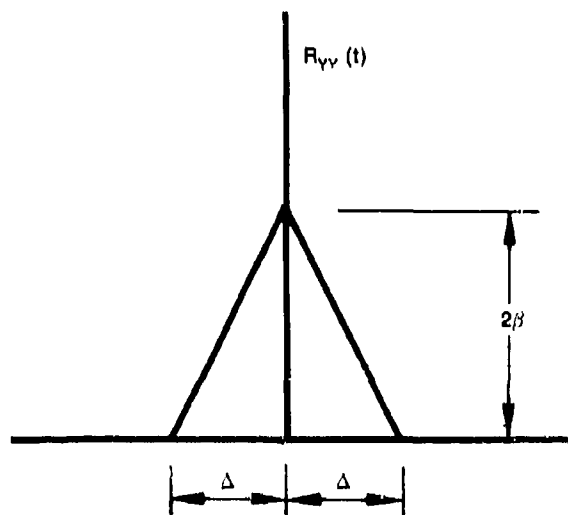
$$d\bar{a} = m(\bar{a}, t)dt + \sigma(\bar{a}, t)dB(t) \tag{42}$$

where m is called the drift coefficient, σ the diffusion coefficient, and $B(t)$ is a unit Brownian motion process (also called the Wiener's process), which has the property that $dB(t_1)$ and $dB(t_2)$ are independent for $t_1 \neq t_2$.

The correlation time of $Y(t)$ may be defined as follows:

$$\tau_{cor} = \frac{\int_0^{\infty} \tau |R_{YY}(\tau)| d\tau}{\int_0^{\infty} |R_{YY}(\tau)| d\tau} \tag{43}$$

Substitution of Equation (41) into Equation (43) results in $\tau_{cor} = \Delta/3$.



FD 255639

Figure 52. Autocorrelation Function of Random Process $Y(t)$

Strictly speaking, the $\bar{a}(t)$ process in Equation (42) is an approximation of that in Equation (40), and they could be represented more clearly by two different symbols; however, the same symbol will be used in this report for both processes as long as no confusion will result.

Stratonovich (Reference 25) has given the required formulas to compute the drift and diffusion coefficients from the original physical equation when the Markov approximation is justified. In the case of Equation (40)

$$\begin{aligned} m &= Q\mu + \int_{-\tau_0}^0 Q \frac{Q}{a} E[Y(t)Y(t+\tau)]d\tau \\ &= Q\mu + Q \frac{Q}{a} \beta\Delta = Q\left(\mu + \beta\Delta \frac{Q}{a}\right) \end{aligned} \quad (44)$$

$$\sigma^2 = 2 \int_{-\tau_0}^0 Q^2 E[Y(t)Y(t+\tau)]d\tau = 2Q^2\beta\Delta \quad (45)$$

where $\tau_0 > \Delta$. These equations imply that Q and $\partial Q/\partial a$ vary slowly within the integration interval to justify their being taken outside the integrals. Thus, the integrals account basically for the contribution towards the drift and diffusion due to the correlation between the past and the present "excitations" $Y(t)$. This contribution is *lumped* at the *present*, when m and σ are used in Equation (42). The replacement of Equation (40) by Equation (42) amounts to substituting $Y(t)$ by a white noise. Theoretically, the substitution introduces a small error associated with a small probability for da to become negative. This error is negligible so long as the drift dominates the diffusion, which should be verified in each practical case. Stratonovich's formulas are applicable to other types of correlation functions for $Y(t)$ as long as Q and dQ/da vary slowly within an interval of τ where such a correlation is not negligibly small. In this case, the lower limit of integration can even be extended to $-\infty$. Stratonovich's method is known as the stochastic averaging method, originally proposed on a physical ground, but later proved rigorously by Khasminskii (Reference 27) and given a rigorous mathematical interpretation.

The transition probability density $q_a(a, t | a_0, t_0)$ of the Markov process $\bar{a}(t)$ is a conditional probability density which describes the distribution of $\bar{a}(t)$ under the condition that the initial crack size is $\bar{a}(t_0) = a_0$ at an earlier time t_0 . It is governed by the following Fokker-Planck equation (Reference 26):

$$\frac{q_a}{t} + \frac{1}{a} \left[Q \left(\mu + \beta \Delta \frac{Q}{a} \right) q_a \right] - \frac{1}{a^2} (Q^2 \beta \Delta q_a) = 0 \quad (46)$$

or by the adjoint of Equation (46):

$$\frac{q_a}{t_0} + \left[Q \left(\mu + \beta \Delta \frac{Q}{a_0} \right) \right] \frac{q_a}{a_0} + Q^2 \beta \Delta \frac{1}{a_0^2} q_a = 0 \quad (47)$$

subject to the condition,

$$q_a(a, t_0 | a_0, t_0) = \delta(a - a_0) \quad (48)$$

In Equation (46) Q is treated as a function of " a " which is a sample value of the crack size $\bar{a}(t)$, whereas in Equation (47) it is treated as a function of a_0 . These equations are also known as the Kolmogorov's forward and backward equations, respectively.

3. Time to Reach a Given Crack Size

We now focus our attention on the random time when the crack size $\bar{a}(t)$ reaches a specific value a_c . This event may be considered as the passage for the first time across an absorbing boundary. Introduce $g(a, t | a_0, t_0)$ such that

$$g(a, t | a_0, t_0) da = \text{Prob} | a \leq \bar{a}(t) \leq a + da | a_0 \leq \bar{a}(\tau) < a_c, t_0 \leq \tau < t, \\ a_0 \leq a < a_c \quad (49)$$

Although g is similar to q_{a_a} , it is not a probability density since its integration on a from a_0 to a_c is generally smaller than one. In fact, g describes only the sample functions which do not reach the absorbing boundary a_c before time t . However, g also satisfies the Kolmogorov backward equation, Equation (47).

The integration of g yields

$$G(t) = \int_{a_0}^{a_c} g(a, t | a_0, t_0) da \\ = \text{Prob survival in } (t_0, t) | \bar{a}(t_0) = a_0 \quad (50)$$

Here the dependence of G on a_0 and t_0 has been suppressed. The $G(t)$ function also satisfies the Kolmogorov backward equation, namely,

$$\frac{G}{t_0} + Q \left(\mu + \beta \Delta \frac{Q}{a_0} \right) \frac{G}{a_0} + Q^2 \beta \Delta \frac{1}{a_0^2} G = 0 \quad (51)$$

subject to the following conditions:

$$G(t_0) = 1 \quad (52)$$

$$G(\infty) = 0 \quad (53)$$

Condition (53) indicates that sooner or later fatigue failure will occur. Letting $\tau = t - t_0$, we obtain

$$-\frac{\partial G}{\partial \tau} + Q\left(\mu + \beta \Delta \frac{\partial Q}{\partial a_0}\right) \frac{\partial G}{\partial a_0} + Q^2 \beta \Delta \frac{\partial^2}{\partial a_0^2} G = 0 \quad (54)$$

Now $G(t_0) - G(t) = 1 - G(t)$ is the probability that first passage (reaching the crack size a_c) occurs prior to t . This is the distribution function of the random first passage time T ; i.e.,

$$F_T(\tau) = 1 - G(t_0 + \tau) \quad (55)$$

The probability density of T follows from a differentiation of Equation (55):

$$P_T(\tau) = -\frac{\partial}{\partial \tau} G(t_0 + \tau) \quad (56)$$

The average first passage time is

$$E[T] = -\int_0^\infty \tau \frac{\partial G}{\partial \tau} d\tau = \int_0^\infty G(t_0 + \tau) d\tau \quad (57)$$

In obtaining the second part of Equation (57) use has been made of the condition (53).

Integrating Equation (54) and using Equations (56) and (57), we obtain an equation for the average first passage time:

$$1 + Q\left(\mu + \beta \Delta \frac{\partial Q}{\partial a_0}\right) \frac{d}{da_0} E[T] + Q^2 \beta \Delta \frac{d^2}{da_0^2} E[T] = 0 \quad (58)$$

The above second order equation requires two boundary conditions, one of which is clearly

$$E[T] = 0, \quad \text{if } a_0 = a_c \quad (59)$$

We shall assume that another condition is

$$\frac{d}{da_0} E[T] = 0, \quad \text{if } a_0 = 0 \quad (60)$$

Equations for higher order moments can also be derived from Equation (54). Note that

$$E[T^n] = -\int_0^\infty \tau^n \frac{\partial G}{\partial \tau} d\tau = n \int_0^\infty \tau^{n-1} G(t_0 + \tau) d\tau \quad (61)$$

Multiplying Equation (54) by τ^n and integrating on τ , we obtain

$$(n+1)E[T^n] + Q \left(\mu + \beta \Delta \frac{\partial Q}{\partial a_0} \right) \frac{d}{da_0} E[T^{n+1}] + Q^2 \beta \Delta \frac{d^2}{da_0^2} E[T^{n+1}] = 0 \quad (62)$$

subject to the conditions:

$$E[T^{n+1}] = 0, \quad \text{if } a_0 = a_c \quad (63)$$

$$\frac{d}{da_0} E[T^{n+1}] = 0, \quad \text{if } a_0 = 0 \quad (64)$$

It is clear that Equation (64) which includes Equation (60) as a special case implies that $a_0 = 0$ is a reflective boundary. Equation (62) can be used recursively to obtain higher moments from the lower order moments. Equation (62) reduces to Equation (58) when $n = 0$.

Note that Equation (62) is first order in $dE[T^{n+1}]/da_0$ which can be solved readily. Let $Q = Q_0 f(a_0)$ where Q_0 has the unit of length/time and $f(\cdot)$ is a dimensionless function. We obtain

$$\frac{d}{da_0} E[T^{n+1}] = - \frac{1}{f} \exp \left(- \frac{\mu}{\beta \Delta} \int \frac{da_0}{Q} \right) J_n \quad (65)$$

where

$$J_n = \frac{n+1}{\mu Q_0} \int_0^{a_0} E[T^n] d \left[\exp \left(- \frac{\mu}{\beta \Delta} \int \frac{da_0}{Q} \right) \right] \quad (66)$$

in which the common practice of using the same symbol for the integration variable and limit of integration has been adopted for convenience. This solution satisfies condition (64). Equation (65) implies that $d/da_0 E[T^{n+1}]$ is nonpositive or $E[T^{n+1}]$ is non-increasing when the initial crack size a_0 is increased, which is physically reasonable.

The $(n+1)$ th moment of T follows from integration of Equation (65):

$$E[T^{n+1}] = - \int_{a_0}^{a_c} \frac{d}{da_0} E[T^{n+1}] da_0 \quad (67)$$

which satisfies condition (63).

4. Power-Law Crack Propagation

We now consider a special form for the Q function which has been proposed by several authors (References 13 through 16):

$$Q = Q_0 (\bar{a}/a_0)^b \quad (68)$$

and in the case of backward equations, we have $Q = Q_0(a_0/a_c)^b$. In this case, the integration in Equations (66) and (67) can be carried out in closed form. Specifically

$$\int \frac{da_0}{Q} = \begin{cases} \frac{a_c}{Q_0} \left(\frac{u^{1-b}}{1-b} \right), & b \neq 1 \\ \frac{a_c}{Q_0} \ln u, & b = 1 \end{cases} \quad (69)$$

where $u = a_0/a_c$. To compute $E[T]$, we require J_0 . From Equation (66) and with $n = 0$,

$$J_0 = \begin{cases} \frac{1}{Q_0 \mu} \left[\exp \left(\frac{k}{1-b} u^{1-b} \right) - H(1-b) \right], & b \neq 1 \\ \frac{1}{Q_0 \mu} u^k, & b = 1 \end{cases} \quad (70)$$

where $k = \frac{a_c \mu}{\beta \Delta Q_0}$ and H is the Heaviside function, i.e.,

$$H(1-b) = \begin{cases} 1, & b < 1 \\ 0, & b > 1 \end{cases} \quad (71)$$

Equations (69) and (70) are substituted into the expression for $dE[T]/da_0$ which is then integrated to obtain $E[T]$; the results are

$$E[T] = \begin{cases} \frac{a_c}{Q_0 \mu} \left\{ \frac{1}{1-b} (1 - u^{1-b}) + H(1-b) \left(\frac{1}{k} \right) \left[\exp \left(- \frac{k}{1-b} \right) - \exp \left(- \frac{k}{1-b} u^{1-b} \right) \right] \right\}, & b \neq 1 \\ - \frac{a_c}{Q_0 \mu} \ln u, & b = 1 \end{cases} \quad (72)$$

To compute $E[T^2]$ we require

$$J_1 = \frac{2}{\mu Q_0} \int_0^{a_0} E[T] d \left[\exp \left(\frac{\mu}{\beta \Delta} \int \frac{da_0}{Q} \right) \right] \quad (73)$$

Substituting Equation (72) into Equation (73), we obtain

$$\begin{aligned} \frac{Q_0^2 \mu^2}{2a_c} J_1 = & \left[\frac{1}{1-b} - \frac{1}{k} \left(\frac{k}{1-b} u^{1-b} - 1 \right) \right] \exp \left(\frac{k}{1-b} u^{1-b} \right) \\ & + H(1-b) \left\{ \frac{1}{k} \exp \left(- \frac{k}{1-b} \right) \left[\exp \left(\frac{k}{1-b} u^{1-b} \right) - 1 \right] \right. \\ & \left. - \frac{1}{1-b} (u^{1-b} + 1) - \frac{1}{k} \right\}, \quad b \neq 1 \end{aligned} \quad (74)$$

$$\frac{Q_0^2 \mu^2}{2a_c} J_1 = u^k \left(\frac{1}{k} - \ln u \right), \quad b = 1 \quad (75)$$

In obtaining Equation (75), we have used the formula

$$\begin{aligned} \int_0^1 u^a \ln u \, du &= - \int_0^1 u^a \, du \int_u^1 \frac{dv}{v} \\ &= (a+1)^{-2} x^{a+1} [(a+1) \ln x - 1] \end{aligned} \quad (76)$$

The second part of Equation (76) follows from changing the order of integration.

Substitute Equations (74) and (75), respectively, into the expression for $dE[T^2]/da_0$ and integrate:

$$\begin{aligned} \frac{Q_0^2 \mu^2}{2a_c^2} E[T^2] = & \frac{1}{1-b} \left(\frac{1}{1-b} + \frac{1}{k} \right) (1 - u^{1-b}) - \frac{1}{2(1-b)^2} (1 - u^{2(1-b)}) \\ & + H(1-b) \left\{ \frac{1}{k^2} + \exp \left(- \frac{k}{1-b} \right) \left[\frac{2}{k^2} + \frac{1}{k(1-b)} (3 - u^{1-b}) \right] \right. \\ & \left. - \exp \left(- \frac{k}{1-b} u^{1-b} \right) \left[\frac{1}{k(1-b)} (1 + u^{1-b}) + \frac{2}{k^2} + \frac{1}{k^2} \exp \left(\frac{k}{1-b} \right) \right] \right\}, \\ & b \neq 1 \end{aligned} \quad (77)$$

$$\frac{Q_0^2 \mu^2}{2a_c^2} E[T^2] = \ln u \left(\frac{1}{2} \ln u - \frac{1}{k} \right), \quad b = 1 \quad (78)$$

In obtaining Equation (78) we have used the formula:

$$\int_x^1 \frac{1}{u} \ln u \, du = - \int_x^1 \frac{1}{u} \, du \int_u^1 \frac{1}{v} \, dv = - \frac{1}{2} (\ln x)^2 \quad (79)$$

The second part of Equation (79) follows from an interchange of the order of integration.

5. Estimation of Model Parameters

The estimation of the parameters of a mathematical model will be illustrated by use of two examples. Refer again to Figure 50 which shows the crack propagation time-histories of some

specimens selected from the fractographical data of 7475-T7351 aluminum fastener holes available in Reference 23. The data set is identified as WPB, indicating that the specimens were drilled with Winslow Spacemetric machines (W), with a proper drilling technique (P), and subjected to a given B-1 bomber load spectrum (B). The data set has been censored to include only those specimens having fatigue crack growth through the crack length interval from 0.004 inch to 0.04 inch (corner crack). This censoring procedure is necessary in order to normalize the data set to zero life at 0.004 inch, thus obtaining a homogeneous crack growth data base. The resulting data set consists of 16 specimens. Within a small crack size range, the power-law propagation, Equation (68), was shown to be valid (References 13 through 17).

The parameters of our mathematical model, specialized to a power-law crack propagation that fits the behavior of the above WPB specimens, have been estimated using the experimental data. We began by taking logarithms on the two sides of Equation (68), with $Q \approx Q_0(a/a_c)^b$ to yield

$$\log \frac{da(t)}{dt} = b \log a(t) + \log(Q_0/a_c^b) + \log X(t) \quad (80)$$

Variations of $\log da/dt$ versus $\log a$ were plotted for the 16 specimens in the WPB data set as shown in Figure 53. Implicit in the mathematical model is the assumption that all points would fall along a single straight line if the random element $\log X(t)$ were not present. Since $X(t)$ has been assumed to be a stationary random process, the mean and the standard deviation of $\log X(t)$ are constants. A linear regression analysis was then carried out to estimate the slope, the intercept, and the standard deviation of the random element $\log X(t)$. The slope is equal to b , and the intercept is $\log(Q_0/a_c^b)$.

The results obtained from the 16 specimens are

$$b = 0.92971,$$

$$Q_0/a_c^b = 1.1051 \times 10^{-4},$$

$$\sigma_{\log X(t)} = 0.087635$$

The linear regression analysis implies that each point in Figure 53 has been treated as an independent sampling of a Gaussian random variable. Thus, estimates of the mean and variance of $X(t)$ itself can be computed from those of $\log X(t)$, using the log-normal to normal conversion formulas; namely,

$$\mu_X = \exp \left(\frac{1}{2} [\sigma_{\log X(t)} \ln 10]^2 \right) = \mu \quad (81)$$

$$\sigma_X^2 = \mu_X^2 \left\{ \exp [\sigma_{\log X(t)} \ln 10]^2 - 1 \right\} = 2\beta \quad (82)$$

Application of Equations (81) and (82) resulted in

$$\mu = 1.0206, \quad \beta = 0.021643$$

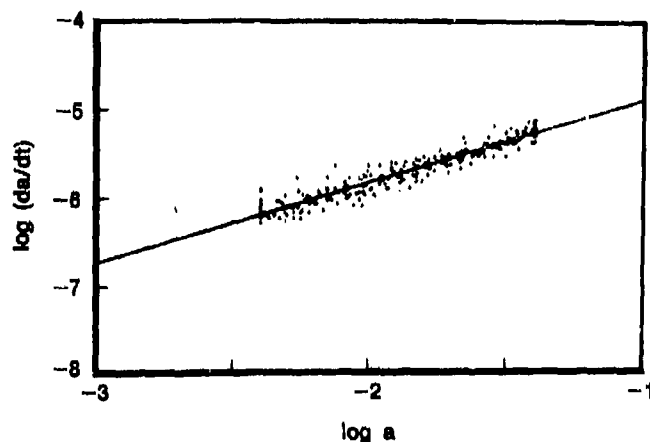


Figure 53. Regression Analysis for the Estimation of Model Parameters for WPB Fastener Holes

The rationale behind these conversion rules is the use of linear regression to obtain the mean and standard deviation for $\log X(t)$. It does not necessarily require that $X(t)$ must be log-normal. In fact, when the crack size $X(t)$ is treated as a diffusive Markov process in an approximate sense, the "excitation" process $X(t)$ is also effectively replaced by a constant mean μ plus a Gaussian white noise. Of course, this replacement excitation process cannot be log-normal.

Having the values of b , Q_0 , μ and β , the mean and mean-square values of the time T to reach a given crack size a_0 can be computed using Equations (72) and (78) for different values of $k = a_0\mu/(\beta\Delta Q_0)$, or equivalently for different values of Δ . Figure 54 shows the results of such computations, in terms of $E[T]$ and $E[T] \pm \sigma_T$, where $\sigma_T = (E[T^2] - E[T]^2)^{1/2}$ is the standard deviation of T . The mean values $E[T]$ are practically uninfluenced by the choice of Δ since the last two terms in Equation (72) are several orders of magnitude smaller than the first term. However, the statistical dispersion σ_T increases as Δ increases. This Δ - σ_T relationship agrees with our earlier observation concerning the results of Yang (References 1, 22), and of Virkler, Hillberry and Goel (References 3 and 4), the former case being equivalent to $\Delta \rightarrow \infty$ and the latter case to $\Delta \rightarrow 0$. Estimates of the mean $E[T]$ and standard deviation, σ_T , of T were also obtained directly from the data of the 16 specimens, and the results plotted in Figure 55. Comparison between Figures 54 and 55 shows that $\Delta = 8,000$ is a reasonable choice for this particular mathematical model and data set.

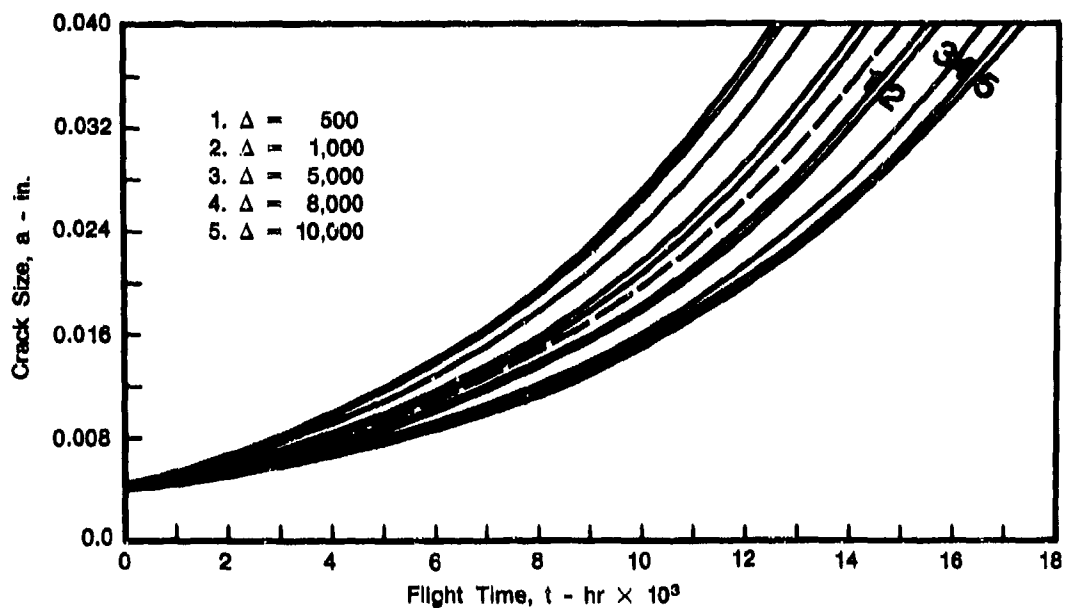


Figure 54. Theoretical Mean and Standard Deviation of Random Time to Reach Various Crack Sizes Computed for Different Δ Values for WPB Fastener Holes

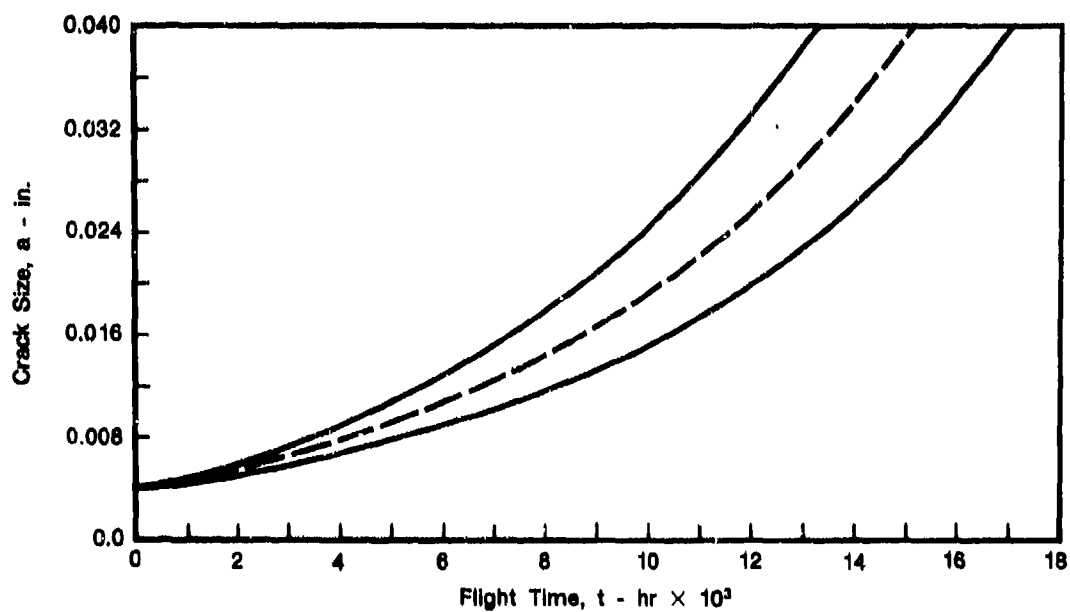


Figure 55. Mean and Standard Deviation of Random Time to Reach Various Crack Sizes Computed Directly from Some Actual Time-Histories of WPB Fastener Holes

Some computer simulated sample functions using the present mathematical model described in Equations (34) and (35) are shown in Figure 56. These have been obtained using parameters $\mu_x = 1.0206$, $\sigma_x^2 = 0.043286$, $b = 0.92971$, $Q_0/a_c^b = 1.1051 \times 10^{-4}$, $\Delta = 8,000$ and an average Poisson pulse rate of $\lambda = 0.1$. Their general characteristics are remarkably similar to the actual records in Figure 50.

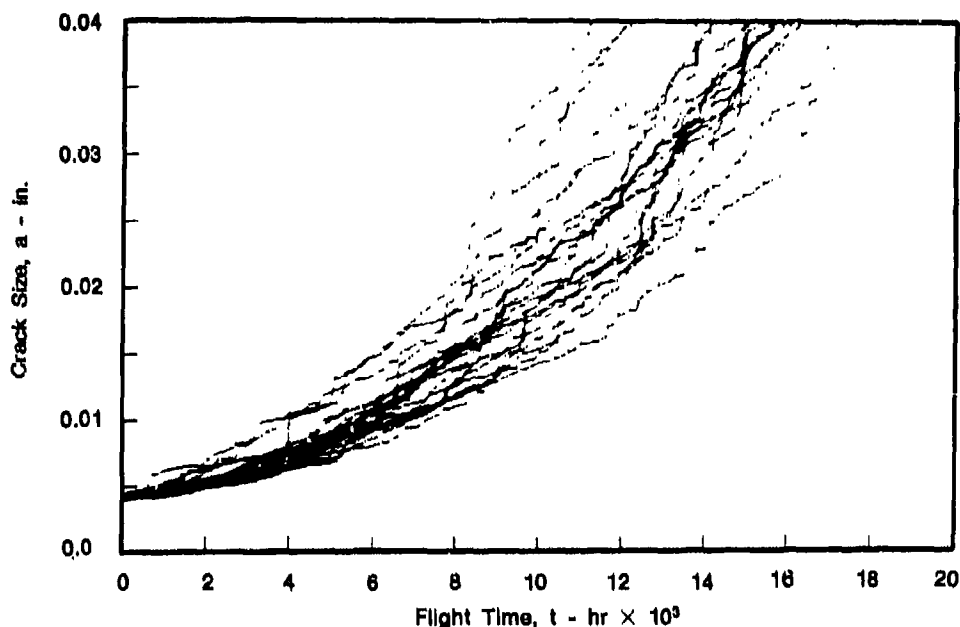


Figure 56. Simulated Sample Functions of Crack Propagation Time-Histories for WPB Fastener Holes

It has been suggested that the distribution of the time T to reach a given crack size a_c can be approximated by a two-parameter Weibull distribution (Reference 1),

$$F_T(t) = P[T \leq t] = 1 - \exp[-(t/\beta_0)^{\alpha_0}] \quad (83)$$

in which α_0 and β_0 are, of course, related to the values of $E[T]$ and σ_T . Approximate distribution functions of T thus computed are shown in Figure 57 as solid curves for $a_c = 0.01, 0.02$ and 0.04 inch, respectively. Also displayed in Figure 57 as circles, triangles and rectangles are the corresponding distributions of the test results obtained from Figure 50. It is observed from Figure 57 that on the basis of the approximation, Equation (83), the test results correlate very well with the present statistical fatigue crack propagation model.

For additional comparison, the above procedure has been applied to another set of data, to be referred to as XWPB where X signifies a 15% load transfer in the fasteners and WPB has the same meaning as before. This second data set also has been censored to include only those with a crack length growth from 0.004 to 0.07 inch, resulting in a total of 22 specimens. The crack propagation time-histories of these specimens are shown in Figure 58. The linear regression analysis for the estimation of model parameters, illustrated in Figure 59, resulted in

$$b = 0.985, Q_0/a_c^b = 2.4414 \times 10^{-4}, \sigma_{\log X(t)} = 0.12896$$

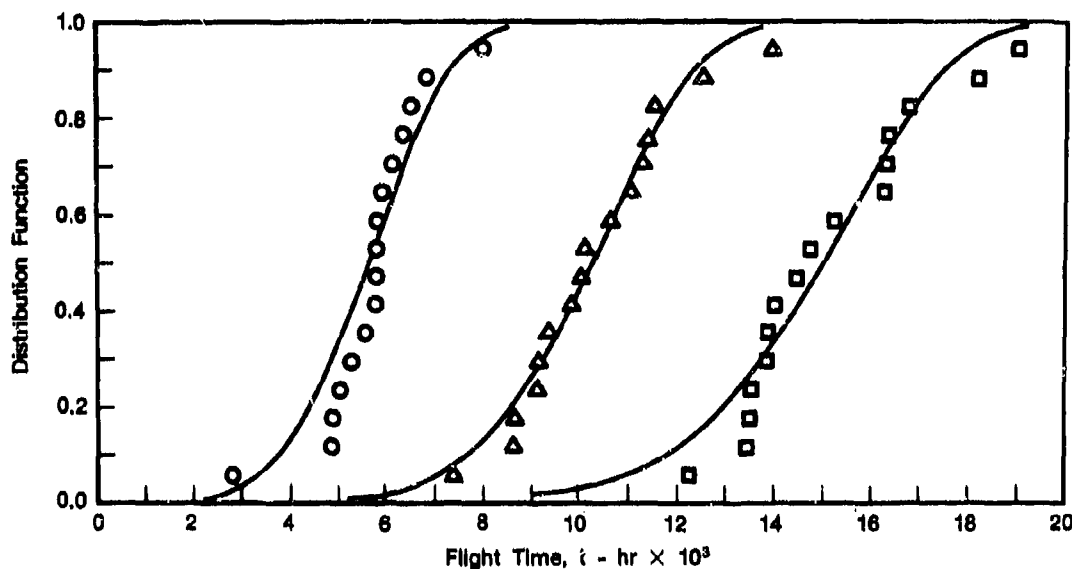


Figure 57. Comparison Between Weibull-Type Approximation for the Distributions of Random Time to Reach a Given Crack Size and Actual Test Results for WPE Fastener Holes

An application of Equations (81) and (82) yielded

$$\mu = 1.0451, \quad \beta = 0.0503$$

The computed $E[T] \pm \sigma_T$ curves for a number of Δ values are shown in Figure 60. When they are compared with the specimen mean and specimen standard deviation, shown in Figure 61, the best agreement is obtained for $\Delta = 8000$. Approximate distributions of the random times to $a_c = 0.008, 0.025$ and 0.07 , based on a Weibull form, Equation (83), are shown in Figure 62, along with the sample distributions. Computer generated simulations using $\Delta = 8000$ and $\lambda = 0.1$ are shown in Figure 63. Again, excellent theoretical and experimental correlations are seen in this second example.

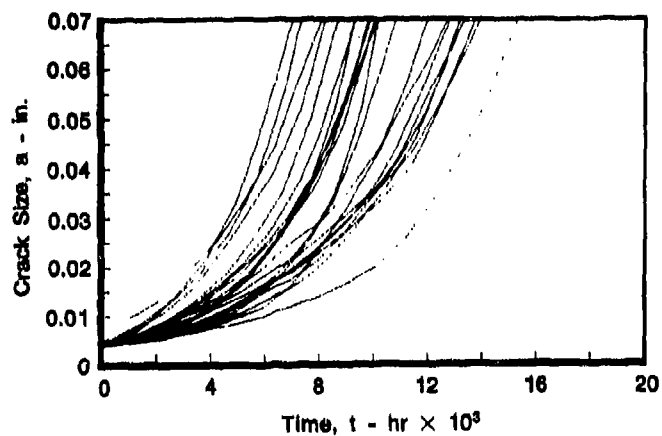


Figure 58. Actual Crack Propagation Time-Histories of Some XWPB Fastener Holes

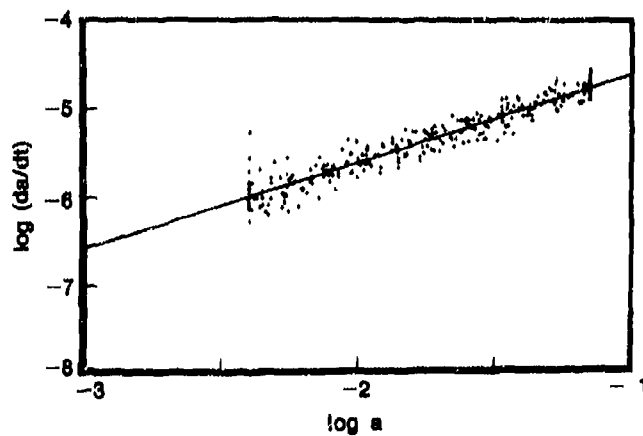


Figure 59. Regression Analysis for the Estimation of Model Parameters for XWPB Fastener Holes

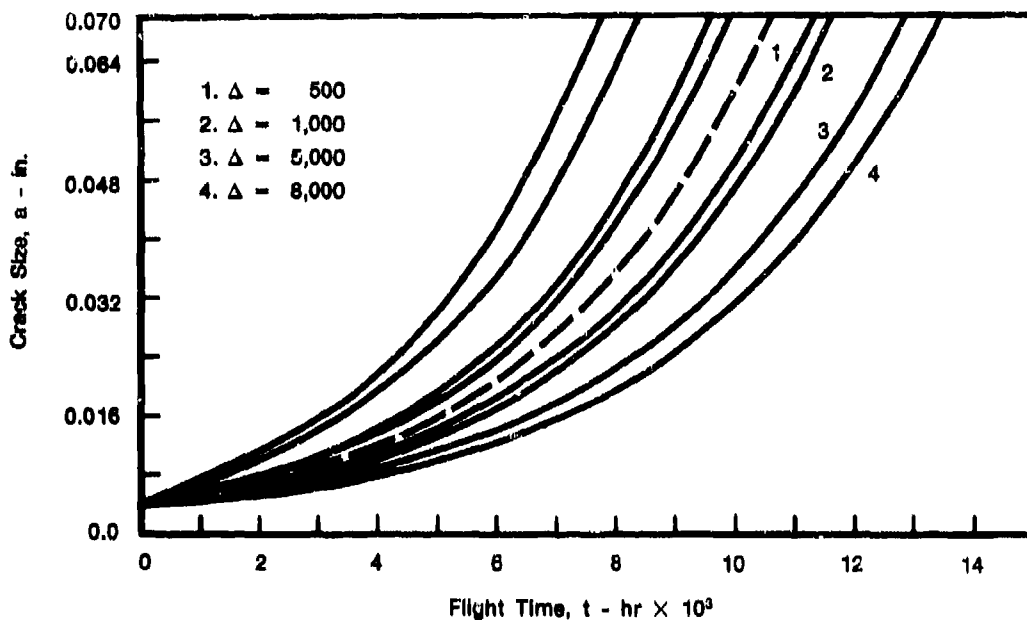


Figure 60. Theoretical Mean and Standard Deviation of Random Time to Reach Various Crack Sizes Computed for Different Δ Values for XWPB Fastener Holes

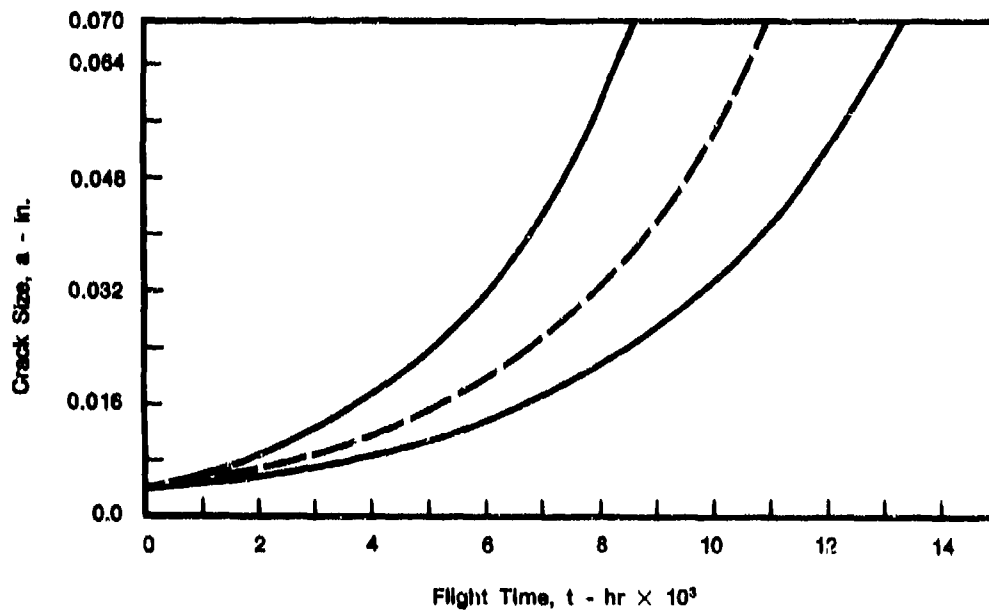


Figure 61. Mean and Standard Deviation of Random Time to Reach Various Crack Sizes Computed Directly from Some Actual Time-Histories of XWPB Fastener Holes

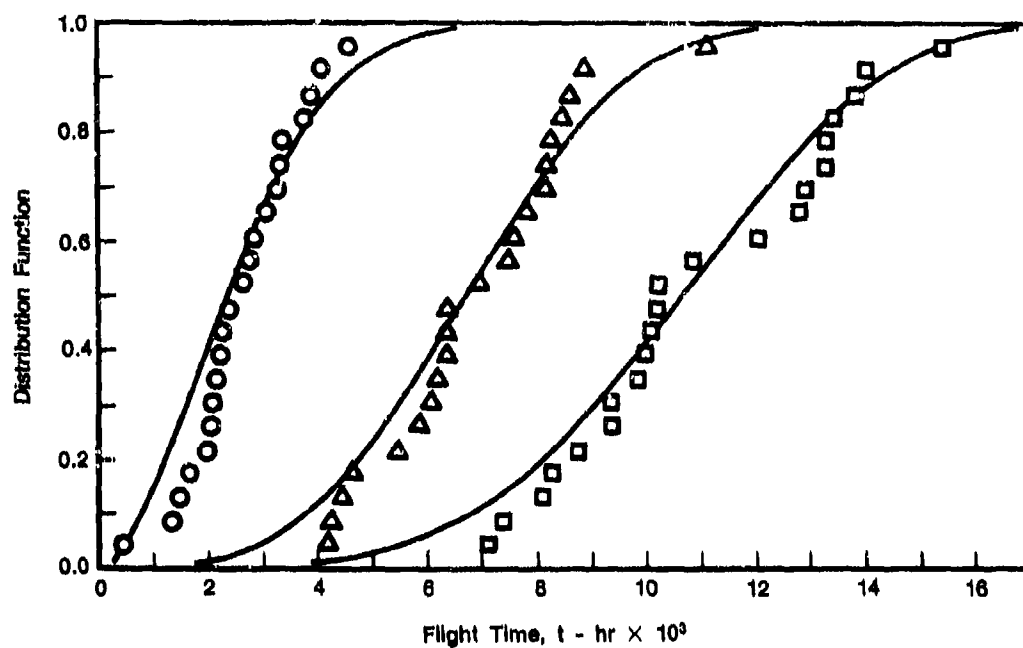


Figure 62. Comparison Between Weibull-Type Approximation for the Distribution of Random Time to Reach a Given Crack Size and Actual Sample Distribution of XWPB Fastener Holes

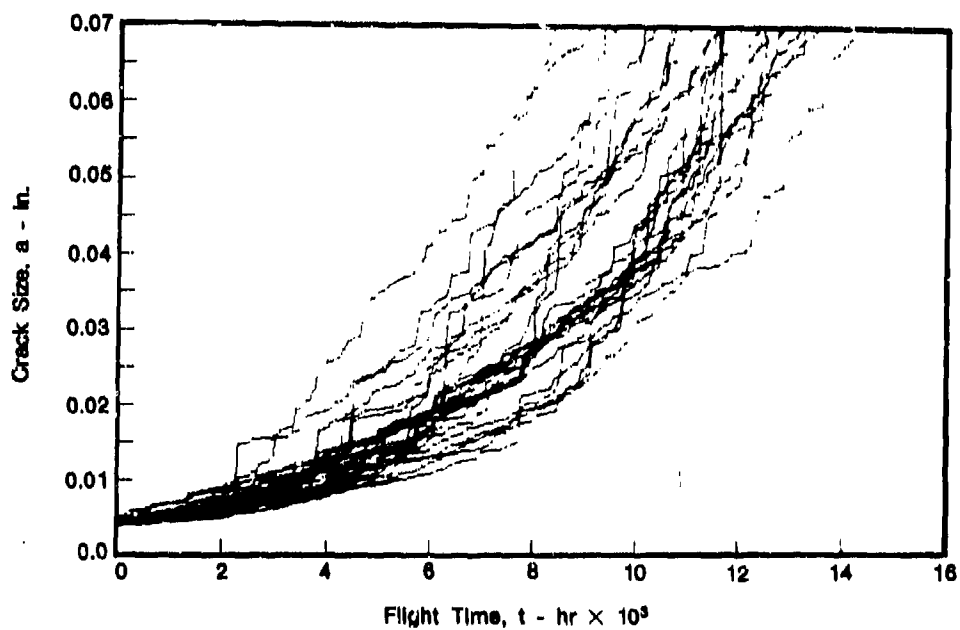


Figure 63. Simulated Sample Functions of Crack Propagation Time-History for XWPB Fastener Holes

SECTION VII

CONCLUSIONS

1. Spectrum Loading

A fracture mechanics-based statistical model developed in Reference 1 for the prediction of fatigue crack growth behavior under any single test condition has been extended to the case of spectrum loading. The distributions of propagation life to reach any given crack size and the crack size at any specific number of load cycles were obtained. A specific block loading was chosen and applied to IN100 laboratory test specimens to obtain statistically meaningful crack propagation test data for the verification of the statistical model. The same block loading was used for the theoretical prediction of the crack propagation behavior of IN100 based on the model. Comparison of the theoretical results with the verification test data indicated a reasonable correlation. The model provided conservative predictions of both the mean behavior and the variability of the data. Thus, the proposed fracture mechanics-based statistical model is quite practical, since it requires only a small nonhomogeneous data base for predicting crack propagation under spectrum loading. Crack growth retardation or acceleration effects due to the applied spectrum (temperature, loading) must be addressed in further work on this model. However, the theoretical model is judged appropriate for practical applications due to its simplicity and conservative predictions.

2. Related Developments

A statistical model based on the Paris crack growth rate function for fatigue crack growth in IN100 was investigated and applied to test results at various temperatures, loading frequencies, and stress ratios. Again, the distributions of life to reach any specific crack size and the crack size at any specific number of cycles were obtained. Homogeneous test environments were assumed to avoid excessive extrapolation into the region where crack growth data did not exist. The life integration was then based on the best-fitted crack growth rate parameters. This approach was necessary in order to obtain the homogeneous data sets, referred to as the extrapolated test results, for the correlation study.

The correlation between the statistical model and the extrapolated test results was reasonable. Care should be taken in the application of this model as the Paris crack growth rate function is applicable only to a certain region of the stress intensity range. This model is mathematically simple and practical for engineering applications.

Closed form solutions have been obtained for the statistical moments of the random time when a dominant crack reaches a given size for a rather general class of crack growth mechanisms. The key to this success was the approximation of the random crack size by a diffusive Markov process. Theoretically, the approximation introduced an error associated with the possibility for the crack propagation rate to be negative at times. However, in terms of statistical properties, the error was negligible if the tendency for drift dominates the tendency for diffusion. The application of the proposed theory to two real examples seemed to substantiate our contention. The theoretical results have been shown to correlate well with the experimental results when the parameters for the mathematical model were obtained from a linear regression procedure. Since the calculation of a few key parameters using such a procedure does not require a very large data base, the proposed theory is quite practical in view of the limited experimental results available at the present time.

REFERENCES

1. Yang, J. N., G. C. Salivar, and C. G. Annis, Jr., "Statistics of Crack Growth in Engine Materials — Vol. 1: Constant Amplitude Fatigue Crack Growth at Elevated Temperatures," Air Force Wright Aeronautical Laboratories Technical Report, AFWAL-TR-82-4040, June 1982.
2. Larsen, J. M., B. J. Schwartz, and C. G. Annis, Jr., "Cumulative Damage Fracture Mechanics Under Engine Spectra," Technical Report AFML-TR-79-4159, Air Force Materials Laboratory, WPAFB, Jan. 1980.
3. Virkler, D. A., B. M. Hillberry and P. K. Goel, The Statistical Nature of Fatigue Crack Propagation, *Journal of Engineering Materials and Technology*, ASME, 101, 148-152 (1979).
4. Virkler, D. A., B. M. Hillberry and P. K. Goel, The Statistical Nature of Fatigue Crack Propagation, Air Force Flight Dynamics Laboratory, Technical Report AFFDL-TR-78-43, WPAFB (1978).
5. Lin, Y. K., and J. N. Yang, "On Statistical Moments of Fatigue Crack Propagation," paper to appear in *Journal of Engineering Fracture Mechanics*, August 1983.
6. Miller, M. S., and J. P. Gallagher, An Analysis of Several Fatigue Crack Growth Rate (FCGR) Descriptions, in *Fatigue Crack Growth Measurement and Data Analysis*, ASTM-STP 738, 1981, pp. 205-251.
7. Hoepfner, D. W., and W. E. Krupp, Prediction of Component Life by Application of Fatigue Crack Growth Knowledge, *Engineering Fracture Mechanics*, 6, 47-70 (1974).
8. Swanson, S. R., F. Cicci and W. Hoppe, Crack Propagation in Clad 7079-T6 Aluminum Alloy Sheet Under Constant and Random Amplitude Fatigue Loading, Fatigue Crack Propagation, ASTM-STP415, 312-362 (1967).
9. Smith, S. H., Random Loading Fatigue Crack Growth Behavior of Some Aluminum and Titanium Alloys, *Structural Fatigue in Aircraft*, ASTM-STP404 (1966).
10. Yang, J. N., Statistics of Random Loading Relevant to the Fatigue, *Journal Engr. Mech. Div.*, ASCE, 100, No. EM3, 469-475 (1974).
11. Yang, J. N., and W. H. Trapp, Reliability Analysis of Aircraft Structures Under Random Loading and Periodic Inspection, *AIAA Journal*, 12, 1623-1630 (1974).
12. Wood, H. A., R. M. Engle, J. P. Gallagher and J. M. Potter, Current Practice on Estimating Crack Growth Damage Accumulation With Specific Application to Structural Safety, Durability and Reliability, U. S. Air Force Flight Dynamics Lab., AFFDL-TR-75-32, WPAFB (1976).
13. Yang, J. N., and S. D. Manning, Distribution of Equivalent Initial Flaw Size, 1980 *Proceedings of Annual Reliability and Maintainability Symposium*, 112-120 (1980).

14. Yang, J. N., Statistical Estimation of Economic Life for Aircraft Structures, *Proc. AIAA/ASME/ASCE/AHS SDM Conf.*, St. Louis, 240-248, (1979), *Journal of Aircraft*, AIAA, Vol. 17, No. 7, 528-535 (1980).
15. Yang, J. N., S. D. Manning and W. R. Garver, Durability Methods Development, Volume V — Durability Analysis Methodology Development, Air Force Flight Dynamics Laboratory, AFFDL-TR-3118, Vol. 5 (1979).
15. Rudd, J. L., J. N. Yang, S. D. Manning and W. R. Garver, Durability Design Requirements and Analysis for Metallic Airframe, in *Design of Fatigue and Fracture Resistant Structures*, ASTM-STP 761, 1982, pp. 133-151.
17. Yang, J. N., Statistical Crack Growth in Durability and Damage Tolerant Analyses, *Proc. AIAA/ASME/ASCE/AHS 22nd Structures, Structural Dynamics, and Materials Conference*, 38-44 (1980).
18. Birnbaum, Z. W., and S. C. Saunders, A New Family of Life Distribution, *Journal of Applied Probability*, 319-327 (1969).
19. Birnbaum, Z. W., and S. C. Saunders, Estimation for a Family of Life Distributions with Applications to Fatigue, *Journal of Applied Probability*, 328-347 (1969).
20. Bogdanoff, J., A New Cumulative Damage Model — Part 4, *Journal of Applied Mechanics*, ASME, 47, 40-44 (1980).
21. Kozin, F., and J. Bogdanoff, A Critical Analysis of Some Probabilistic Models of Fatigue Crack Growth, *Journal of Engineering Fracture Mechanics*, 14, 59-89 (1981).
22. Yang, J. N., G. C. Salivar, Statistical Modeling of Fatigue-Crack Growth in a Nickel-Based Superalloy, to appear in *Journal of Engineering Fracture Mechanics*, August 1983.
23. Norohna, P. J., et al., Fastener Hole Quality, Vol I, Air Force Flight Dynamics Lab., AFFDL-TR-78-206, WPAFB (1978).
24. Lin, Y. K., Probabilistic Theory of Structural Dynamics, McGraw-Hill Book Co. (1967). Reprinted by R. E. Krieger Publishing Co. (1976).
25. Stratonovich, R. L., *Topics in the Theory of Random Noise, Vol. II*, translated by R. A. Silverman, Gordon and Breach, New York (1967).
26. Arnold, L., *Stochastic Differential Equations: Theory and Applications*, John Wiley and Sons, Inc., New York (1974).
27. Khasminskii, R. Z., A Limit Theorem for the Solution of Differential Equations with Random Right Hand Sides, *Theory of Probability and Application*, 11, 390-405 (1966).
28. Lin, Y. K., and J. N. Yang, A Stochastic Theory of Fatigue Crack Propagation, AIAA Paper No. 83-0978, *Proc. AIAA/ASME/ASCE/AHS 24th SDM Conference*, 2-4 May 1983, Lake Tahoe.

APPENDIX

1002396 PWA 1074 MISS. AIR 10 CPN R= 0.10 THICKNESS=12.649 MM PWA= 10.675 KN WIDTH=63.386 MM									
COMPACT SPECIMEN									
NO.	CYCLES	A(MM)	DEL K (MPA* M)	DA/DN (MM/CYCLE)					
1	0	12.59	15.68	9.176E-05					
2	4000	12.95	15.71	6.350E-05					
3	8000	13.21	15.74	5.874E-05					
4	12000	13.44	15.78	6.794E-05					
5	16000	13.71	15.82	6.477E-05					
6	20000	13.97	15.87	7.112E-05					
7	24000	14.26	15.93	7.906E-05					
8	28000	14.57	16.01	8.688E-05					
9	32000	14.92	16.08	6.318E-05					
10	36000	15.17	16.17	9.833E-05					
11	40000	15.57	16.27	8.255E-05					
12	44000	15.90	16.38	8.001E-05					
13	48000	16.22	16.51	1.194E-04					
14	52000	16.70	16.67	3.398E-05					
15	56000	17.07	16.88	1.667E-04					
16	60000	17.74	17.16	1.422E-04					
17	64000	18.31	17.46	1.765E-04					
18	68000	19.01	17.86	1.972E-04					
19	72000	19.80	18.31	1.977E-04					
20	76000	20.60	18.92	2.857E-04					
21	80000	21.74	19.80	3.598E-04					
22	84000	23.18	20.50	4.458E-04					
23	85000	23.62	21.06	9.982E-04					
24	86606	24.62	21.55	1.905E-04					
25	87800	24.81	21.73	2.266E-04					
26	88000	25.04	22.13	6.998E-04					
27	89000	25.74	23.07	1.392E-03					
28	90000	27.13	23.85	2.273E-04					
29	91000	27.36	24.67	2.312E-04					
30	92000	27.59	24.74	1.076E-03					
31	93000	28.67	26.61	2.316E-03					
32	94000	30.98	28.38	5.245E-04					
33	95000	31.51	28.94	1.124E-04					
34	96006	31.82	28.94	1.808E-03					
35	97000	33.63	30.45	5.286E-03					
36	98000	38.92	36.75	1.952E-03					
37	99000	40.87	46.16	3.340E-03					
38	100000	44.21	55.93						

1002397 PWA 1074 MISS. AIR 10 CPN R= 0.10 THICKNESS=12.751 MM PWA= 10.675 KN WIDTH=63.317 MM									
COMPACT SPECIMEN									
NO.	CYCLES	A(MM)	DEL K (MPA* M)	DA/DN (MM/CYCLE)					
1	0	12.69	15.58	1.264E-04					
2	4000	13.20	15.64	1.229E-04					
3	8000	13.69	15.73	1.299E-04					
4	12000	14.21	15.83	1.273E-04					
5	16000	14.72	15.96	1.489E-04					
6	20000	15.32	16.12	1.463E-04					
7	24000	15.91	16.32	1.661E-04					
8	28000	16.57	16.60	2.115E-04					
9	32000	17.42	16.96	2.130E-04					
10	36000	18.27	17.42	2.654E-04					
11	40000	19.33	17.79	3.556E-04					
12	41000	19.69	18.06	5.817E-04					
13	42000	20.27	18.26	9.398E-05					
14	43000	20.36	18.38	3.099E-04					
15	44000	20.67	18.54	2.057E-04					
16	45000	20.88	18.87	8.293E-04					
17	46000	21.71	19.19	1.460E-04					
18	47000	21.85	19.31	1.791E-04					
19	48000	22.03	19.56	5.537E-04					
20	49000	22.59	20.13	1.013E-03					
21	50000	23.60	20.61	2.438E-04					
22	51000	23.84	20.76	1.461E-04					
23	52000	23.99	21.10	7.010E-04					
24	53000	24.69	22.02	1.464E-03					
25	54000	26.16	22.77	2.210E-04					
26	55000	26.39	22.96	2.019E-04					
27	56000	26.58	23.53	9.995E-04					
28	57000	27.58	25.09	2.050E-03					
29	58000	29.63	26.51	4.965E-04					
30	59000	30.12	27.00	3.289E-04					
31	60000	30.45	28.21	1.584E-03					
32	61000	32.64	32.27	3.909E-03					
33	62000	35.95	37.19	1.236E-03					
34	63000	37.18	39.84	1.053E-03					
35	64000	38.23	47.76	4.426E-03					
36	65000	42.66							

1002398 PWA 1074 MISS. AIR 10 CPN R= 0.10 THICKNESS=12.649 MM PWA= 10.675 KN WIDTH=63.355 MM									
COMPACT SPECIMEN									
NO.	CYCLES	A(MM)	DEL K (MPA* M)	DA/DN (MM/CYCLE)					
1	0	12.55	15.69	1.464E-04					
2	4000	13.13	15.76	1.381E-04					
3	8000	13.69	15.87	1.845E-04					
4	12000	14.42	15.97	6.159E-05					
5	16000	14.67	16.06	1.305E-04					
6	20000	15.19	16.19	1.181E-04					
7	24000	15.67	16.31	8.668E-05					
8	28000	16.01	16.31	1.575E-04					
9	32000	16.66	16.48	1.575E-04					
10	36000	17.47	16.75	2.057E-04					
11	40000	18.32	17.11	2.140E-04					
12	44000	19.43	17.58	2.762E-04					
13	48000	20.61	18.21	2.956E-04					
14	52000	22.14	19.06	3.819E-04					
15	53000	22.14	19.58	7.630E-06					
16	56000	23.62	20.12	4.911E-04					
17	60000	26.15	21.71	6.345E-04					
18	61000	26.84	23.34	6.835E-04					
19	62000	28.85	24.47	2.015E-03					
20	63000	30.22	26.30	1.364E-03					
21	64000	30.23	27.11	1.778E-05					
22	65000	31.69	28.03	1.453E-03					
23	66000	37.25	33.31	5.565E-03					
24	67000	39.18	41.39	1.928E-03					
25	68000	42.65	49.67	3.467E-03					

1002398 PWA 1074 MISS. AIR 10 CPN R= 0.10 THICKNESS=12.649 MM PWA= 10.675 KN WIDTH=63.355 MM									
COMPACT SPECIMEN									
NO.	CYCLES	A(MM)	DEL K (MPA* M)	DA/DN (MM/CYCLE)					
1	0	12.55	15.69	1.464E-04					
2	4000	13.13	15.76	1.381E-04					
3	8000	13.69	15.87	1.845E-04					
4	12000	14.42	15.97	6.159E-05					
5	16000	14.67	16.06	1.305E-04					
6	20000	15.19	16.19	1.181E-04					
7	24000	15.67	16.31	8.668E-05					
8	28000	16.01	16.40	1.575E-04					
9	32000	16.64	16.75	2.057E-04					
10	36000	17.47	17.11	2.140E-04					
11	40000	18.32	17.58	2.762E-04					
12	44000	19.43	18.21	2.956E-04					
13	48000	20.61	19.58	7.630E-06					
14	52000	22.14	20.12	4.911E-04					
15	53000	22.14	20.12	4.911E-04					
16	56000	23.62	21.71	6.344E-04					
17	60000	26.84	23.14	6.833E-04					
18	61000	26.84	24.47	2.015E-03					
19	62000	28.85	26.30	1.378E-05					
20	63000	30.22	27.11	1.778E-05					
21	64000	30.23	28.03	1.453E-03					
22	65000	31.69	33.31	5.585E-03					
23	66000	37.25	41.39	1.928E-03					
24	67000	39.18	49.67	3.467E-03					
25	68000	42.65							

1002399 FMA 1074 MISS. AIR 10 CPM				
R= 0.0 THICKNESS=12.700 MM				
PMAX= 10.675 KN WIDTH=63.309 MM				
COMPACT SPECIMEN				
NO.	CYCLES	A(MM)	DEL K (MPA* M)	DA/DN (MM/CYCLE)
1	0.	12.63		
2	4000.	13.24	17.39	1.530E-04
3	8000.	13.67	17.46	1.067E-04
4	12000.	13.99	17.52	8.128E-05
5	16000.	14.49	17.61	1.257E-04
6	20000.	14.89	17.71	9.938E-05
7	24000.	15.30	17.83	1.026E-04
8	28000.	15.44	17.91	3.524E-05
9	32000.	16.16	18.05	1.791E-04
10	36000.	16.77	18.30	1.534E-04
11	40000.	17.62	18.61	2.118E-04
12	44000.	18.46	19.02	2.115E-04
13	48000.	19.29	19.47	2.061E-04
14	52000.	20.33	20.04	2.615E-04
15	53000.	20.47	20.43	1.321E-04
16	55000.	21.59	20.86	3.759E-04
17	60000.	22.80	21.74	3.019E-04
18	61000.	23.58	22.54	7.798E-04
19	62000.	24.56	23.31	9.817E-04
20	63000.	25.13	24.01	5.652E-04
21	64000.	25.00	24.22	-1.308E-04
22	65000.	25.94	24.61	9.436E-04
23	66000.	27.64	25.95	1.703E-03
24	67000.	28.15	27.17	5.058E-04
25	68000.	28.26	27.52	1.143E-04
26	69000.	29.17	28.13	9.043E-04
27	70000.	32.20	30.67	3.031E-03
28	71000.	33.06	33.62	8.595E-04
29	72000.	33.52	34.74	4.610E-04
30	73000.	36.29	37.80	2.774E-03

1002400 FMA 1074 MISS. AIR 10 CPM				
R= 9.10 THICKNESS=12.649 MM				
PMAX= 10.675 KN WIDTH=63.353 MM				
COMPACT SPECIMEN				
NO.	CYCLES	A(MM)	DEL K (MPA* M)	DA/DN (MM/CYCLE)
1	0.	12.70		
2	4000.	13.22	15.70	1.283E-04
3	8000.	13.52	15.75	7.557E-05
4	12000.	13.92	15.81	1.016E-04
5	16000.	14.35	15.88	1.060E-04
6	20000.	14.79	15.97	1.114E-04
7	24000.	15.34	16.09	1.372E-04
8	28000.	15.94	16.25	1.502E-04
9	32000.	16.58	16.45	1.591E-04
10	36000.	17.19	16.68	1.530E-04
11	40000.	18.05	16.98	2.140E-04
12	44000.	18.84	17.37	1.988E-04
13	48000.	20.13	17.91	3.223E-04
14	49000.	20.35	18.35	2.184E-04
15	50000.	21.12	18.65	7.671E-04
16	51000.	21.28	18.94	1.600E-04
17	52000.	21.36	19.02	8.001E-05
18	54000.	22.62	19.48	6.331E-04
19	55000.	22.90	20.03	2.756E-04
20	56000.	23.07	20.20	1.740E-04
21	57000.	23.72	20.51	6.426E-04
22	58000.	24.67	21.22	1.157E-03
23	59000.	25.07	21.78	1.981E-04
24	60000.	25.35	21.99	2.819E-04
25	61000.	26.15	22.46	7.937E-04
26	62000.	27.92	23.66	1.775E-03
27	63000.	28.42	24.80	4.978E-04
28	64000.	28.64	25.18	2.159E-04
29	65000.	29.91	26.00	1.273E-03
30	66000.	32.77	28.53	2.865E-03
31	67000.	33.54	31.13	7.633E-04
32	68000.	34.13	32.22	5.931E-04
33	69000.	36.67	35.03	2.544E-03
34	70000.	47.00	53.14	1.032E-02

1002401 FMA 1074 MISS. AIR 10 CPM				
R= 0.10 THICKNESS=12.675 MM				
PMAX= 10.675 KN WIDTH=63.373 MM				
COMPACT SPECIMEN				
NO.	CYCLES	A(MM)	DEL K (MPA* M)	DA/DN (MM/CYCLE)
1	0.	12.55		
2	4000.	12.90	15.65	8.604E-05
3	8000.	13.11	15.67	5.334E-05
4	12000.	13.41	15.71	7.557E-05
5	16000.	13.56	15.73	2.191E-05
6	20000.	13.94	15.77	1.092E-04
7	24000.	14.05	15.82	2.921E-05
8	28000.	14.37	15.86	7.906E-05
9	32000.	14.62	15.92	6.223E-05
10	36000.	14.97	15.99	8.688E-05
11	40000.	15.33	16.08	9.049E-05
12	44000.	15.74	16.18	1.035E-04
13	48000.	16.08	16.30	8.509E-05
14	52000.	16.54	16.43	1.143E-04
15	56000.	16.95	16.59	1.032E-04
16	60000.	17.52	16.78	1.419E-04
17	64000.	18.13	17.03	1.518E-04
18	68000.	18.77	17.33	1.603E-04
19	72000.	19.59	17.70	2.045E-04
20	76000.	20.46	18.18	2.197E-04
21	80000.	21.78	18.85	3.280E-04
22	81000.	22.20	19.43	4.254E-04
23	82000.	22.98	19.86	7.785E-04
24	83000.	23.19	20.22	2.065E-04
25	84000.	23.27	20.33	3.362E-05
26	85000.	23.77	20.55	5.042E-04
27	86000.	24.54	21.05	7.645E-04
28	87000.	25.46	21.75	9.245E-04
29	88000.	25.50	22.17	4.065E-05
30	89000.	26.07	22.44	5.626E-04
31	90000.	28.06	23.63	1.994E-03
32	91000.	28.27	24.73	2.057E-04
33	92000.	28.54	24.98	2.756E-04
34	93000.	29.61	25.82	1.267E-03
35	94000.	32.97	28.52	3.160E-03
36	95000.	33.62	31.43	8.534E-04
37	96000.	34.44	32.63	6.147E-04
38	97000.	37.54	36.10	3.104E-03

1002402 PMA 1074 MISS. AIR 10 CPM R= 0.10 THICKNESS=12.700 MM PMA= 10.675 KN WIDTH=63.353 MM COMPACT SPECIMEN						
NO.	CYCLES	A(MM)	DEL K (MPA* M)	DA/DN (MM/CYCLE)		
1	0.	12.68	15.63	1.041E-04		
2	4000.	13.10	15.68	7.620E-05		
3	8000.	13.40	15.72	7.683E-05		
4	12000.	13.71	15.77	8.541E-05		
5	16000.	14.05	15.84	8.827E-05		
6	20000.	14.40	15.90	7.525E-05		
7	24000.	14.70	15.99	1.026E-04		
8	28000.	15.14	15.99	1.022E-04		
9	32000.	15.55	16.10	1.127E-04		
10	36000.	16.00	16.23	1.127E-04		
11	40000.	16.55	16.39	1.368E-04		
12	44000.	17.03	16.58	1.222E-04		
13	48000.	17.66	16.80	1.579E-04		
14	52000.	18.39	17.10	1.838E-04		
15	56000.	19.20	17.47	2.010E-04		
16	60000.	20.23	17.97	2.575E-04		
17	64000.	21.52	18.66	3.235E-04		
18	68000.	23.03	19.60	3.775E-04		
19	69000.	23.57	20.35	5.398E-04		
20	70000.	24.46	20.91	8.839E-04		
21	71000.	24.66	21.35	2.083E-04		
22	72000.	24.84	21.51	1.816E-04		
23	73000.	25.50	21.87	6.540E-04		
24	74000.	26.66	22.67	1.166E-03		
25	75000.	27.00	23.37	3.328E-04		
26	76000.	27.19	23.62	1.956E-04		
27	77000.	28.15	24.19	9.598E-04		
28	78000.	29.98	25.67	1.831E-03		
29	79000.	30.41	26.97	4.242E-04		
30	80000.	30.71	27.42	3.035E-04		
31	81000.	32.16	28.54	1.453E-03		
32	82000.	35.56	32.14	3.399E-03		
33	83000.	36.47	36.12	9.081E-04		
34	84000.	37.54	38.27	1.069E-03		
35	85000.	41.45	44.82	3.907E-03		

1002403 PMA 1074 MISS. AIR 10 CPM R= 0.10 THICKNESS=12.624 MM PMA= 10.675 KN WIDTH=63.363 MM COMPACT SPECIMEN						
NO.	CYCLES	A(MM)	DEL K (MPA* M)	DA/DN (MM/CYCLE)		
1	0.	12.57	15.72	1.365E-04		
2	4000.	13.12	15.77	9.049E-05		
3	8000.	13.46	15.83	1.067E-04		
4	12000.	13.91	15.91	1.019E-04		
5	16000.	14.31	16.00	1.137E-04		
6	20000.	14.77	16.09	9.271E-05		
7	24000.	15.14	16.23	1.534E-04		
8	28000.	15.75	16.40	1.362E-04		
9	32000.	16.30	16.61	1.591E-04		
10	36000.	16.93	16.79	7.966E-05		
11	40000.	17.25	17.04	2.076E-04		
12	44000.	18.08	17.44	2.216E-04		
13	48000.	19.97	17.98	2.966E-04		
14	52000.	20.15	19.61	3.588E-04		
15	56000.	21.42	18.71	3.169E-04		
16	60000.	22.85	20.35	5.664E-04		
17	61000.	23.42	21.02	1.163E-03		
18	62000.	24.58	21.73	2.159E-04		
19	63000.	24.75	21.57	1.727E-04		
20	64000.	24.97	21.73	2.159E-04		
21	65000.	25.68	22.13	7.087E-04		
22	66000.	27.31	23.19	1.634E-03		
23	67000.	27.44	24.04	1.308E-04		
24	68000.	27.80	24.28	3.581E-04		
25	69000.	28.84	25.00	1.035E-03		
26	70000.	31.40	27.03	2.559E-03		
27	71000.	31.92	29.00	5.132E-04		
28	72000.	32.30	29.63	3.874E-04		
29	73000.	34.26	31.38	1.960E-03		
30	74000.	39.58	38.29	5.323E-03		
31	75000.	41.51	46.47	1.927E-03		

1002404 PMA 1074 MISS. AIR 10 CPM R= 0.10 THICKNESS=12.725 MM PMA= 10.675 KN WIDTH=63.457 MM COMPACT SPECIMEN						
NO.	CYCLES	A(MM)	DEL K (MPA* M)	DA/DN (MM/CYCLE)		
1	0.	12.72	15.59	9.525E-05		
2	4000.	13.10	15.62	3.239E-05		
3	8000.	13.23	15.64	4.921E-05		
4	12000.	13.43	15.67	6.826E-05		
5	16000.	13.70	15.67	-1.588E-05		
6	20000.	13.64	15.69	-3.492E-06		
7	24000.	13.62	15.70	7.366E-05		
8	28000.	13.92	15.73	1.270E-05		
9	32000.	13.97	15.76	5.207E-05		
10	36000.	14.18	15.78	1.587E-05		
11	40000.	14.24	15.81	5.080E-05		
12	44000.	14.44	15.85	3.969E-05		
13	48000.	14.60	15.89	6.572E-05		
14	52000.	14.87	15.99	1.295E-04		
15	56000.	15.38	16.08	2.858E-05		
16	60000.	15.50	16.21	1.851E-04		
17	64000.	15.53	16.10	7.620E-06		
18	68000.	16.27	16.38	6.064E-05		
19	72000.	16.51	16.48	8.255E-05		
20	76000.	16.84	16.68	1.775E-04		
21	80000.	17.55	17.01	2.029E-04		
22	84000.	18.36	17.39	1.997E-04		
23	88000.	19.16	17.75	1.391E-04		
24	92000.	19.72	18.19	2.496E-04		
25	96000.	20.72	19.35	5.970E-05		
26	100000.	22.84	20.05	2.222E-04		
27	101000.	22.90	20.27	3.454E-04		
28	102000.	23.13	20.43	8.636E-04		
29	103000.	23.47	20.27	3.454E-04		
30	104000.	23.56	21.15	8.636E-04		
31	105000.	25.25	21.92	1.105E-04		
32	107000.	25.40	22.15	4.305E-04		
33	108000.	25.83	22.79	9.868E-04		
34	109000.	26.81	24.36	2.262E-03		
35	110000.	29.09	26.02	8.293E-04		
36	111000.	29.91	26.64	2.476E-04		
37	112000.	30.15	27.83	1.689E-03		
38	113000.	31.84	34.10	6.500E-03		
39	114000.	38.34	44.00	1.962E-03		
40	115000.	40.30				

1002405 PMA 1074 MISS. AIR 10 CPM				
R= 0.10 THICKNESS=12.751 MM				
PMAK= 10.675 KN WIDTH=63.396 MM				
COMPACT SPECIMEN				
NO.	CYCLES	A(MM)	DEL K (MPA* M)	DA/DN (MM/CYCLE)
1	0.	12.65	15.56	1.121E-04
2	4000.	13.10	15.61	7.557E-05
3	8000.	13.40	15.65	7.048E-05
4	12000.	13.68	15.69	5.461E-05
5	16000.	13.90	15.75	1.235E-04
6	20000.	14.39	15.75	1.118E-04
7	24000.	14.84	15.85	1.118E-04
8	28000.	15.16	15.94	8.033E-05
9	32000.	15.61	16.04	1.133E-04
10	36000.	16.11	16.18	1.238E-04
11	40000.	16.61	16.35	1.241E-04
12	44000.	17.09	16.52	1.216E-04
13	48000.	17.84	16.77	1.867E-04
14	52000.	18.51	17.09	1.667E-04
15	56000.	19.34	17.46	2.092E-04
16	60000.	20.40	17.97	2.638E-04
17	62000.	21.16	18.51	3.791E-04
18	63000.	21.46	18.85	3.061E-04
19	64000.	21.50	18.96	3.937E-05
20	65000.	22.06	19.17	5.626E-04
21	66000.	22.95	19.67	8.839E-04
22	67000.	22.64	19.88	3.099E-04
23	68000.	22.90	19.86	2.642E-04
24	69000.	23.82	20.30	9.144E-04
25	70000.	24.46	20.90	6.375E-04
26	71000.	24.72	21.27	2.667E-04
27	72000.	24.85	21.43	1.308E-04
28	73000.	25.79	21.89	9.360E-04
29	74000.	27.02	22.85	1.227E-03
30	75000.	28.18	24.00	1.168E-03
31	76000.	28.52	24.77	3.353E-04
32	77000.	29.64	25.55	1.118E-03
33	78000.	32.11	27.66	2.473E-03
34	79000.	33.02	29.96	9.118E-04
35	80000.	34.00	31.40	9.817E-04
36	81000.	35.75	33.71	1.744E-03

1002406 PMA 1074 MISS. AIR 10 CPM				
R= 0.10 THICKNESS=12.700 MM				
PMAK= 10.675 KN WIDTH=63.434 MM				
COMPACT SPECIMEN				
NO.	CYCLES	A(MM)	DEL K (MPA* M)	DA/DN (MM/CYCLE)
1	0.	12.90	15.64	6.064E-05
2	4000.	13.14	15.67	9.493E-05
3	8000.	13.52	15.73	9.398E-05
4	12000.	13.90	15.79	7.811E-05
5	16000.	14.21	15.79	7.811E-05
6	20000.	14.53	15.85	8.065E-05
7	24000.	14.82	15.92	7.271E-05
8	28000.	15.29	16.01	1.165E-04
9	32000.	15.66	16.12	9.334E-05
10	36000.	16.18	16.26	1.308E-04
11	40000.	16.79	16.45	1.518E-04
12	44000.	17.42	16.68	1.565E-04
13	48000.	18.18	16.97	1.908E-04
14	52000.	18.95	17.33	1.921E-04
15	56000.	19.93	17.79	2.451E-04
16	60000.	21.09	18.41	2.911E-04
17	64000.	22.59	19.27	3.727E-04
18	65000.	23.19	20.01	6.083E-04
19	66000.	23.78	20.46	5.893E-04
20	67000.	23.99	20.77	2.019E-04
21	68000.	24.19	20.93	2.007E-04
22	69000.	24.66	21.20	4.737E-04
23	70000.	25.95	21.94	1.293E-03
24	71000.	26.10	22.58	1.448E-04
25	72000.	26.36	22.76	2.667E-04
26	73000.	27.19	23.27	8.230E-04
27	74000.	28.93	24.53	1.740E-03
28	75000.	29.54	25.79	6.064E-04
29	76000.	29.71	26.24	1.740E-04
30	77000.	31.00	27.10	1.290E-03
31	78000.	34.30	30.16	3.294E-03
32	79000.	35.13	33.51	8.344E-04
33	80000.	35.76	34.87	6.350E-04
34	81000.	38.87	36.85	3.103E-03

1002407 PMA 1074 MISS. AIR 10 CPM				
R= 0.10 THICKNESS=12.713 MM				
PMAK= 10.675 KN WIDTH=63.487 MM				
COMPACT SPECIMEN				
NO.	CYCLES	A(MM)	DEL K (MPA* M)	DA/DN (MM/CYCLE)
1	0.	12.75	15.60	9.652E-05
2	4000.	13.14	15.64	7.493E-05
3	8000.	13.44	15.68	5.368E-05
4	12000.	13.65	15.72	6.953E-05
5	16000.	13.93	15.77	7.080E-05
6	20000.	14.21	15.83	8.128E-05
7	24000.	14.54	15.83	7.557E-05
8	28000.	14.84	15.89	9.271E-05
9	32000.	15.21	15.98	8.700E-05
10	36000.	15.56	16.07	1.419E-04
11	40000.	16.13	16.21	1.419E-04
12	44000.	16.55	16.37	1.070E-04
13	48000.	17.43	16.61	2.200E-04
14	52000.	17.91	16.89	1.194E-04
15	56000.	18.61	17.15	1.734E-04
16	60000.	19.50	17.55	2.235E-04
17	61000.	19.78	17.86	2.756E-04
18	62000.	20.31	18.09	5.359E-04
19	63000.	20.55	18.32	2.413E-04
20	64000.	20.63	18.42	7.620E-05
21	65000.	21.25	18.64	6.223E-04
22	66000.	21.54	18.93	2.934E-04
23	67000.	21.68	19.07	1.384E-04
24	68000.	21.83	19.17	1.436E-04
25	71000.	23.26	19.72	4.771E-04
26	72000.	23.46	20.32	1.994E-04
27	73000.	24.02	20.61	5.588E-04
28	74000.	25.27	21.33	1.245E-03
29	75000.	25.23	21.84	3.429E-05
30	76000.	25.45	21.92	2.146E-04
31	77000.	26.49	22.47	1.049E-03
32	78000.	27.91	23.62	1.416E-03
33	79000.	28.36	24.56	4.534E-04
34	80000.	28.71	24.97	3.416E-04
35	81000.	29.81	25.76	1.102E-03
36	82000.	33.03	28.37	3.222E-03
37	83000.	33.85	31.28	8.166E-04
38	84000.	34.27	32.28	4.204E-04
39	85000.	37.01	35.13	2.741E-03